



JRC EXTERNAL STUDY REPORT

Generic vehicle model N2A & N3D

Sebik, M., Kodajkova, Z.

2023

This publication is an External Study prepared for the Joint Research Centre (JRC), the European Commission's science and knowledge service. It aims to provide evidence-based scientific support to the European policymaking process. The contents of this publication do not necessarily reflect the position or opinion of the European Commission. Neither the European Commission nor any person acting on behalf of the Commission is responsible for the use that might be made of this publication. For information on the methodology and quality underlying the data used in this publication for which the source is neither Eurostat nor other Commission services, users should contact the referenced source. The designations employed and the presentation of material on the maps do not imply the expression of any opinion whatsoever on the part of the European Union concerning the legal status of any country, territory, city or area or of its authorities, or concerning the delimitation of its frontiers or boundaries.

Contact information

Name: Martin Larcher

Email: jrc-public-spaces@ec.europa.eu

EU Science Hub

<https://joint-research-centre.ec.europa.eu/jrc>

JRC135531

PDF ISBN 978-92-68-09590-4 doi:10.2760/968550 KJ-02-23-236-EN-N

Luxembourg: Publications Office of the European Union, 2023

© European Union, 2023



The reuse policy of the European Commission documents is implemented by the Commission Decision 2011/833/EU of 12 December 2011 on the reuse of Commission documents (OJ L 330, 14.12.2011, p. 39). Unless otherwise noted, the reuse of this document is authorised under the Creative Commons Attribution 4.0 International (CC BY 4.0) licence (<https://creativecommons.org/licenses/by/4.0/>). This means that reuse is allowed provided appropriate credit is given and any changes are indicated.

For any use or reproduction of photos or other material that is not owned by the European Union permission must be sought directly from the copyright holders.

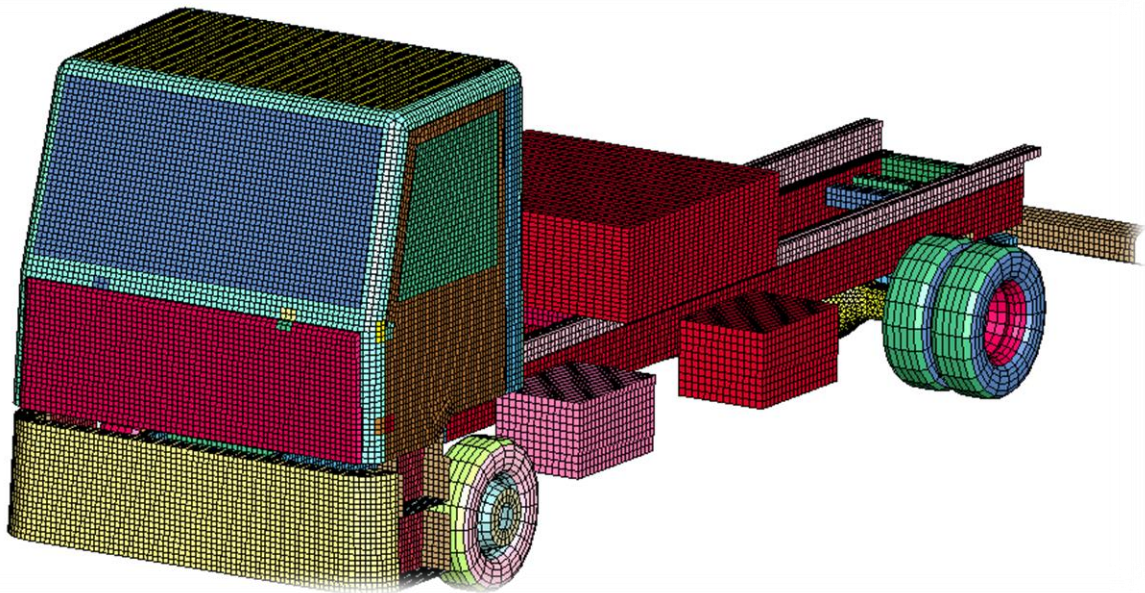
How to cite this report: Sebik, M. and Kodajkova, Z., *Generic vehicle model N2A and N3D*, European Commission, Ispra, 2023, JRC135531.

TECHNICAL REPORT SVS FEM s.r.o.

QUOTATION NUMBER: VN-22260-1 __ JRC model N2	PROJECT NUMBER: ZAK-22263	REVISION: 3	DATE: 9. 10. 2023
--	-------------------------------------	--------------------	--------------------------

Generic vehicle model N2A & N3D

SUPPLIER:	CUSTOMER:
COMPANY: SVS FEM s.r.o. ADDRESS: Trnkova 3104/117c, 628 00 Brno AUTHORS: Ing. Marek Šebík, Ing. Zuzana Kodajková	COMPANY: European Commission - Joint Research Centre ADDRESS: Joint Research Centre, T.P. 441 Directorate for Space, Security and Migration Safety and Security of Buildings I-21027 Ispra (VA) Italy CONTACT PERSON: Dr.-Ing. Martin Larcher



The model will be distributed with the EU Public Licence and the report should be distributed freely and without any specific legal restrictions. The distribution will be managed by European Commission - Joint Research Centre.

Contents

1	Introduction.....	3
2	Main characteristics.....	4
3	FE model.....	6
3.1	Solution method.....	6
3.2	Unit system.....	6
3.3	Model structure.....	7
3.4	Geometry model.....	8
3.5	FE mesh.....	11
3.6	Material models.....	13
3.7	Connections and constraints.....	17
3.8	Loading.....	20
3.9	Initial and boundary conditions.....	20
3.10	Contacts.....	20
3.11	Parameters.....	21
4	Model testing.....	32
4.1	Vehicle in idle.....	32
4.1.1	Objective.....	32
4.1.2	Results.....	32
4.1.3	Conclusion.....	34
4.2	Linear track.....	35
4.2.1	Objective.....	35
4.2.2	Results.....	35
4.2.3	Conclusion.....	37
4.3	Curb test.....	38
4.3.1	Objective.....	38
4.3.2	Results.....	38
4.3.3	Conclusion.....	44
4.4	Crash test – rigid wall.....	45
4.4.1	Objective.....	45
4.4.2	Results.....	47
4.4.3	Conclusion.....	56

4.5	Crash test – bollard	57
4.5.1	Objective	57
4.5.2	Experimental data	57
4.5.3	Results	58
4.5.4	Conclusion	69
5	Summary	70
6	References.....	71
7	Attachments	73
8	Appendix A: Geometry reverse engineering example	74

1 Introduction

Security in public spaces is one of the key responsibilities of all governments and municipalities in the modern world. These days, the security is threatened also by vehicle attacks, which have already happened in many cities all over the world. This kind of terrorist attack poses a challenge on developers of barrier systems who try to mitigate them with their products. Testing of the barriers plays a key role in the development process. However, real testing of the barriers is very expensive. The development is therefore very often driven by realistic computer simulations (finite element numerical simulations – FE simulations). A tremendous advantage of the simulations is their ability to answer many questions regarding behaviour of the system before the real crash test is performed. Moreover, the simulations can quickly predict results of the crash tests under various conditions such as- various impact angles, various attacking vehicles, various impact velocities.

To support these defensive efforts of both academic and commercial researchers Joint Research Centre (JRC) has started a series of workshops “Numerical simulation for hostile vehicle mitigation”. At these workshops various institutions across Europe are sharing their knowledge and experience related to the numerical simulations of vehicle attack mitigation. During these discussions it turned out that there is a need for generic vehicle models that would represent vehicle categories prescribed by standards like IWA 14 or CWA 16221 (a superseding ISO standard ISO 22343 (Parts 1 and 2) has been released recently).

Such generic vehicle models could open a new and more generalized approach to virtual barrier testing. According to the standards, for a certification of a barrier a single crash test must be performed. However, in assessing a barrier in a real application it could be useful to analyse several crash test scenarios with varying conditions. It must be noted that this approach (varying impact speed, impact angle, friction, etc.) has been already adopted by many researchers ([1,3,4]). But these sensitivity analyses are exclusively done by keeping the vehicle characteristics fixed, even if real vehicles of a same category can vary significantly (brand, fitness, wheelbase, mass distribution, etc.). With a generic vehicle model, which can be modified easily through parameters, and which is not computationally expensive, the vehicle properties can also be varied. Furthermore, to get general probabilistic assessment of the barrier performance, a robustness analysis could be easily applied.

On the initiative of the JRC, SVS FEM s.r.o. took the first step in this effort and in 2022 the first model for this purpose – model of N1 vehicle was released [2]. Subsequently, the second generic vehicle model corresponding to the N2A and N3D category (IWA 14) was prepared. This technical report is a description of this generic model (N2A and N3D category) and can be used as a manual for its applications.

It must be also noted that these FE models are significantly different from the typical vehicle FE models used by manufacturers as both types of the models serve different purpose. Vehicle manufacturers employ FE models for the development of individual vehicle components, with the primary goal of meeting industry standards, enhancing occupant safety, reducing weight, and streamlining manufacturing processes. Consequently, it is crucial to provide detailed predictions for every structure within the vehicle. On the other hand, presented models are used for development of the barriers. In these tests, the vehicle itself can be viewed more as a loading condition for the object under analysis.

We would like to gratefully acknowledge Marco Barbi and Giuseppe Cordua who helped us with their expert knowledge on vehicle crash simulations, so that we could verify and improve our most important modelling assumptions.



2 Main characteristics

Vehicle category N2A and N3D

The model represents a vehicle from category N2A or N3D according to the standard IWA 14 (see tab 1). Since these categories are relatively similar to each other it shall be possible to obtain a vehicle from both of these categories just by selecting appropriate input parameters of the model. N2A vehicles have 2-axle configuration (optional flat bed, open side curtain, or rigid box), minimal unladen mass 3 575 kg and total mass 7 200 kg ± 400 kg. N3D vehicles have 2-axle configuration (optional flat bed, open side curtain, or rigid box), minimal unladen mass 6 200 kg and total mass 12 000 kg ± 400 kg.

Parametr	min	max	Model default
Test vehicle mass	6 800 kg	12 400 kg	9 600 kg
Min unladen mass	3 575 kg		
Max ballast		5800 kg	
Length	6 090 mm	10 800 mm	8 500 mm
Width	2 200 mm	2 725 mm	2 310 mm
Wheel base	3 480 mm	6 700 mm	5 090 mm
Height from ground to chasis rail at the front	340 mm	1 070 mm	720 mm

Tab. 1: Parameters' ranges (according to the standard IWA 14) + model default values

Generalization

The vehicle model is generic. The generic vehicle model represents both required categories (N2A, N3D) commercially used within the EU and does not reflect any specific brand - or model-dependent features. The most common vehicle brands belonging to described categories are Iveco, DAF, Mercedes-Benz, Man, Scania, Volvo, Renault.

Validity of the model

The model is validated by basic tests (vehicle in idle, linear track curb test and rigid wall test) according to CEN/TR 16303. The results of the curb test simulation are compared with experimental data. The model is also validated by comparison with experimental data at frontal impact to a bollard.

Parametrization

The model is parametrized to allow user to easily modify key attributes of the vehicle (velocity, mass distribution, dimensions, crash related stiffness, suspension properties). This enables the model to represent any real vehicle within the N2A and N3D category (various age, fitness, brand, size, mass, ...). Parametrization makes the model suitable also for stochastic studies.

Solution efficiency

From computational perspective, the model shall be as effective as possible. There was an effort taken to eliminate too detailed structure features and keep only the parts and features relevant for the crash test. The minimum timestep varies with input parameters. Default version of the model achieves timestep of 3 μ s (3 μ s = 0.003 ms). The model is computationally effective without mass scaling¹.

Convertibility to other codes

The original version of the model was developed for Ansys LS-DYNA but is convertible to other FE codes as well. There are no strictly Ansys LS-DYNA related features. In particular, the model is being converted by the JRC for calculations with the EUROPLEXUS software.

¹ Mass scaling is a technique of artificially increasing the mass on the parts where the critical time step becomes prohibitively small. This technique allows to control efficiently the CPU time of the simulations, but would require a verification that the artificially added mass does not influence the expected result.

3 FE model

3.1 Solution method

The model is prepared for explicit simulations in Ansys LS-DYNA R13. For detailed description of keywords mentioned in this report see LS-DYNA manual [5].

3.2 Unit system

The model is prepared in consistent unit system:

mm, ms, kg, kN, GPa, J

If not stated otherwise, the values in this report are in this unit system as well.

3.3 Model structure

The model input is split into several input files for clarity and easier editing of individual parts. The recommended model structure for a crash test simulation with this vehicle model is: main input file (Main.k) which references main input files of the barrier (Barrier_Main.k), the road (Road_Main.k) and the vehicle (Vehicle_Main.k) (see fig. 1). Content of input files Main.k, Barrier_Main.k and Road_Main.k depends on specific crash test scenario and is not a subject of this work nor this report. Due to this recommended model structure, Barrier_Main.k and Road_Main.k can be changed independently from the vehicle model. In this model structure, the analysis settings (*CONTROL keywords) and output settings (*DATABASE keywords) are in the Main.k input file.

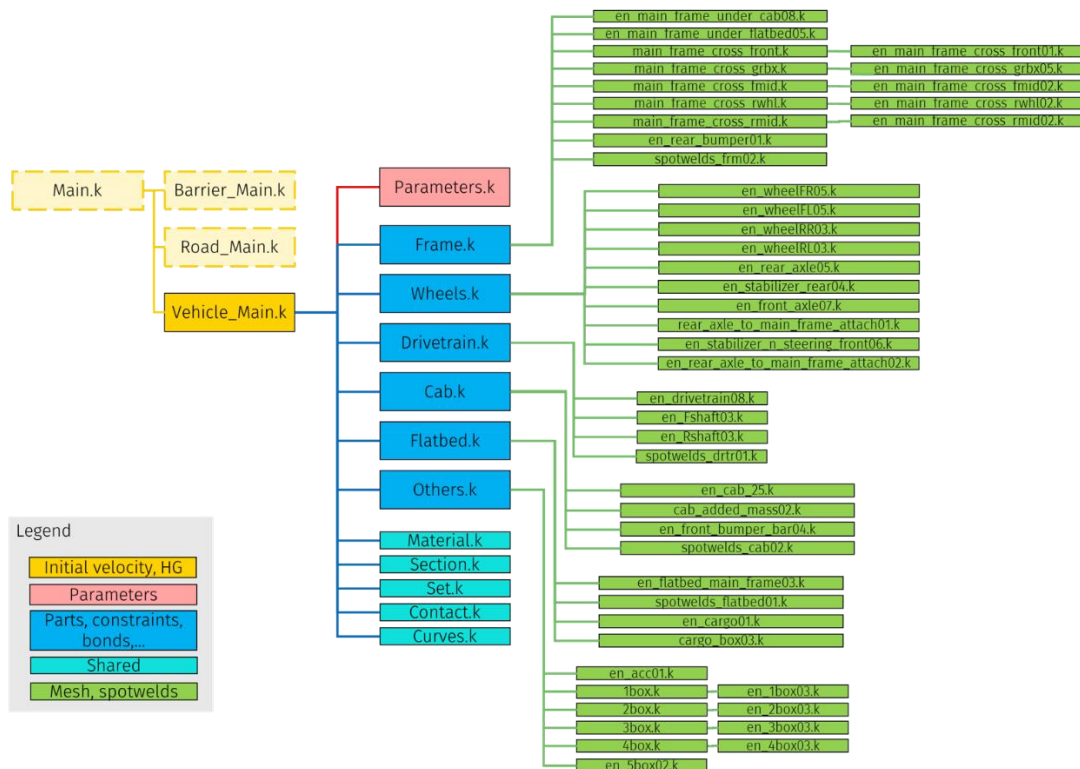


Figure 1: Model structure

Vehicle_Main.k includes the initial velocity definition and the hourglass control. Input file Parameters.k contains key input parameters (see chap. 3.11 Parameters). Frame.k, Wheels.k, Drivetrain.k, Cab.k, Flatbed.k and Others.k are input files devoted to major sections of the vehicle. These input files reference corresponding input files with the mesh (element, nodes) and constraints like rigid connections or kinematic joints. Input files from the category “Shared” contain the material library (Material.k), the element type definitions (Section.k), various sets like sets of nodes, sets of segments, sets of parts (Set.k), contacts (Contact.k) and curves (Curves.k).

Numbering of the model is summarized in the table 2. For simple use of the model there are already several sets of parts prepared:

- PART SET ID 2 – ALL TIRES: for vehicle-road contact, tires only
- PART SET ID 6 – PARTS CONTACTING GROUND W/O TIRES: for vehicle-road contact, all vehicle parts except tires
- PART SET ID 10 – PARTS TO CRASH: for vehicle-barrier contact
- PART SET ID 11 – BEAM PARTS FOR CONTACTS: for vehicle-barrier, vehicle-road and vehicle single surface contacts, beam parts only

3.4 Geometry model

As mentioned before, the aim of this model is not to represent a specific vehicle but to create a generic N2A/N3D category vehicle (according to standard IWA 14). For this reason, it is important to include in the model only those features of the vehicle's construction that are independent of the brand and model and are present (in some form) in every vehicle of the specified categories. Another aspect that determines the decision of which vehicle parts should be included and which should be omitted is the requirement for solution speed while achieving sufficient calculation accuracy.

The vehicle model is designated for the design process of the barriers and will be used in simulations in which the barriers are the main subjects of interest. The vehicle model therefore includes only parts relevant for the global stiffness, mass distribution and global behaviour of the vehicle during the crash event. In these analyses, the vehicle model must produce a correct loading on the barrier. On the other hand, the crash effects on parts which only negligibly contribute to the overall behaviour of the vehicle like dashboard, seats, components of passive safety and so on are unimportant for these analyses and they can be omitted (only their mass is considered).

The geometry of the generic model was based on several vehicles of these categories of brands: Iveco, Man, Daf, Scania, Volvo and Renault (see fig. 2). Since the technical drawings and CAD data of contemporary vehicles are proprietary, the geometry for this model is based on reverse engineering (physical measurements of several complete or partially disassembled vehicles, photos, and product brochures [8-28]). Examples of photos from this process are attached in appendix A.

Ansys Spaceclaim was used for the geometry creation, editing and preprocessing. All the parts had to be prepared for meshing, which means eliminating components and features considered as insignificant.



Figure 2: Vehicle geometry: a) Renault Midlum 220.12, b) Man TGM 18.290 , c) Iveco Crusor 180C33, d) Generic model of vehicle

From a geometrical point of view the model consists of 2 basic components: a cabin and a chassis.

Cabin

For the generic vehicle model the cabin was chosen as daily (this type of cabin does not provide extra space for sleeping, bed nor extra storage). The dimensions of the generic cabin were chosen as the average based on studies of available online sources [8-28] and from direct measurements (see appendix A). The largest vehicles of N3D category are represented by MAN TGM 18.290 (blue in fig. 3 and 6), and the smallest permissible vehicles of N2A category are represented by Renault Midlum 220.12 (red in fig. 3 and 6). The schematic representation of the generic cabin's geometry is shown as green in figure 3. Main dimensions of generic geometry of cabin are depicted in figure 4. The final geometry of the generic cabin is shown in figure 5. The dimensions of the cabin are not parametrized, only the position of the cabin can be changed as a result of changes of other dimension parameters (frame-ground clearance).

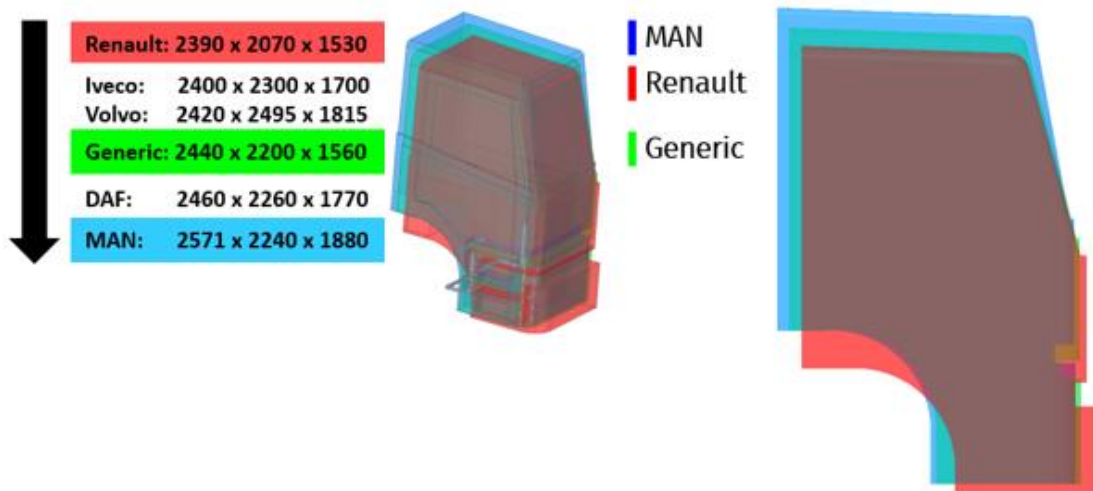


Figure 3: Generic geometry of cabin compared to chosen representatives

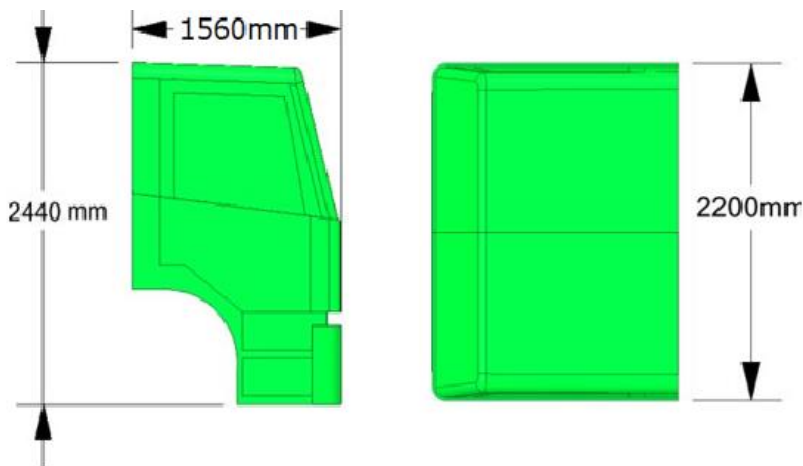


Figure 4: Basic dimensions of generic geometry of cabin

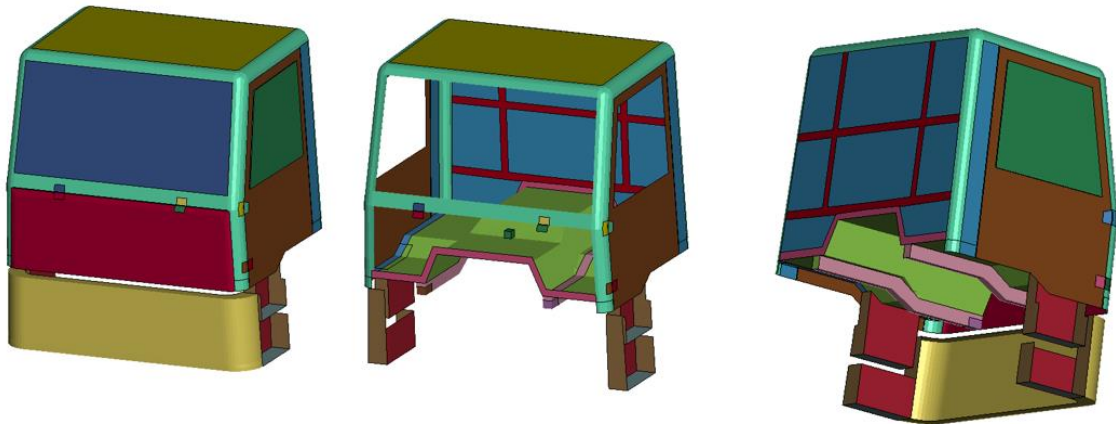


Figure 5: Geometry of generic cabin

Chassis

Firstly, default geometry of the rest of the vehicle components (frame, wheels, engine, etc.) was created as the average of the largest representative (MAN TGM 18.290) and the smallest representative (Renault Midlum 220.12). Secondly, in order to maximize generality of the model, this default geometry was updated based on the findings from manufacturers' brochures [8-28] and discussion with relevant experts. Simultaneously it was also decided which dimensions and positions should be parameterized.

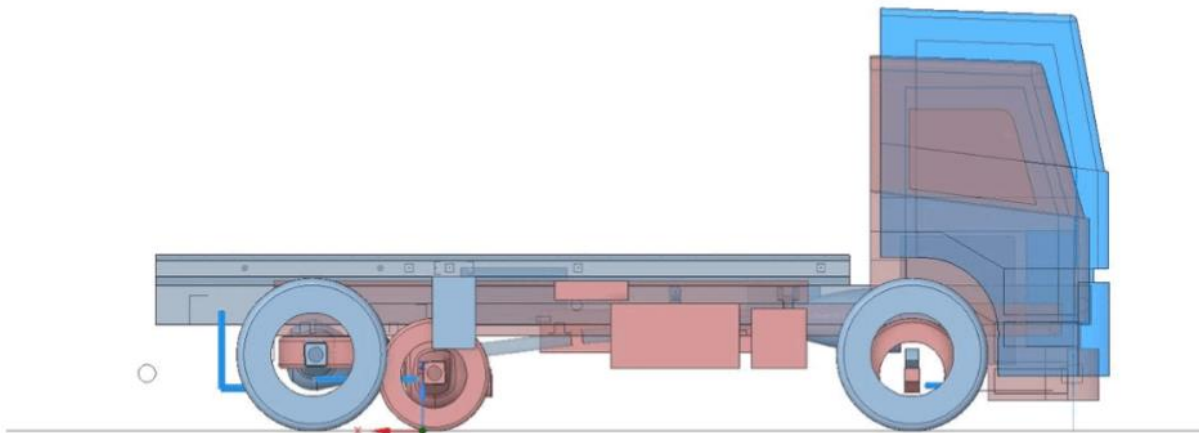


Figure 6: Vehicle of category N2A (red) and category N3D (blue)

3.5 FE mesh

The finite element mesh was created in Ansys LS-PrePost based on the default geometry of the vehicle presented in the previous chapter. The mesh consists of solid, shell and beam elements. However, with respect to the nature of most of the vehicle parts most of them are modelled with shell elements.

Engine, gearbox, front axle and rear axle with differential, wheels hubs and accelerometer in the cabin, are modelled with solid elements. Stabilizers of wheels, steering rods, various simplified connections, and holders of the generic boxes are modelled with beam elements. Beam elements are also used for additional reinforcements of cabin steps and front bumper (see figure 7).

The mesh was created with the focus on uniformity and shape regularity (see figure 8). The characteristic length of the elements is 14 - 47 mm. Warp²age² of elements was kept below 23 degrees. Quadrilateral linear elements are strongly preferred over triangular linear elements (quadrilateral elements have better accuracy). Detailed views of the FE mesh of the cabin and chassis are displayed in figure 9. The total counts of nodes and elements are in table 2.

Entity		Nodes	Solid elements	Shell elements	Beam elements	Discrete elements	Element mass
ID range	min	1	55 561	1	143 301	60 121	215 001
	max	420 007	420 000	409 609	407 189	214 003	215 006
Count		159 593	65 219	113 251	428	26	6

Tab. 2: Mesh statistics

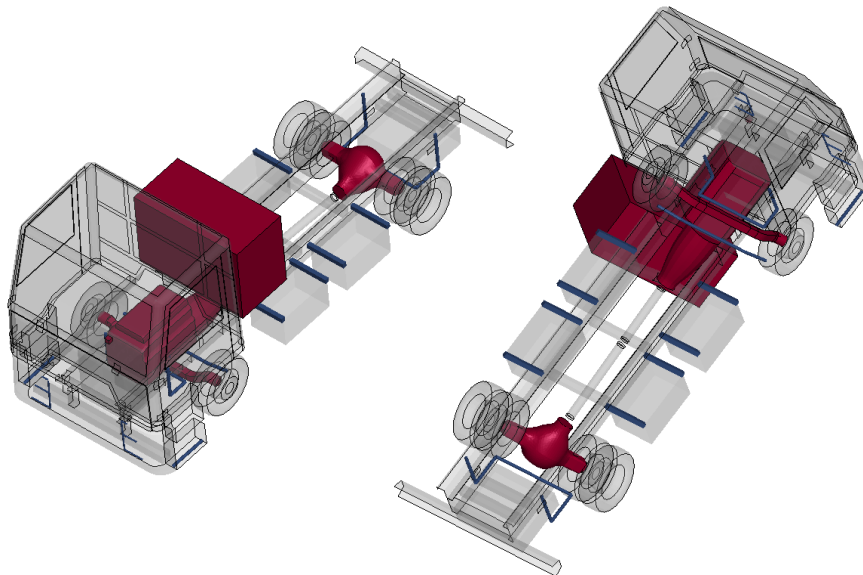


Figure 7: Element types on the vehicle model (solids – red; shells – transparent grey, beams – blue)

² Warp²age – angle between normals to two planes formed by splitting the quad element along diagonals. Warp²age reflects how much a quad element is not planar (planar quad has warp²age 0°).

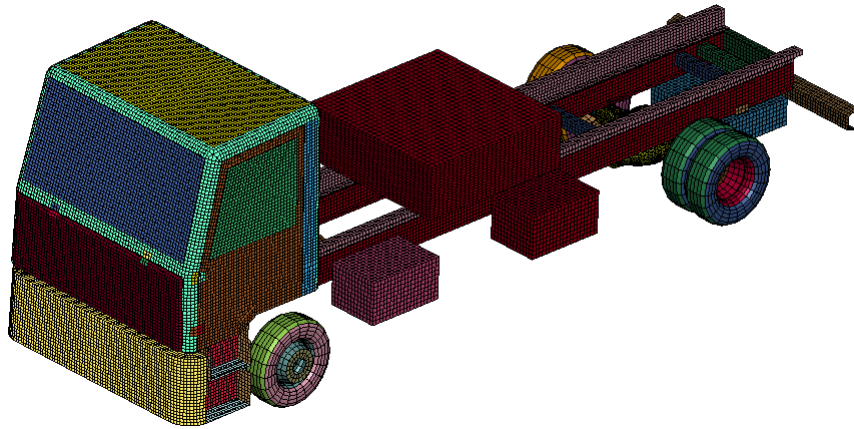


Figure 8: FE mesh of generic vehicle model

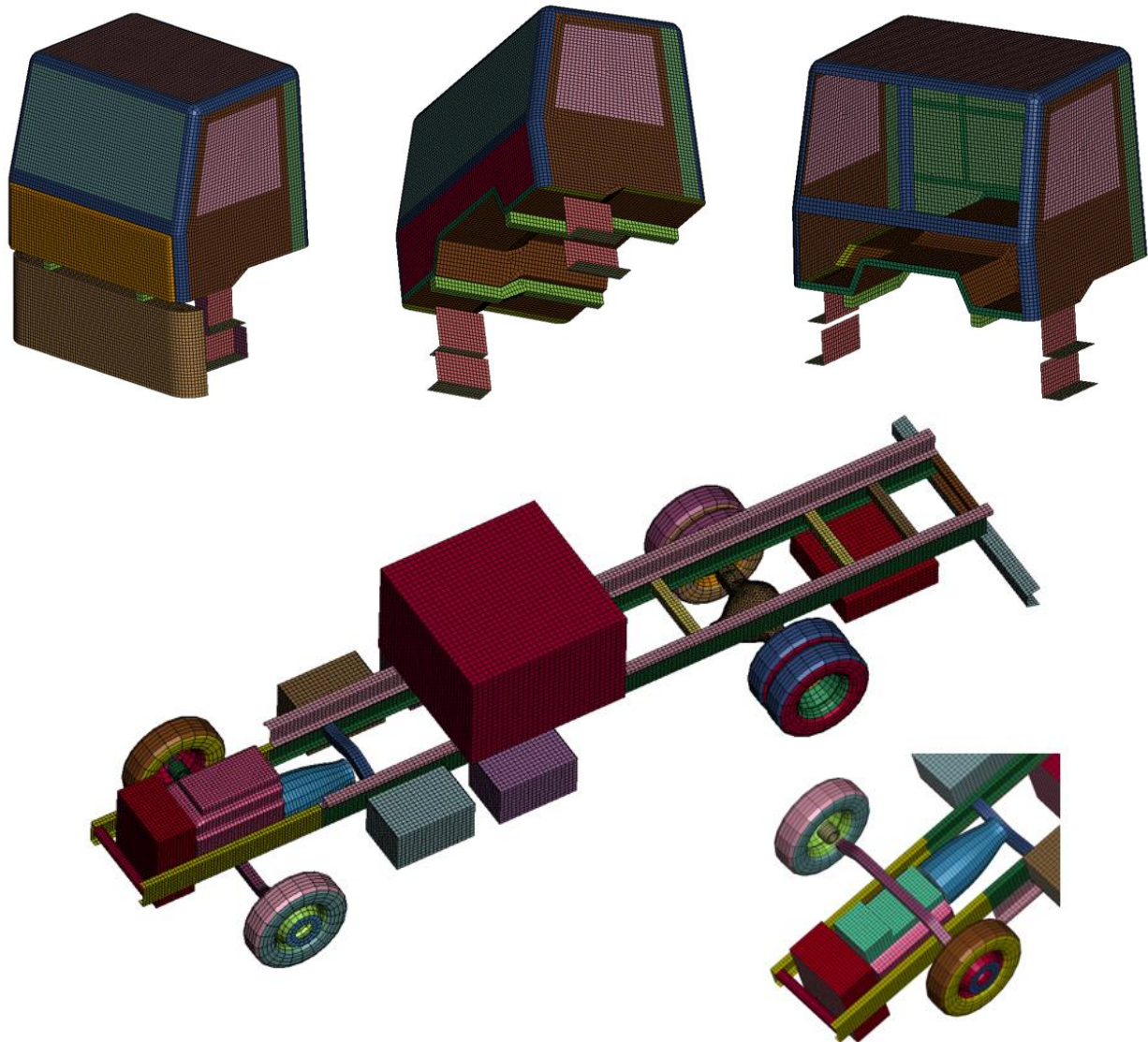


Figure 9: FE mesh of cabin and frame

3.6 Material models

There are only 5 basic constitutive laws used in the FE model in order to increase the convertibility of the model to other FE codes. These are:

- Rigid material model (*MAT_RIGID)
- Elastic material model (*MAT_ELASTIC)
- Bilinear elasto-plastic material model (*MAT_PIECEWISE_LINEAR_PLASTICITY)
- Piecewise linear elasto-plastic material model (*MAT_PIECEWISE_LINEAR_PLASTICITY)
- Crushable foam material model (*MAT_CRUSHABLE_FOAM)

Majority of parts in this vehicle model use material models with simple failure criterion based on equivalent plastic strain.

It must be noted that for the purposes of mass parametrization of the model, the density of particular material models can be altered to artificial higher or lower values. More details on this are provided in the chapter 3.11 Parameters/mass.

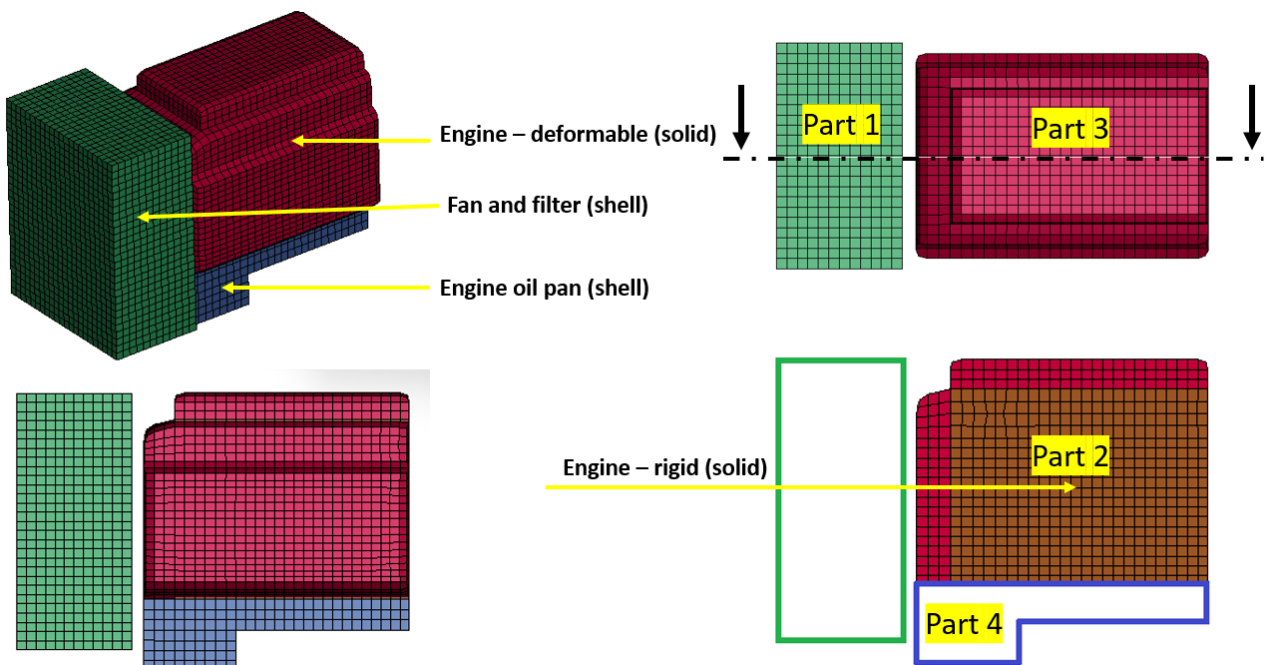


Figure 10: Main components of the engine compartment

Rigid material model is used for engine (inner part), gearbox, cargo, generic boxes, drive shaft, hubs, rear axle and accelerometer. Also “dummy” parts (usually single shell elements) helping with attachment of certain parts or allowing parametrized FE mesh transformation (e.g. attachment of wheels) are defined with rigid material model.

The engine consists of several parts (see fig. 10). The first part, which is modelled with shell elements, represents the stiffness of components such as filters, cooler, fan, etc. This part uses bilinear elasto-plastic material model with $E = 70 \text{ GPa}$, $\mu = 0.28$, $S_y = 0.1 \text{ GPa}$, $E_{\tan} = 0.01 \text{ GPa}$ and $\epsilon_{\text{fail}} = 0.5$.

During the vehicle testing it was found that rigid part (part 2, see fig. 10) “engine” may cause a significant contact force peak when the vehicle impacts to the barrier. To avoid this, there was an extra part (part 3) introduced which covers the rigid engine block and which is deformable (see fig. 10). The role of this part is to mimic deformable behaviour of the softer parts which are located in the surroundings of the engine

(plastic covers, hoses, tubes, valves, hoses, clamps etc). This part uses crushable material model with nonlinear bulk stiffness described with a curve (crushable foam material model).

The oil pan is modelled with shell elements and this part uses bilinear elasto-plastic material model with $E = 210 \text{ GPa}$, $\mu = 0.28$, $S_y = 0.3 \text{ GPa}$, $E_{tan} = 1.5 \text{ GPa}$ and $\epsilon_{fail} = 0.5$.

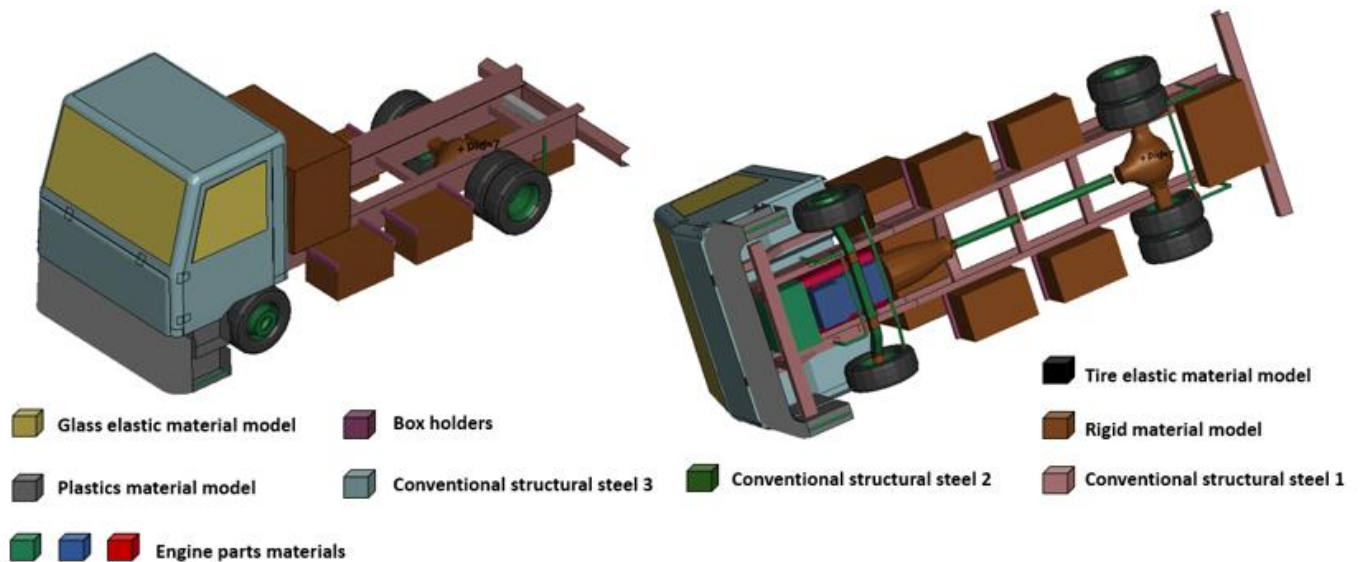


Figure 11: Material models

Majority of the parts are prescribed with conventional structural steel (see fig. 11). Conventional structural steel #1 [6] is defined as piecewise elasto-plastic material model with $E = 210 \text{ GPa}$, $\mu = 0.28$, $S_y = 0,6 \text{ GPa}$, $E_{tan} = 1.14 \text{ GPa}$ with failure $\epsilon_{fail} = 0.2-0,4$. Plasticity is governed by curve (see fig. 12).

Conventional structural steel #2 [6] is defined as piecewise elasto-plastic material model with $E = 207 \text{ GPa}$, $\mu = 0.28$, $S_y = 0.450 \text{ GPa}$. Plasticity is governed by curve (see fig. 13), $\epsilon_{fail} = 0.3$.

Conventional structural steel #3 [6] is defined as piecewise elasto-plastic material model with $E = 210 \text{ GPa}$, $\mu = 0.28$, $S_y = 0.350 \text{ GPa}$. Plasticity is governed by curve (see fig. 14), $\epsilon_{fail} = 0.3$.

Elastic material model is used for windows and tyres. For windows there is $E = 72 \text{ GPa}$ and $\mu = 0.22$. Elastic material model of tyres is prescribed with $E = 0.3 \text{ GPa}$ and $\mu = 0.45$ to match overall stiffness of composite structure of tyres modelled with single layer of shell elements (details in chapter *Model testing*).

Plastic parts (front bumper, cab step side, cab step back, cab step floor) are modelled with bilinear elasto-plastic material with $E = 40 \text{ GPa}$, $\mu = 0.30$, $S_y = 0.05 \text{ GPa}$ and $E_{tan} = 0.10 \text{ GPa}$, $\epsilon_{fail} = 0.1$.

Box holders are modelled with bilinear elasto-plastic material with $E = 210 \text{ GPa}$, $\mu = 0.30$, $S_y = 0.2 \text{ GPa}$.

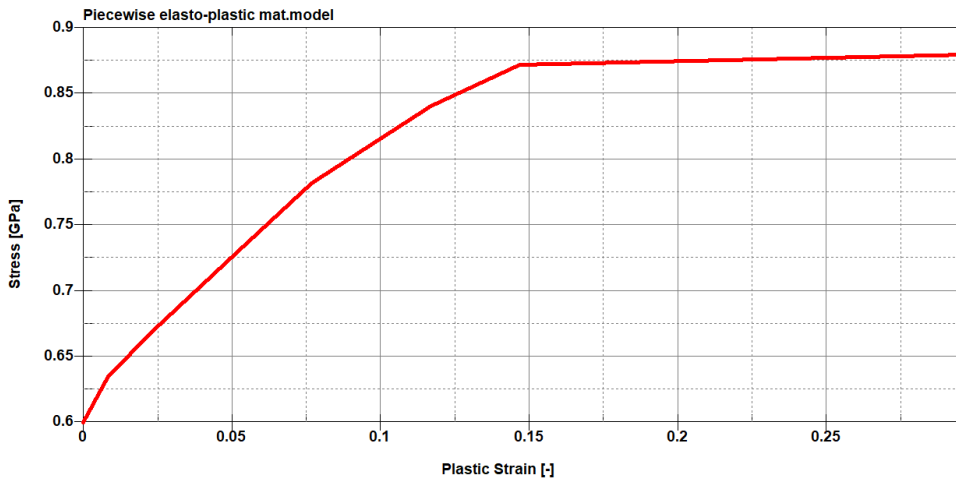


Figure 12: Conventional structural steel #1 plasticity curve

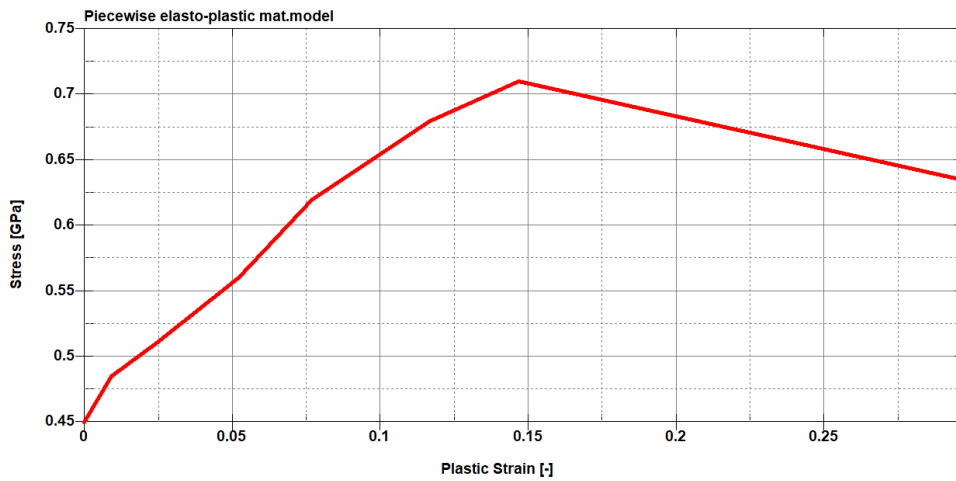


Figure 13: Conventional structural steel #2 plasticity curve

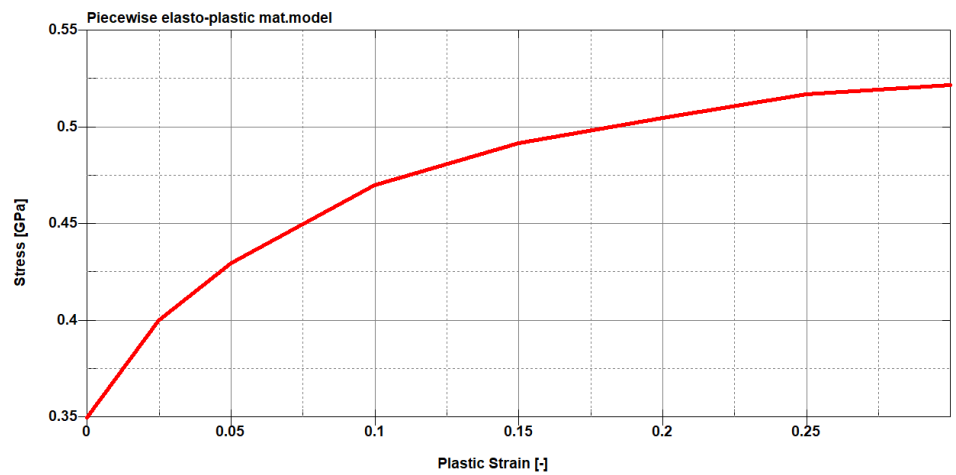


Figure 14: Conventional structural steel #3 plasticity curve

At the bollard crash validation case (chapter 4.5) it turned out that rigid connection frame – engine and frame – gearbox is not sufficient. For this reason, there were added four mounting points (2 sides, 2 at gearbox) with beam elements which represent the engine mounts and allow bilinear elasto-plastic behaviour and even failure criterion of the connection (see fig. 15). The material properties of these beams are: $E = 210 \text{ GPa}$, $\mu = 0.3$, $S_y = 0.2 \text{ GPa}$ and, $\epsilon_{\text{fail}} = 5$. This kind of simplified modelling of the engine mounts allows convenient control over the behaviour of this connection.

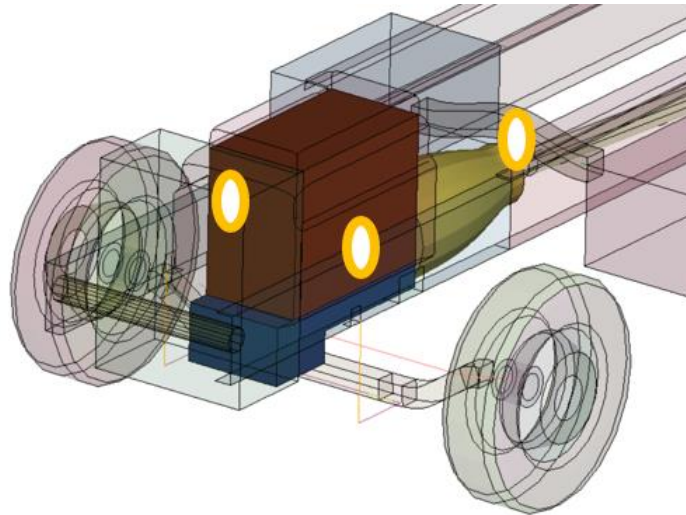


Figure 15: Engine – frame connection

Detailed definitions of all material models used in the vehicle model can be found in `\Vehicle\Shared\Material.k`.

3.7 Connections and constraints

Weld connections are modelled with rigid connections `*CONSTRAINED_SPOTWELD`, `*CONSTRAINED_NODAL_RIGID_BODY`, most of them without failure criterion (see fig. 16 and 17). Attachment of the longitudinal frame to the flatbed longerons and also attachment of the cab brackets to longitudinal frame is done with rigid connection `*CONSTRAINED_SPOTWELD` with no failure. Attachment of the windshield and cab windows is realised with rigid connection `*CONSTRAINED_SPOTWELD` with failure. Similarly, the attachments of the front and the gearbox crossmembers and bumper to the frame are also done with `*CONSTRAINED_SPOTWELD` with failure (figure 17).

In cases which include rigid bodies the connection is done with `*CONSTRAINED_EXTRA_NODES` keyword.

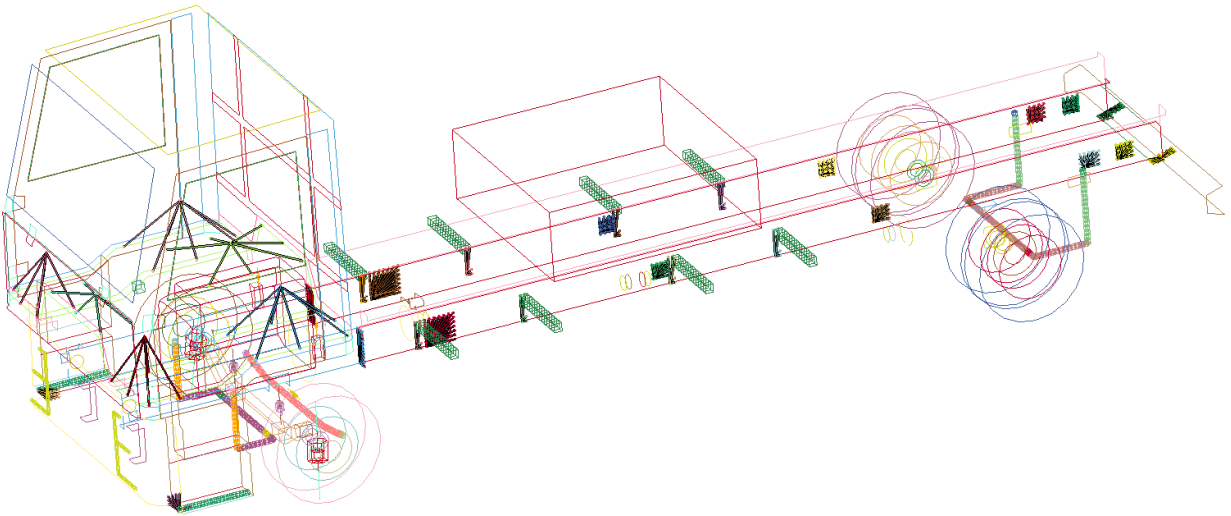


Figure 16: Nodal rigid bodies

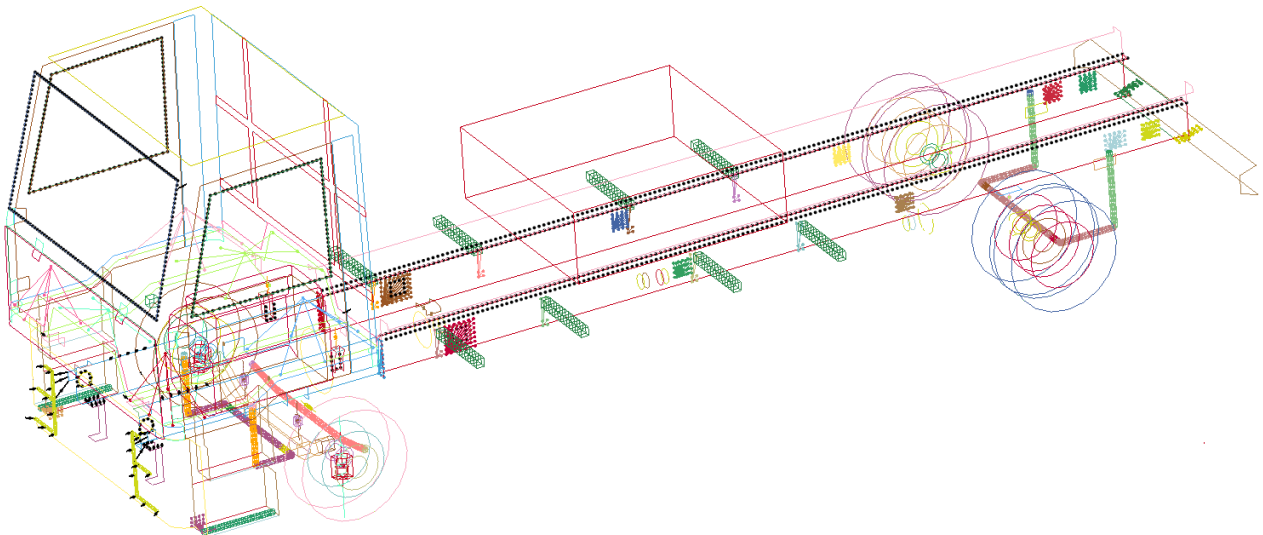


Figure 17: Spotwelds

Connection between the engine and the gearbox and between the differential and the rear wheels' hubs are also regarded as rigid (figure 18).

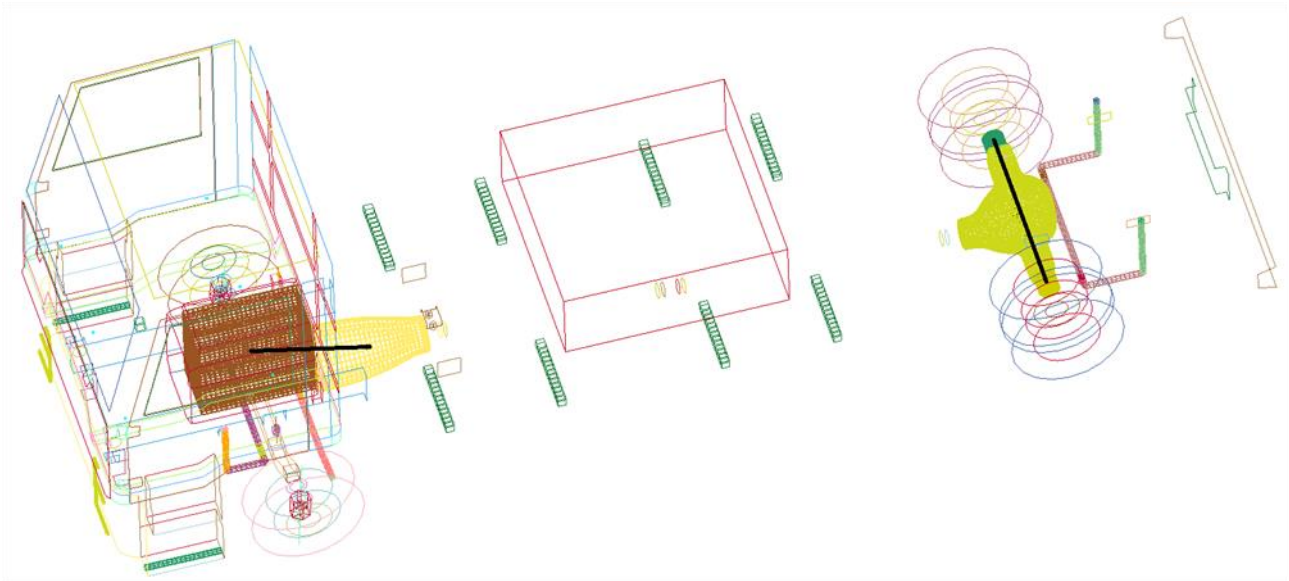


Figure 18: Rigid connections between engine and gearbox; rear axle and hubs of the rear wheels

Axles are attached to the frame with kinematic joints and spring and damper elements (see fig. 19 and 20). Detailed description of the spring and damper elements is in chapter *Parameters*. Up-down movement of the front axle is allowed due to the vertical translational joints. The movement of the front axle stabilizer is allowed through spherical joints. Spherical joints are also used to allow movement of the steering rod. Front wheels' turning is allowed due to the revolute joints. The positions of joints of the default vehicle complies with Ackermann principle (see fig. 20).

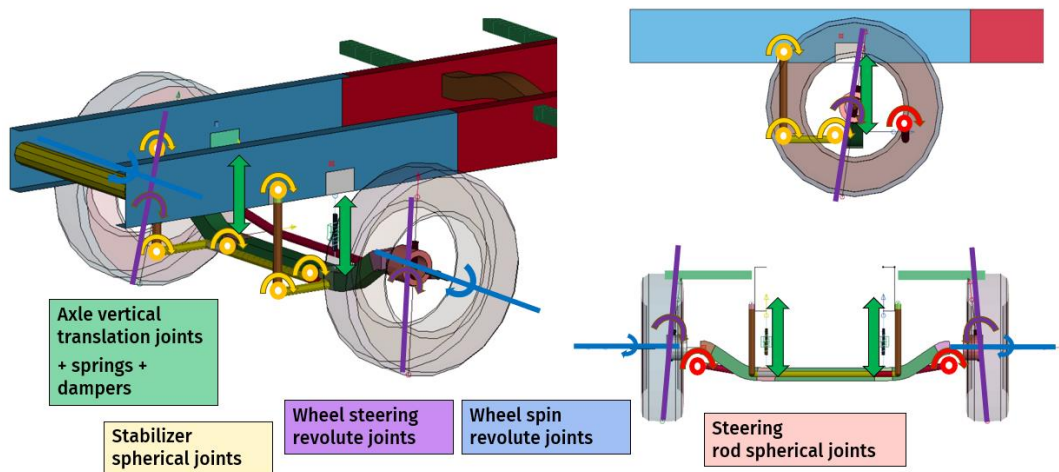


Figure 19: Kinematic joints of the front wheels

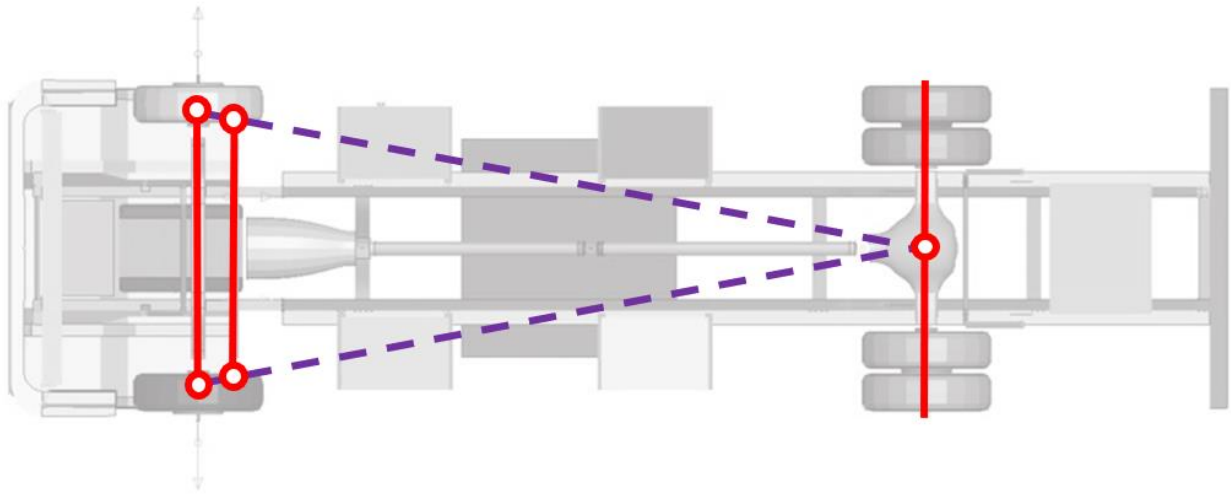


Figure 20: Ackermann steering principle

Up-down movement of the rear axle is allowed due to the vertical translational joints. The movement of the rear axle stabilizer is allowed due to spherical joints. Rotation of each rear wheel is also allowed due to revolute joints (see fig. 21).

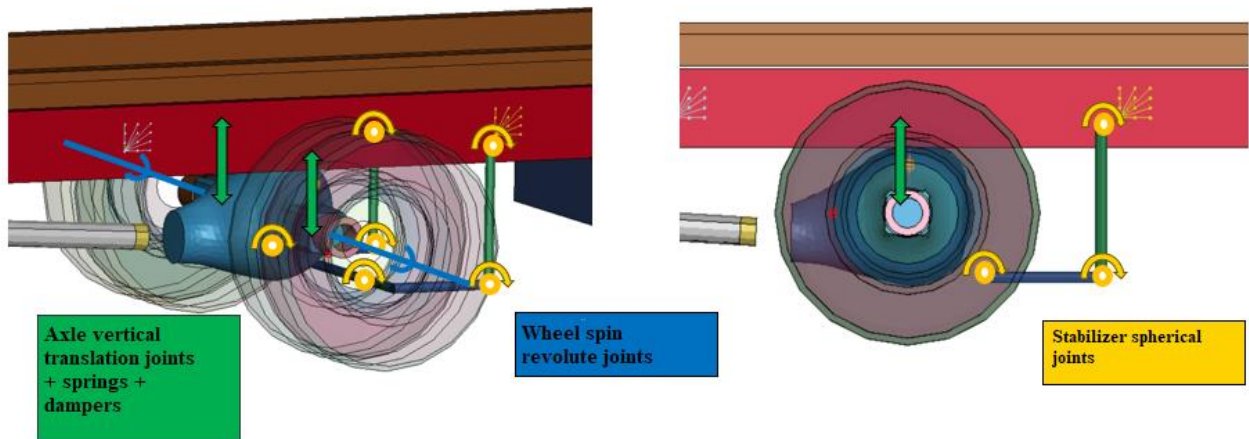


Figure 21: Kinematic joints of the rear wheels

3.8 Loading

Gravity

Gravity is prescribed on the model with the keyword `*LOAD_BODY_Z` which applies acceleration on all parts of the model. This keyword is present in the input file "Main.k".

Tyre Pressure

The tyres are loaded with a uniform internal pressure of 850 kPa for both the front wheels and the rear wheels.

3.9 Initial and boundary conditions

The vehicle model is given an initial velocity through the keyword "INITIAL_VELOCITY_GENERATION". This condition is applied to all parts of the vehicle except wheels to prescribe translational initial velocity. Two additional initial conditions are applied on the front and rear wheels to prescribe translational and angular initial velocities. The values of translational and angular initial velocities are derived from the parameter "VELKMH".

3.10 Contacts

Interaction between parts of the vehicle is prescribed with `*CONTACT_AUTOMATIC_SINGLE_SURFACE` and `*CONTACT_AUTOMATIC_NODES_TO_SURFACE`. Friction coefficient for these contacts is 0.3. Majority of parts are in these global contacts (see fig. 22).

Detailed properties of the contacts can be found in `\Vehicle\Shared>Contact.k`.

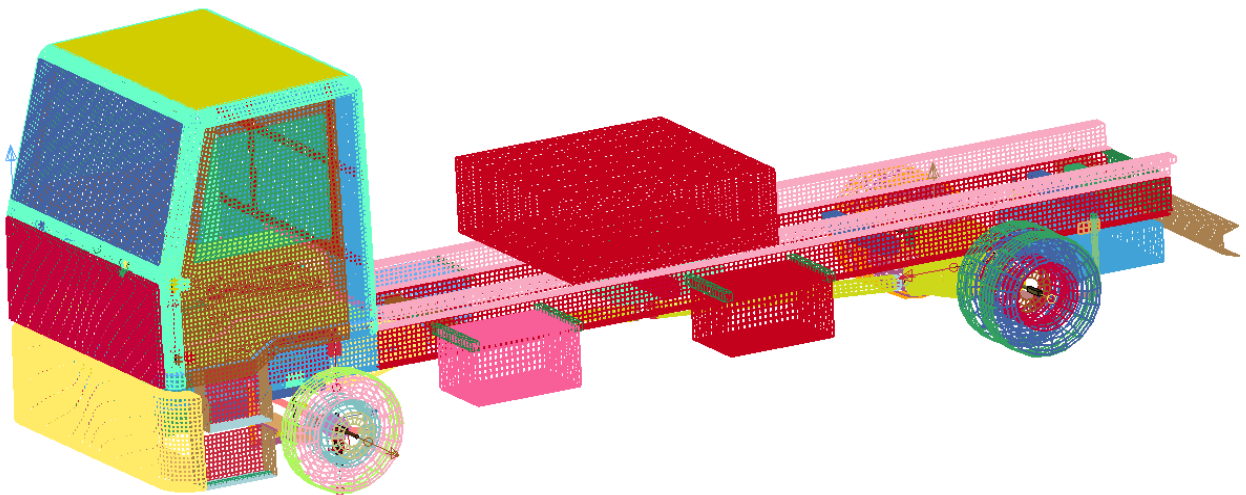


Figure 22: Global contacts of vehicle model

3.11 Parameters

Key input parameters are in a separate input file: “\Vehicle\Parameters.k”.

The parameters in this input file are divided into 6 groups (see fig. 23):

- Initial velocity
- Dimensions
- Mass
- Crash-related stiffness
- Turning
- Suspension

In the first section of this input file there are listed the main (basic) parameters (*PARAMETER). These parameters are meant to be changed by the user to easily modify the vehicle model. In the second section of the “Parameters.k” input file there are derived parameters. These are prescribed with an expression (*PARAMETER_EXPRESSION) and they are derived from the main parameters. The expressions of derived parameters are not meant to be changed by the user.

*PARAMETER	\$ DIMENSIONS	\$ Cargo X position mm	\$ CRASH-RELATED STIFFNESS	\$ SUSPENSION
\$ VELOCITY	\$ Vehicle length mm	\$ (375, 4390)	\$ Frame fitness	\$ [FRONT]
\$ Velocity km/h	\$ (6090, 10800)	R CRGXPOS 2000	\$ Relative value of frame fitness	\$
R VELKMH 48	R VEHL 8500	\$	\$ 1 = good shape;	\$ Stiffness of linear part of the spring
\$	\$ Wheelbase mm	\$ (-775, 775)	\$ 0 = bad shape	kn/mm
\$ MASS	\$ (3480, 6700)	R CRGYPOS 0	\$ (0, 1)	R FSPRING 0.12
\$ Cab additional mass kg	R WHBASE 5090	\$	R FRAMFIT 1.0	\$
RCABADMAS 300	\$	\$ Cargo length (X dir) mm	\$ Frame front crossmember	\$ Spring stopper upper bound mm
\$	\$ Wheel track mm	\$ (750, 8780)	spotwelds	R FSPUPB 70
\$ Cargo mass kg	R WHTRCK 1980	R CRGSIZ 1500	\$ Failure limit normal force kN	\$ Spring stopper lower bound mm
R CARGMASS 4790	\$	\$	R FRCMSN 100	R FSPLOB 80
\$	\$ Wheel outer diameter mm	\$ Cargo width (Y dir) mm	\$	\$
\$ Engine mass kg	\$ (752, 1075)	R CRGSIZ 1500	\$ Frame front crossmember	\$ Damper constant kN/(mm/ms)
R ENGMAS 750	R WHODIA 910	\$ (750, 1500)	spotwelds	R FDAMP 1.50
\$	\$ Frame - Ground clearance mm	R CRGZSIZ 1000	\$ Failure limit shear force kN	\$ [REAR]
\$ Gearbox mass kg	\$ (420, 1070)	\$	R FRCMSS 70	\$
R GBXMASS 106	R CGRCLR 720	\$ Frame profile thickness (C	\$ Frame front bumper bar spotwelds	\$ Stiffness of linear part of the spring
\$	\$	DIMENSION) mm	\$ Failure limit normal force kN	kn/mm
\$ Box 1 mass kg	\$ Bumper rear Z position mm	\$ (4, 8)	R FRBMPSN 60	R RSPRING 0.030
R BOX1MASS 300	\$ (350, 550)	R FCDIMO 0	\$	\$
\$	R RBMPZPOS 425	\$	\$ Frame front bumper bar spotwelds	\$ Spring stopper upper bound mm
\$ Box 2 mass kg	\$	\$ Frame profile height (A	\$ Failure limit shear force kN	R RSPUPB 100
R BOX2MASS 100	\$	DIMENSION) mm	R FRBMPS5 30	\$
\$	\$ TURNING	\$ (170, 270)	\$	\$ Spring stopper lower bound mm
\$ Box 3 mass kg	\$ Stiffness of linear part of the	R FADIMO 0	\$ Cab frame attachment rear springs	R RSPLOB 100
R BOX3MASS 100	torsion spring kN*mm/rad	\$	\$ Failure limit effective plastic strain	\$
\$	\$ FTSPRING 1000	\$	R CABATEPS 0.500	\$ Damper constant kN/(mm/ms)
\$	\$	\$	\$	R RDAMP 7.00
\$ Box 4 mass kg	\$ Damper constant	\$	\$	\$
R BOX4MASS 30	kN*mm/(rad/ms)	\$	\$	\$
\$	R FTDAMP 8e5	\$	\$	\$
\$	\$	\$	\$	\$
\$ Box 5 mass kg	\$ Spring turn bound rad	\$	\$	\$
R BOX5MASS 50	R FSPTB 0.2	\$	\$	\$
\$	\$	\$	\$	\$

Figure 23: Input of main parameters

Main parameters are always accompanied with comments describing the meaning of the parameter, recommended range and its unit. There are default vales of main parameters already pre-set. The default values were used throughout the initial model testing (see chapter 4).

Allowed range of initial velocity is not stated as the applicability of the model with respect to various velocities has not been tested yet. So far the applicability can be assumed only based on the initial model testing (velocities 16 km/h, 48 km/h and 100 km/h). Allowed ranges of mass, crash related stiffness, suspension and turning parameters are not stated either as this would require comprehensive statistical analysis of mass distribution of vehicles of N2A and N3D categories which is beyond the extend of this project. Allowed ranges of dimension parameters are corresponding to limit values prescribed by standard IWA 14. Allowed ranges of wheelbase, wheel outer diameter and frame profile dimensions are based on all data

collected during this project (reverse engineering, product brochures [8-28]). Allowed ranges of the rest of dimension parameters are defined in order not to exceed model limits or its reasonable proportions.

Default values of the parameters are matching average values of the ranges given by the standard (see tab. 1). Default values of suspension, turning and crash-related stiffness were obtained with calibration at the test cases described in chapter 4. The rest of the default values are chosen as average values of properties observed on the set of real vehicles which were analysed during this project (reverse engineering, product brochures [8-28]).

Note that for users' convenience some of the parameters are in different units than the unit system of the model (e.g. Velocity km/h).

Derived parameters are helping to set up the model and to achieve desired model variations. Note that due to the wide potential of model variations some of the input parameters cannot guarantee absolute agreement with final values (for example mass values can be slightly inaccurate because of the dimension parameters, connections, and shared nodes).

1) Initial velocity:

Initial velocity is prescribed with main parameter VELKMH (km/h). This main parameter is then used for calculation of derived parameters: translational initial velocity TRVEL (mm/ms) and angular initial velocity ANGVEL (rad/ms). These derived parameters are the input for *INITIAL_VELOCITY_GENERATION keywords which are located in "Vehicle_Main.k" input file.

2) Dimensions:

Variations of dimensions can be set by the user through main parameters from group "DIMENSIONS" (see fig. 23). Based on the main parameters and dimensions of original mesh a set of derived parameters (translational shifts and directional scaling of mesh) is calculated. These derived parameters are then applied on the model through *INCLUDE_TRANSFORM and *DEFINE_TRANSFORM keywords.

Note that with these parameters also the centre of gravity and inertia of the vehicle can be changed. Figure 24 shows the main parameterized dimensions.

Due to the wide potential range of model variations, it is not guaranteed that all the combinations of input variables would provide reasonable model setup. The user must consider prescribed dimensions with respect to the rest of the model in order to prevent absurd setups.



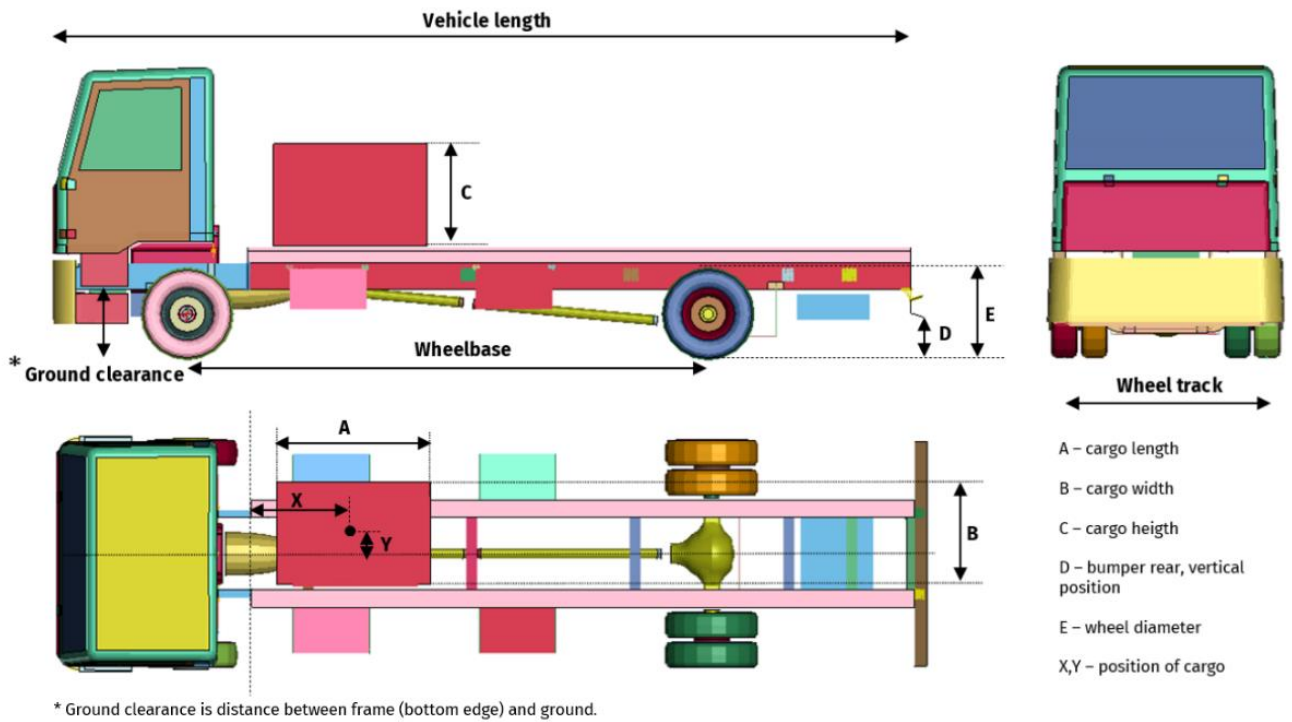


Figure 24: Main parameters of dimensions

Basic dimensions

User can change vehicle length, wheelbase, wheel track, wheel outer diameter, chassis ground clearance, and height of the rear bumper. Size and cargo position can be changed with parameters as well. Examples of dimensional variations can be seen in figure 25.

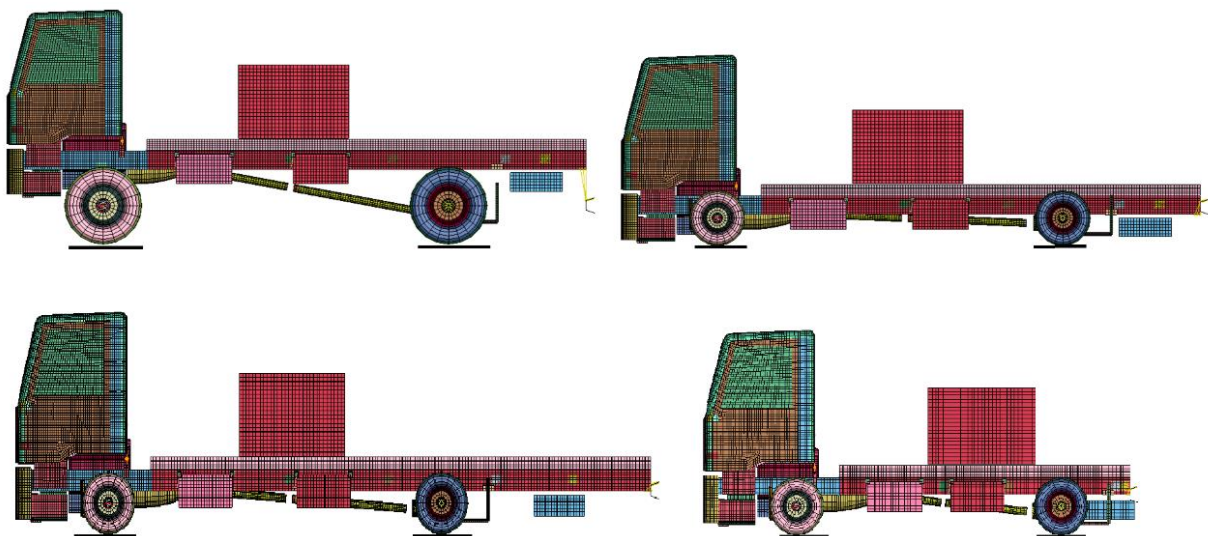


Figure 25: Examples of variations of dimensions

Frame cross section

The user can also change the dimensions (A – height and C – thickness) of the cross section of the main frame (see fig. 26).

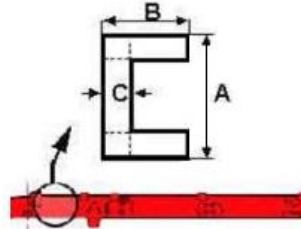


Figure 26: Frame cross section [11]

The user can define A dimension and C dimension of the frame cross section directly or these values can be set automatically. Since there was certain dependency between the wheelbase and the frame dimensions observed, the frame dimensions can be automatically calculated based on this knowledge (see fig. 27 and 28).

If FCDIMO = 0 (C dimension) in the input file “Parameters.k”, then the value is set based on a function, which represents dependency of C dimensions of real N2A and N3D vehicles on their wheelbases (see fig. 27). Otherwise (when FCDIMO ≠ 0) FCDIMO value is taken directly. Range of the values is (4, 8) mm (vehicle manufacturer’s brochure [11]).

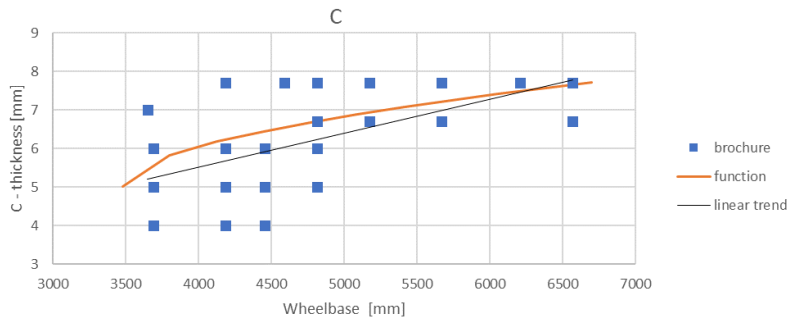


Figure 27: Dependency of the frame thickness on the wheelbase (based on vehicle manufacturer’s brochure [11])

Similarly, if FADIMO = 0 (A dimension) in the input file “Parameters.k” then the value is set based on a function, which represents dependency of A dimensions of real N2A and N3D vehicles on their wheelbases. Otherwise (when FADIMO ≠ 0) FADIMO value is taken directly. Range of the values is (170, 270) mm. Dependency of the frame height on the wheelbase is depicted in figure 28.

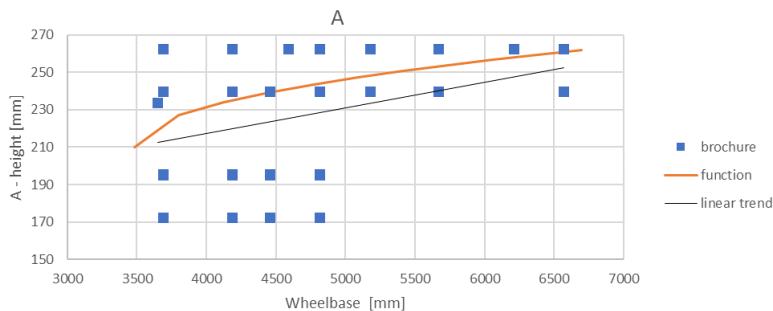


Figure 28: Dependency of the frame height on the wheelbase (based on vehicle manufacturer’s brochure [11])

Dependency of flange of the frame cross section on the wheelbase is depicted in the following graph (see fig. 29).

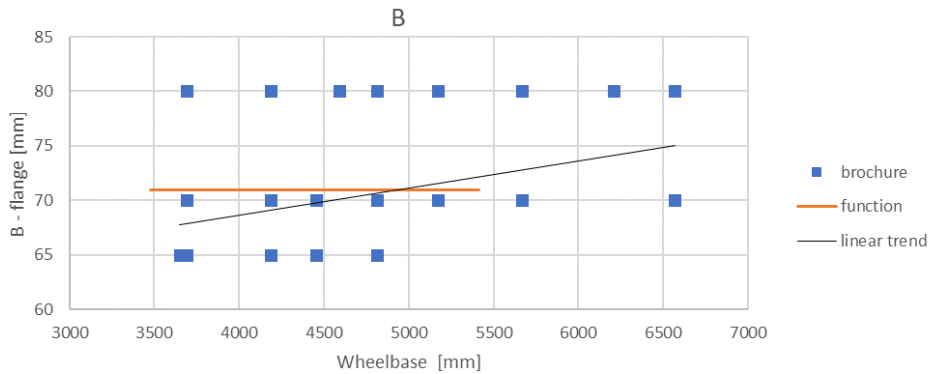


Figure 29: Dependency of the frame flange on the wheelbase (based on vehicle manufacturer's brochure [11])

The graphs show that trends of trends of all dimensions (A, B, C) of the frame cross section increase with increasing wheelbase. In contrary to A and C dimensions which are parametrized (and their values can be easily changed or calculated automatically), the B dimension (frame flange) is fixed to 71 mm since the variations of this parameter are not expected to play significant role in the crash events.

Cross-members

Number, geometry, and positioning of the frame crossmembers are based on observed frame designs of real vehicles in the analysed categories. The frame of the model is reinforced with 7 crossmembers (see fig. 30). Five crossmembers (position 2 – 6) have the same default square profile (100 x 100 mm). The first crossmember (position 1) has circular profile with diameter 100 mm.

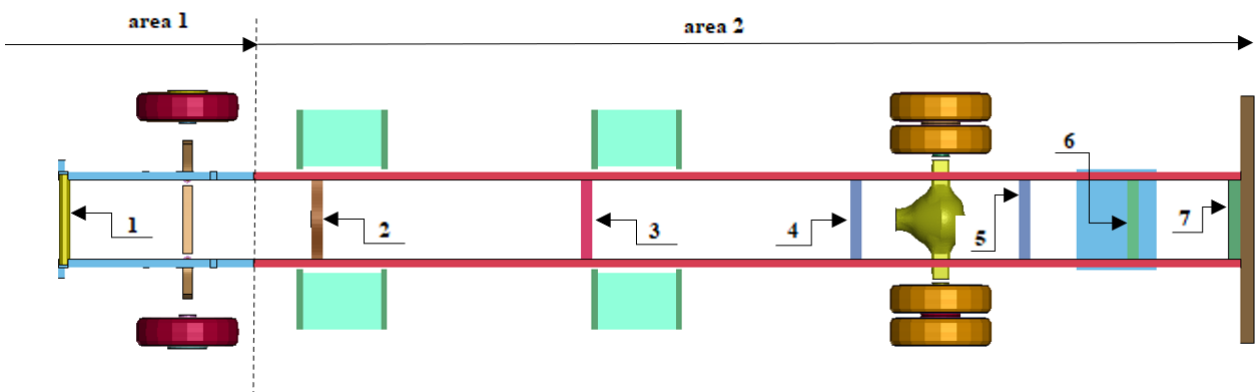


Figure 30: Position of the crossmembers

Computational model is divided to two areas (see fig. 30). The first area basically stays fixed and no modifications of positions of parts in this area in longitudinal direction can be done with the main dimension parameters.

Generic boxes

In the second area, there are five boxes attached to the frame (see fig. 31). The boxes are generic representations of items which are commonly attached to the frame at these positions and cannot be omitted since they affect the overall mass distribution of the vehicle. These items typically include fuel tank, spare wheel, storage boxes, etc. Unfortunately, exact positions of these items on the vehicles cannot be generalized (for example fuel tank can be on front right side, front left side or there can be even more of them). In order to deal with this wide variability of positions, number and types of these items they are modelled as simple rigid boxes with parametrized masses. This approach allows the user to easily set different masses to individual generic boxes and to model various mass distributions this way.

The longitudinal positions of boxes number 1 and 2 remain unchanged. The front face of the boxes is always 1 m from the centre of the front axle. The longitudinal positions of other additional boxes (3-5) vary depending on the dimensions of the vehicle. A diagram with the positions of the crossmembers and generic boxes with respect to the axles is shown in (see fig. 31).

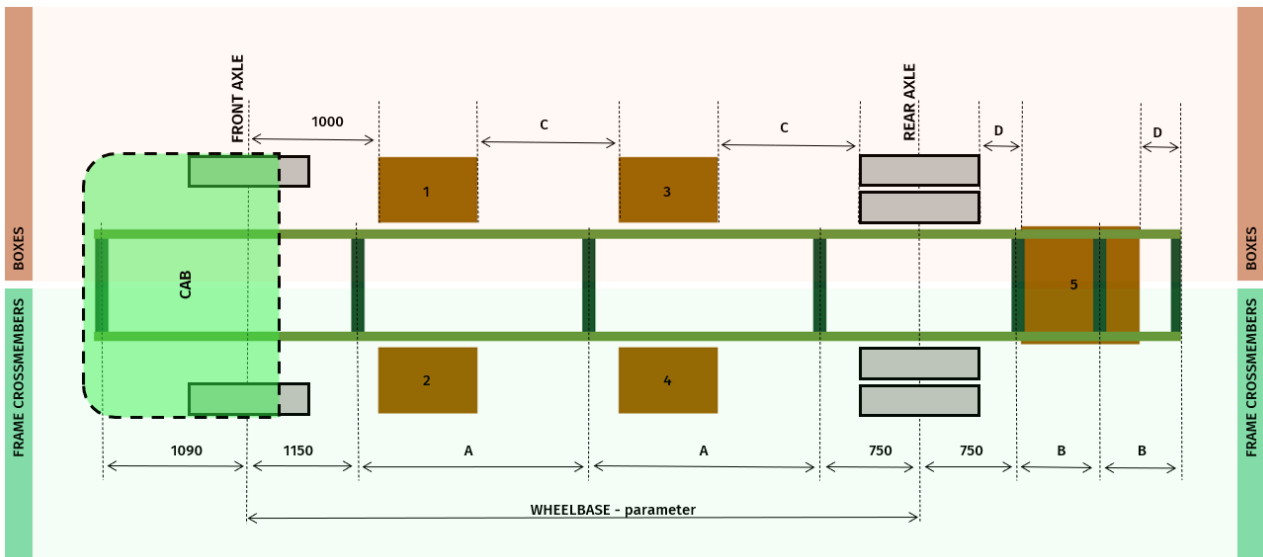


Figure 31: Positions of crossmembers and generic boxes

Tyres

The tyres' dimensions are also very variable within the N2A and N3D categories. The most frequently used tyre types for both vehicle categories are summarized in tab. 3 [11]. It is presumed that the outer diameter has the greatest effect on the global vehicle behaviour during a crash event. For this reason there is only this single parameter (WHODIA) prepared in the input file "Parameters.k" for simple changes of wheel dimensions. Then the default wheel geometry is automatically scaled up/down in radial direction in order to match this parameter.

Tyre size	A [mm]	B [mm]	C [mm]	D [mm] outer diameter	
205/75 R17,5	205	153,75	444,5	752	D 100% D 143%
245/70 R17,5	245	171,5	444,5	787,5	
305/70 R19,5	305	213,5	495,3	922,3	
295/80 R22,5	295	236	571,5	1043,5	
315/80 R22,5	315	252	571,5	1075,5	

Tab. 3: Tyre types for categories N2A and N3D [11]

Ground clearance

The user can also modify the ground clearance of the vehicle using the parameter CGRCLR. This dimension stands for a distance between the bottom of the frame and the ground. The ground clearance is adjustable within the range 425 – 1070 mm. Additionally, the height of the rear bumper can be changed using the parameter RBMPZPOS. The height of the rear bumper from the ground can be set within the range of 350-550 mm.

Cargo

Position and size of the cargo can be easily modified with parameters as well. The position of the cargo centre on the vehicle flatbed is specified with local (flatbed related) coordinates in the X (longitudinal) and Y (lateral) directions (see fig. 24) (CRGXPOS and CRGYPOS). The main dimensions of the cargo (length, width, height) can be changed by the user using the parameters CRGXSIZ, CRGYSIZ and CRGZSIZ. Again, the recommended ranges (min, max) for each parameter are provided in the input file. The user must consider both the position and the dimensions of the cargo with respect to the chosen vehicle size in order to prevent absurd setups. Examples of possible cargo setups are depicted in figure 32.

It must be also noted that the cargo is modelled as rigid since its stiffness properties cannot be generalised. For this reason, using too big cargos (also majority of the examples in fig. 32) can lead to over stiffening of the vehicle model.

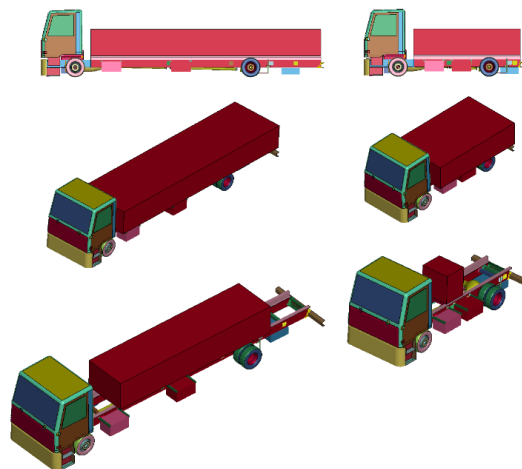


Figure 32: Example of possible dimensions and positions of cargo

3) Mass:

Mass distribution can be changed through main parameters from group “MASS” (see fig. 23). With these parameters, the user defines masses of some of the vehicle parts: engine, gearbox, cab additional mass, cargo and five generic boxes. These main parameters are then transformed to derived density parameters. Density values are then referenced by material models. In case of the cabin, its mass can be adjusted by six additional point masses inside the cabin. These additional masses represent the mass of seats, dashboard, and other components.

Figure 33 shows which parts are related to which mass parameter. Naturally, the overall mass distribution of the vehicle is influenced by these parameters. The density of the rest of the parts is fixed and is not meant for mass distribution adjustment.

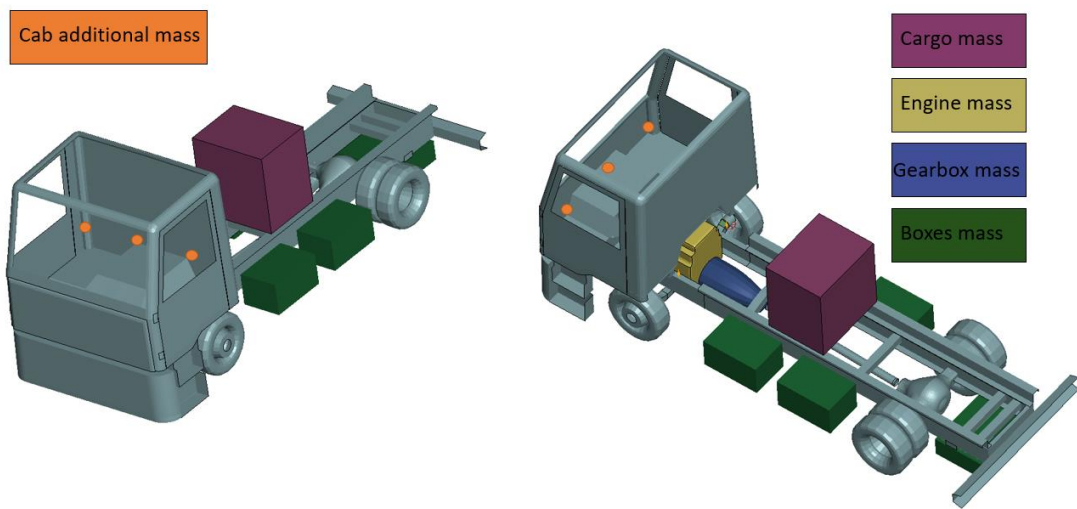


Figure 33: Sets for different mass parameters

For the final check of total mass and mass distribution at the initial time, the user shall read summary of mass in d3hsp file. D3hsp is a key output file of LS-DYNA run. It contains a section "summary of mass" which includes exact final values at the initial time of all parts of the model (even after redistribution due to the constraints and connections).

4) Crash-related stiffness:

The user can modify crash-related stiffness parameters through the main parameters in the "CRASH-RELATED STIFFNESS" group (see fig. 23). These parameters relate to those parts of the vehicle model which significantly influence energy absorption and global behaviour of the vehicle during a crash event. By adjusting these parameters, the user can adapt the crash-related stiffness based on factors as the vehicles age, fitness, or the construction of the front parts of the vehicle.

The user can set the fitness value of the vehicle frame with the parameter FRAMFIT. The value of this parameter ranges from 0 to 1, where FRAMFIT = 1 represents good condition and FRAMFIT=0 represents poor condition (wear, corrosion, etc.) of the frame. The material properties of the frame are then automatically adjusted accordingly. The dependency of the stiffness and the yield stress of the material is based on the findings of the study [7] which was focused on the impact of corrosion on mechanical properties of steel. The dependency between the yield stress and the loss of diameter in this study (see fig. 34) was used to derive functions representing the reduction of the yield stress relative to the decreasing level of fitness (loss of diameter) (see fig. 36). Derived reduction of the elastic stiffness corresponds to the loss of the cross section area as well (see fig. 35). In the vehicle model the maximum fitness (FRAMFIT = 1) of the material corresponds to 100% stiffness (0% diameter loss) and 100% yield stress. On the other hand, minimum fitness (FRAMFIT = 0) corresponds to 56% stiffness (25% diameter loss) and 55% yield stress.

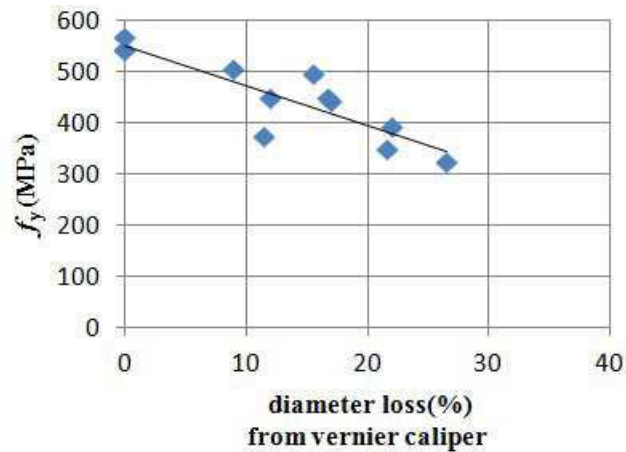


Figure 34: Dependency between the yield stress and the loss of diameter [7]

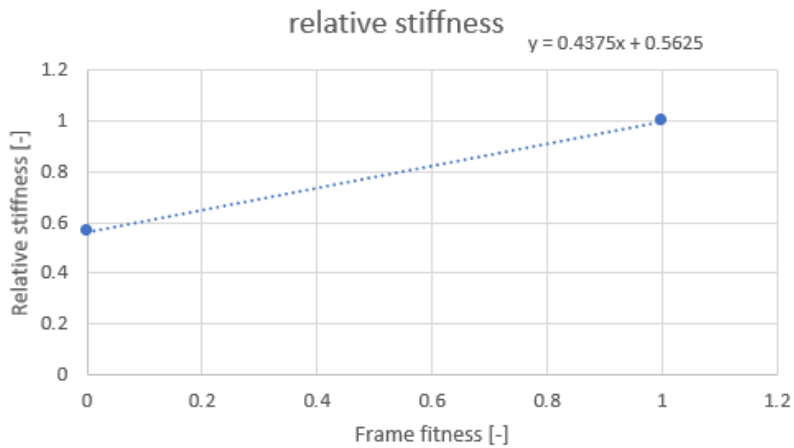


Figure 35: Dependency between the relative stiffness and the frame fitness parameter

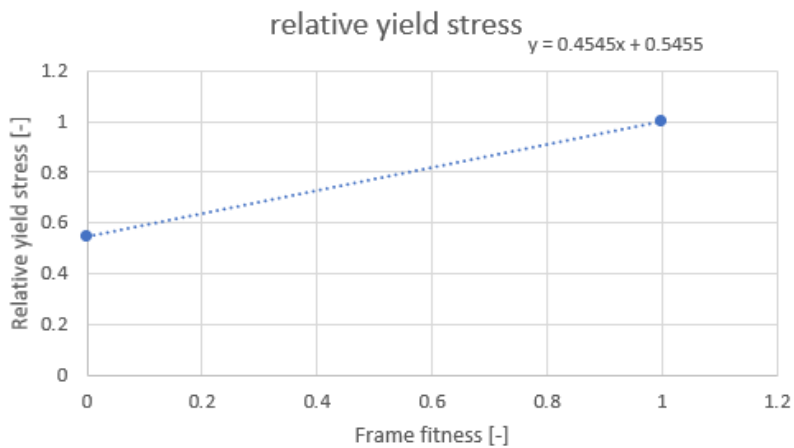


Figure 36: Dependency between the relative yield stress and the frame fitness parameter

The other main parameters affecting the overall vehicle crash-related stiffness are failure limits (normal force - *SN, shear force - *SS, strain - *EPS) of critical connections at the front of the vehicle. The user can easily vary strength of these connections:

- frame longitudinal beams to front crossmember: parameters FRCMSN, FRCMSS
- frame longitudinal beams to gearbox crossmember: parameters FRCMSN, FRCMSS
- front bumper bar attachment to the frame: parameters FRBMPSN, FRBMPSS
- Cab suspension: parameter CABATEPS

5) Suspension and turning:

The user can vary stiffness of linear spring, travel distance (lower and upper bound) and damping coefficient of linear damper separately for front and rear wheels. Both left and right front wheels use the same suspension parameters. Similarly, both left and right rear wheels use the same suspension parameters. Moreover, stiffness and damping of turning of front wheels can be also changed with parameters. Variations of these main parameters can reflect various designs of suspension or fitness/age of the components.

The default values of suspension and turning parameters are based on the testing procedure described in the standard CEN/TR 16303 (see chapter “4”). This testing was performed with the default model dimensions and mass distribution. Please note that in case of significant changes of dimensions and/or mass distribution the default suspension parameters may not be appropriate.

Nonlinear stiffness of suspension consists of 3 springs (see fig. 37) and one damper for each wheel:

- I. Linear spring
- II. Upper bound
- III. Lower bound
- IV. Linear damper

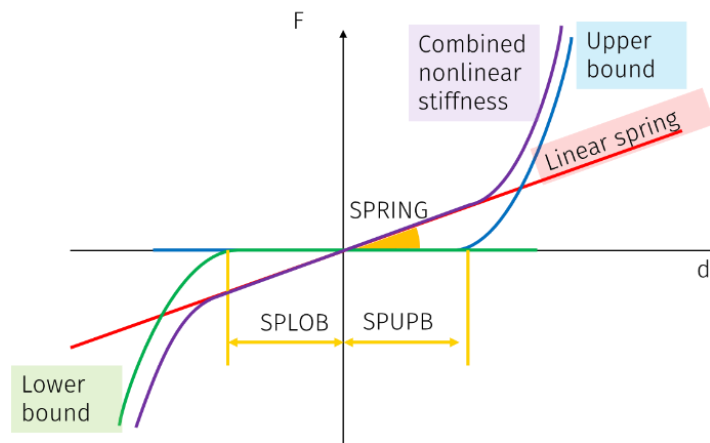


Figure 37: Nonlinear stiffness of suspension

4 Model testing

The first series of model testing was performed by SVS FEM s.r.o. The testing was based on the procedure described by CEN/TR 16303. Since it is not possible to test all of the variations of the parametric vehicle model in all test scenarios, it was tested with the default and experiment-related values only.

4.1 Vehicle in idle

4.1.1 Objective

The model must remain stable in idle for a time, which should correspond to the time needed for the simulations of the crash test. For these purposes the vehicle FE model must stay in idle for 1.5 sec (see fig. 38). There is no initial velocity prescribed to the vehicle model. The only load is gravity acceleration. There is no barrier nor obstacle in front of the vehicle model in this test. The aim of this test is to prove robustness and stability of the model. The behaviour of the model is observed with focus on displacements, stresses, energy balance and contact interfaces. Measurement points were set on the vehicle for evaluation of the vehicle movement (see fig. 39).

4.1.2 Results

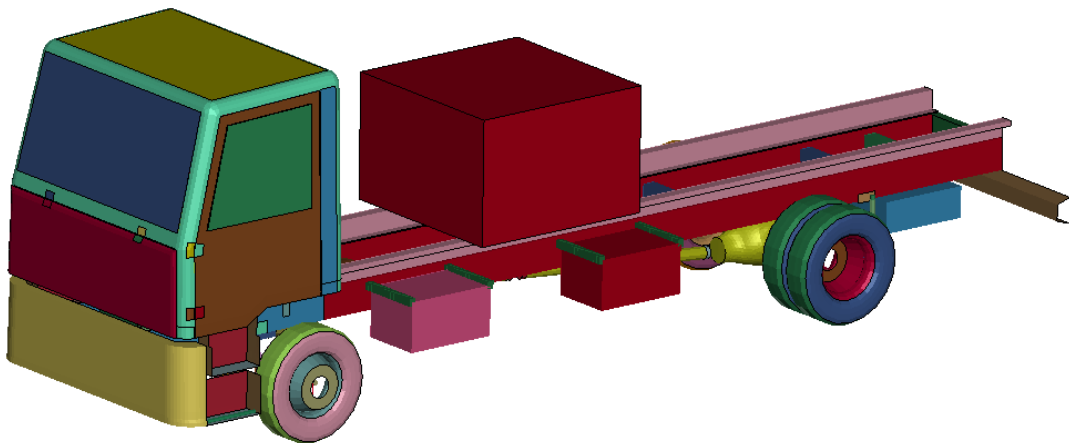


Figure 38: Vehicle in idle after 1.5 sec

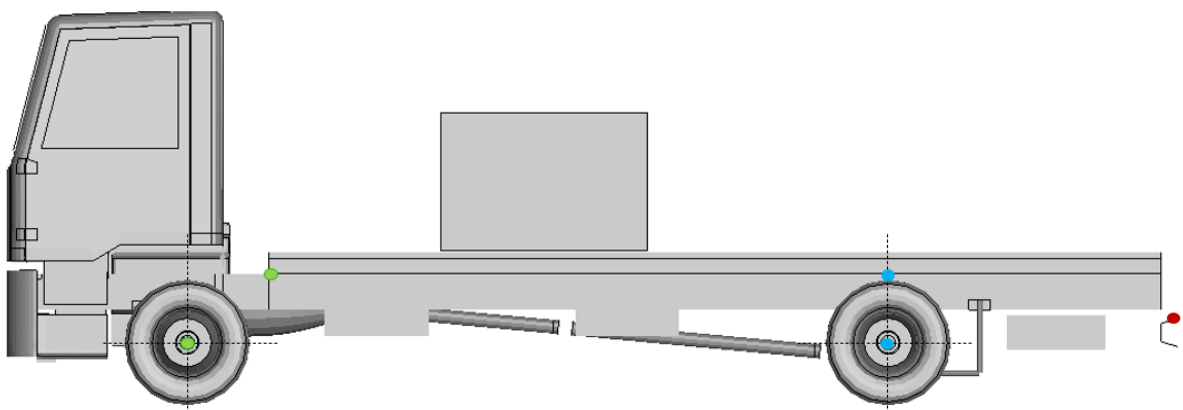


Figure 39: Measurement points on the vehicle

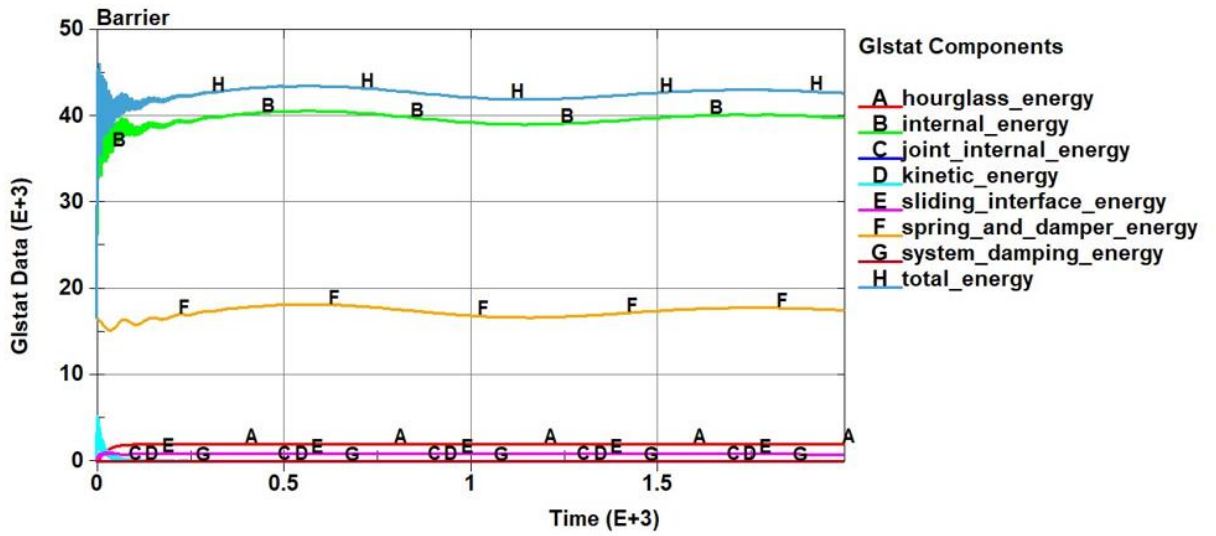


Figure 40: Energy balance

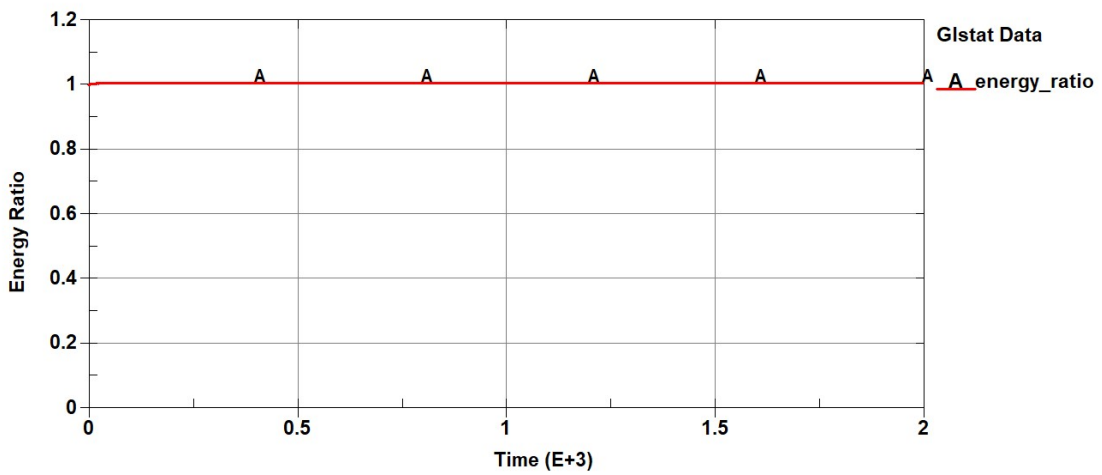


Figure 41: Energy ratio

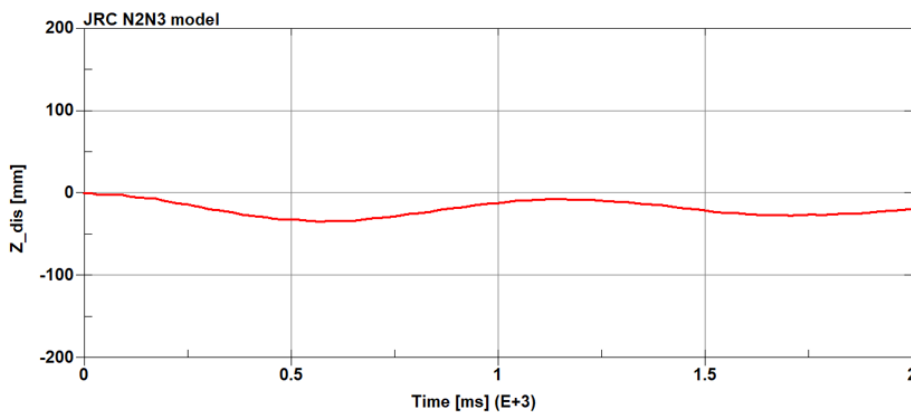


Figure 42: Displacement of the flatbed lead edge (vertical - Z direction)

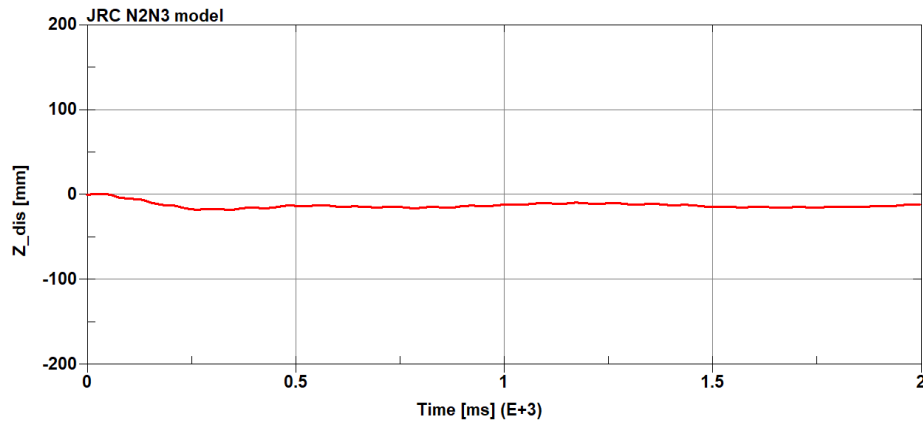


Figure 43: Displacement of the flatbed above rear wheel (vertical – Z direction)

No abnormal deformation nor stresses were observed on the model. Energy balance and energy ratio correspond to vehicle staying in idle. The maximum displacements of the measurement points on the flatbed are about 20 – 30 mm in the vertical direction.

4.1.3 Conclusion

The FE model proved its computational stability, steering stability, and suspension stability, while staying in idle for more than 1.5 sec. The maximum displacements at the monitored points were about 20 – 30 mm in the vertical direction. The mentioned displacements at monitored points were caused by the settling down of the suspension.

4.2 Linear track

4.2.1 Objective

The vehicle FE model is given an initial velocity of 100 km/h and its subsequent motion is observed for another 1.5 sec. The vehicle travels over 40 m during this time period.

4.2.2 Results



Figure 44: Fe model in linear motion (0, 500, 1000, 1500 ms)

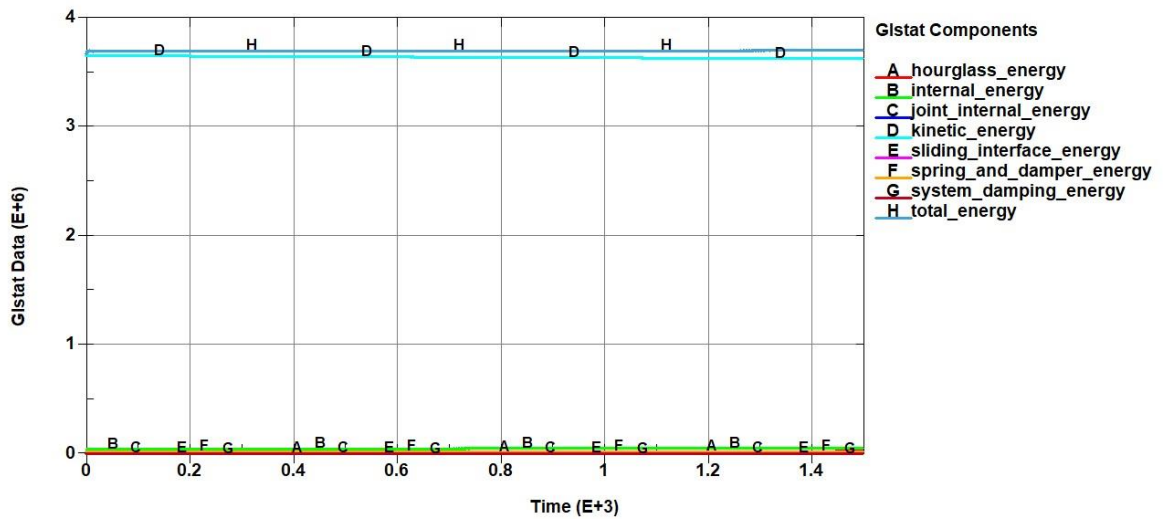


Figure 45: Energy balance

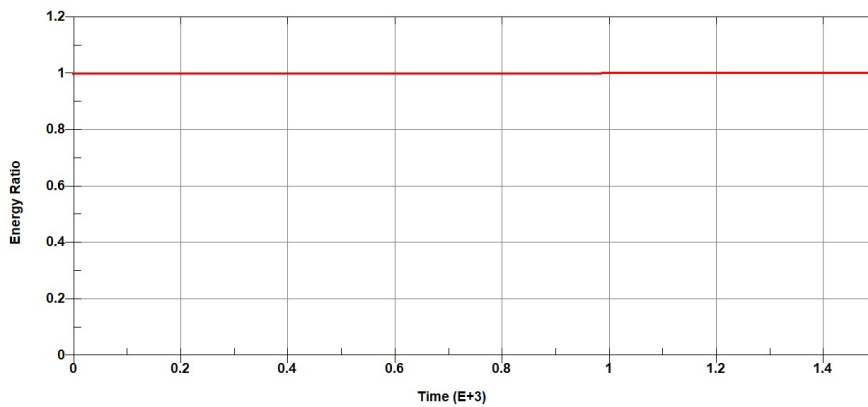


Figure 46: Energy ratio

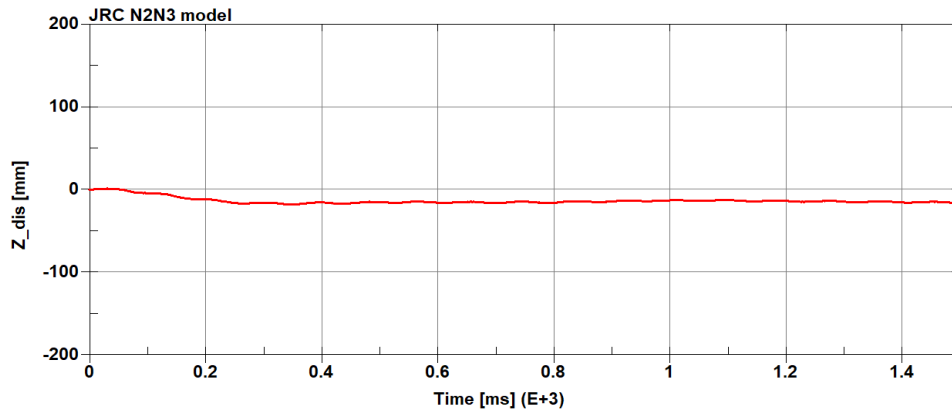


Figure 47: Displacement of the flatbed above rear wheel

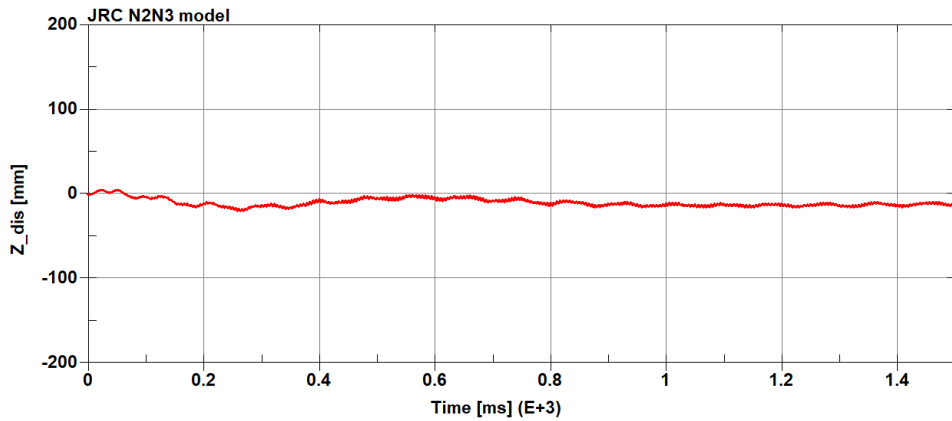


Figure 48: Displacement of the flatbed end

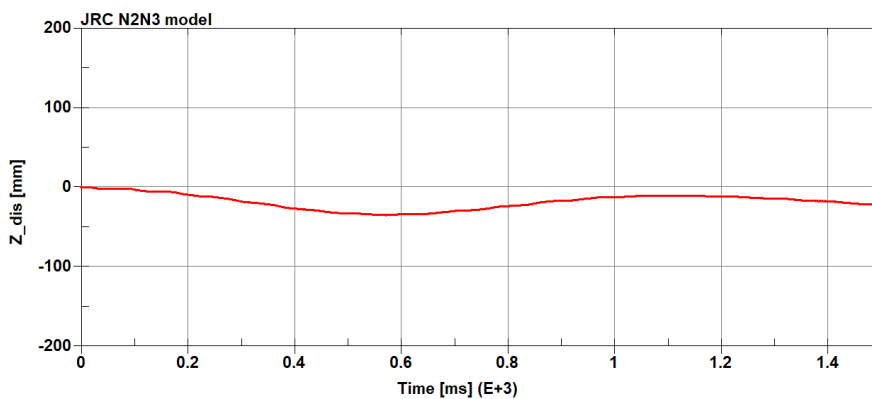


Figure 49: Displacement of the flatbed lead edge

No abnormal deformation nor stresses were observed on the model. Energy balance and energy ratio correspond to vehicle going straight forward for 40 m at 100 km/h. The vehicle kept straight forward linear trajectory with no substantial deceleration or turning (see fig. 50).

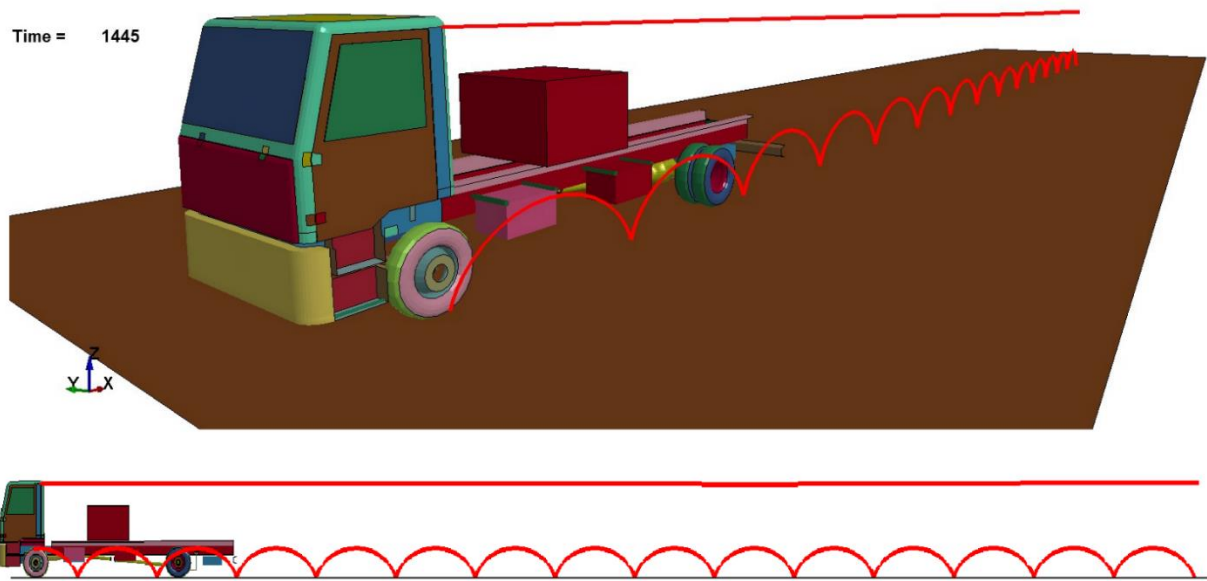


Figure 50: Linear track a distance of 40 m at a speed of 100 km/h

4.2.3 Conclusion

The FE model proved its computational stability, steering stability, and suspension stability, while traveling straight forward for 40 m at 100 km/h (1.5 sec). The displacement at the monitored points were about 20-30 mm.

4.3 Curb test

4.3.1 Objective

In this test the vehicle model is placed in front of a rigid speed bump (see fig.51) and it is given initial velocity of 48 km/h. The speed bump is fixed to the ground. The vehicle model is observed as it goes over the obstacle. During the vehicle's passage over the speed bump, the movement is monitored at the marked points on both the front and rear axles (see fig. 39). These movements are compared with experimental data. There were two simulation runs: front wheels going over the curb, rear wheels going over the curb.

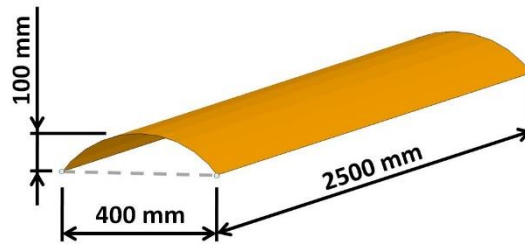


Figure 51: Speed bump dimensions

4.3.2 Results

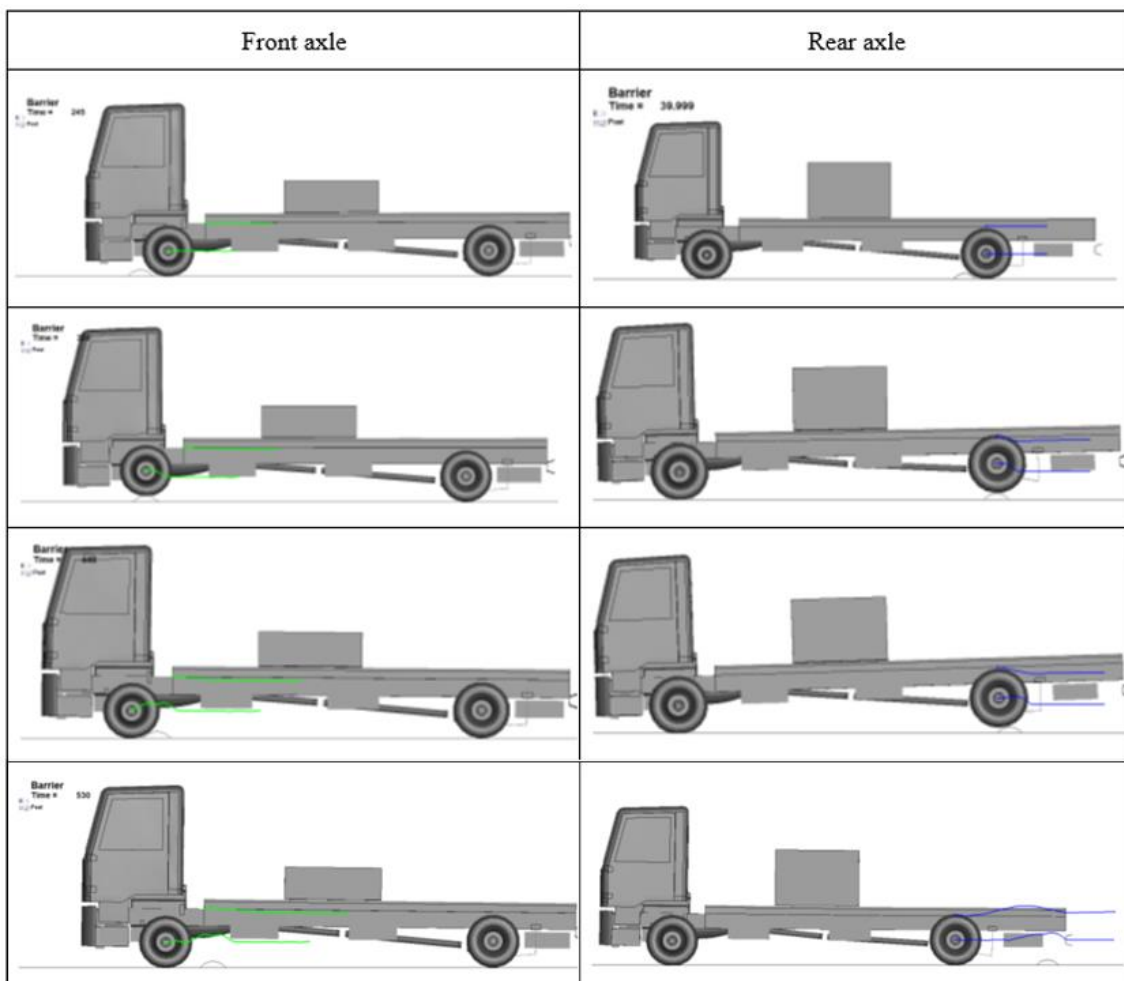


Figure 52: Curb test simulation – N2A/N3D at 16 km/h

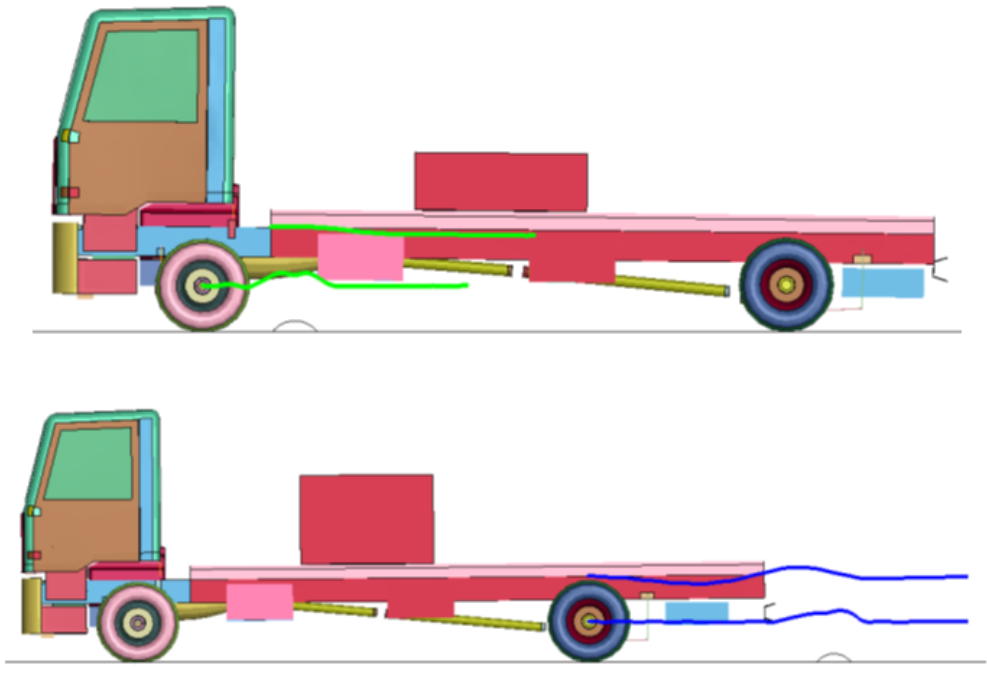


Figure 53: Vehicle model at curb test – trajectories of marked points

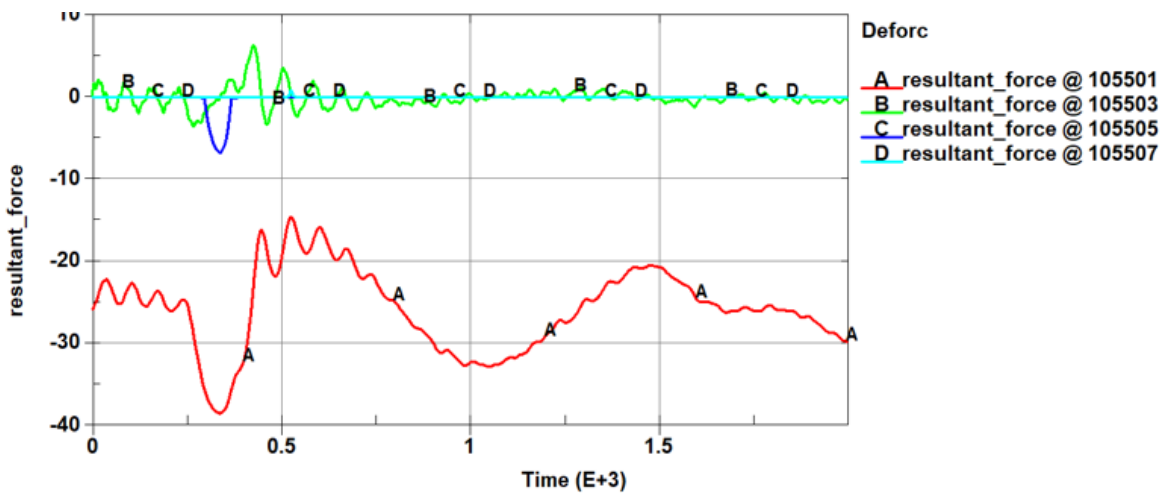


Figure 54: Forces on front right wheel suspension (A – Linear spring, B – Damper, C – Upper bound, D – Lower bound)

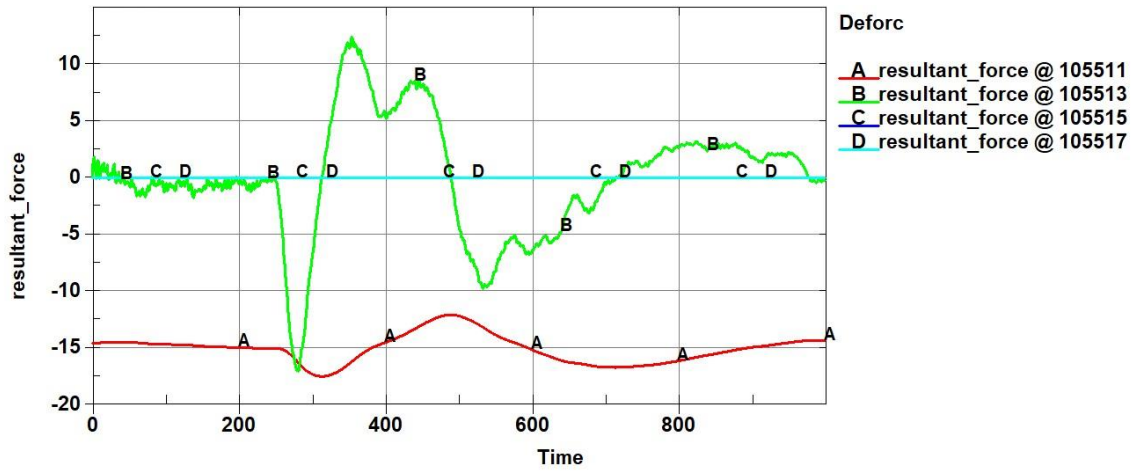


Figure 55: Forces on rear right wheel suspension (A – Linear spring, B – Damper, C – Upper bound, D – Lower bound)

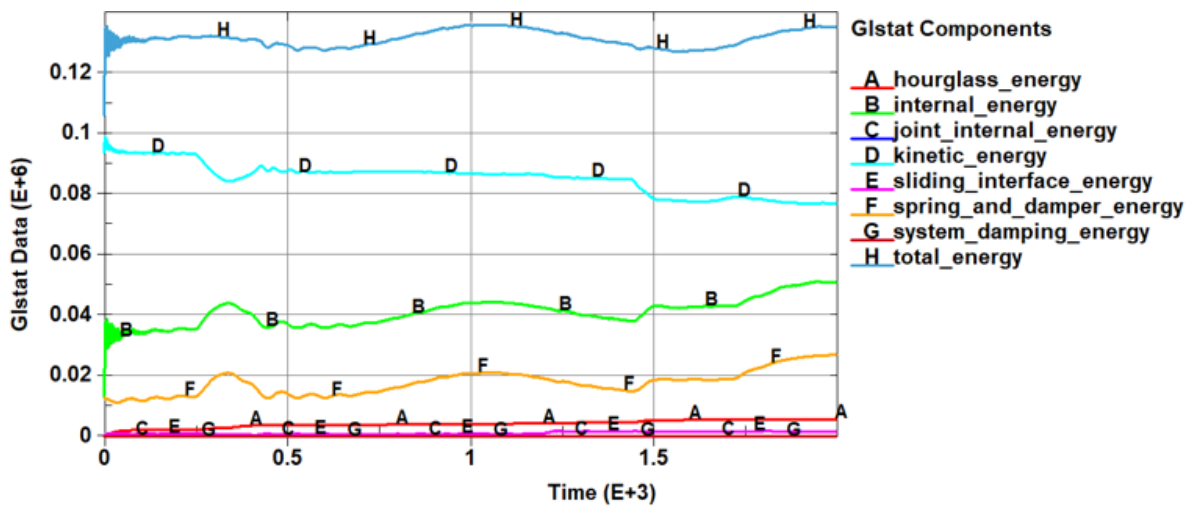


Figure 56: Energy balance – front wheels at the curb test

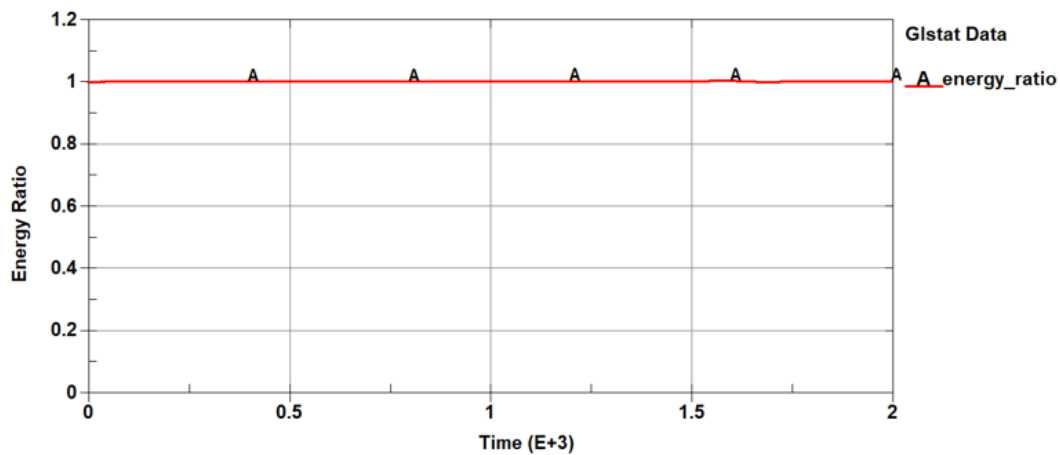


Figure 57: Energy ratio - front wheels at the curb test

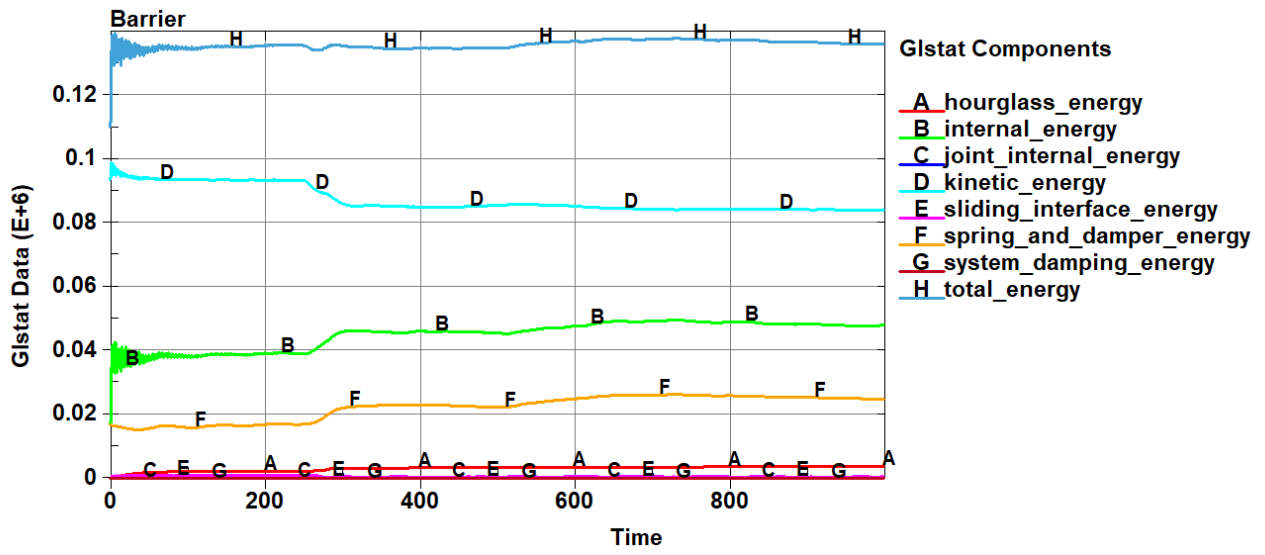


Figure 58: Energy balance - rear wheels at the curb test

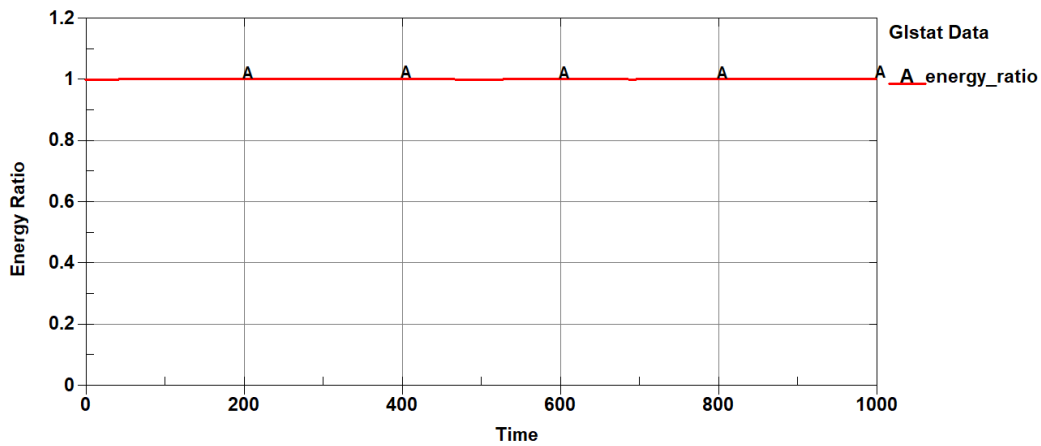


Figure 59: Energy ratio - rear wheels at the curb test



Figure 60: Curb test experiment – 16 km/h

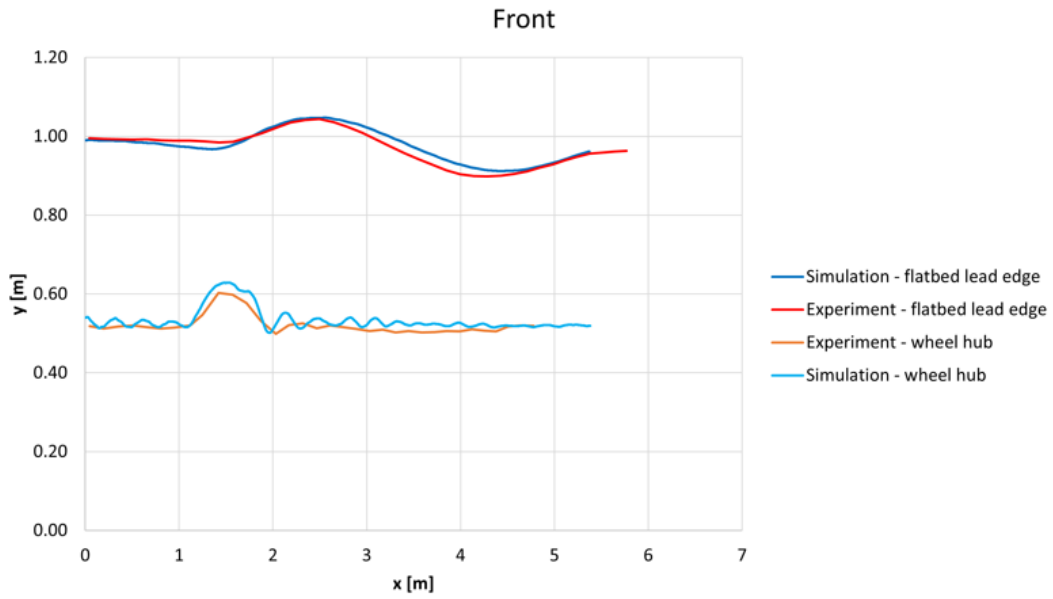


Figure 61: Curb test – sideview trajectory comparison simulation vs experiment – front axle

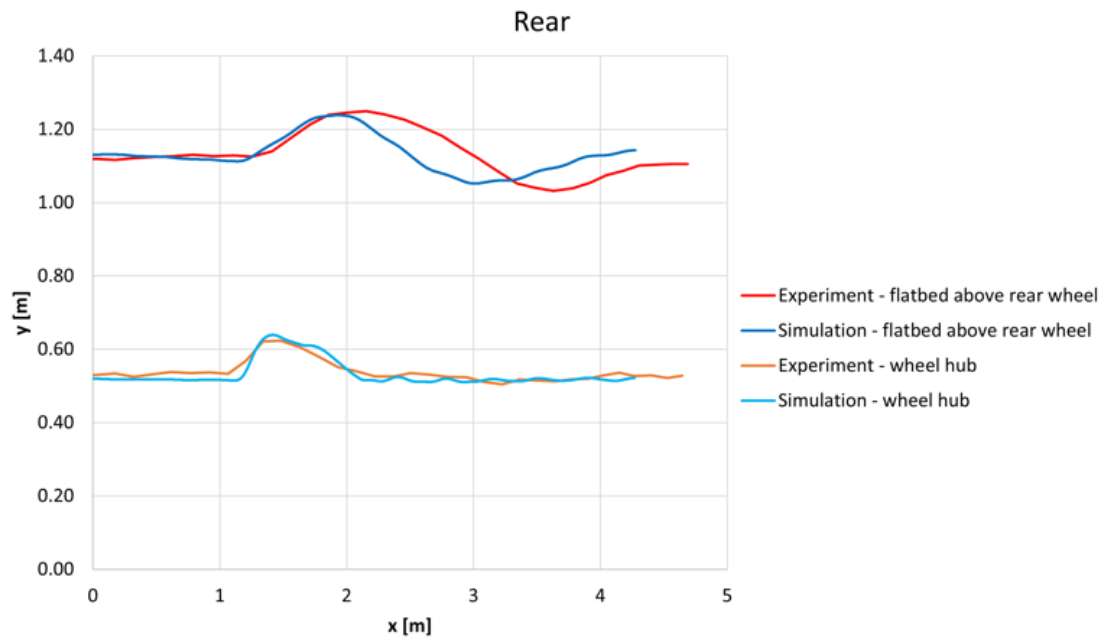


Figure 62: Curb test – sideview trajectory comparison simulation vs experiment – rear axle

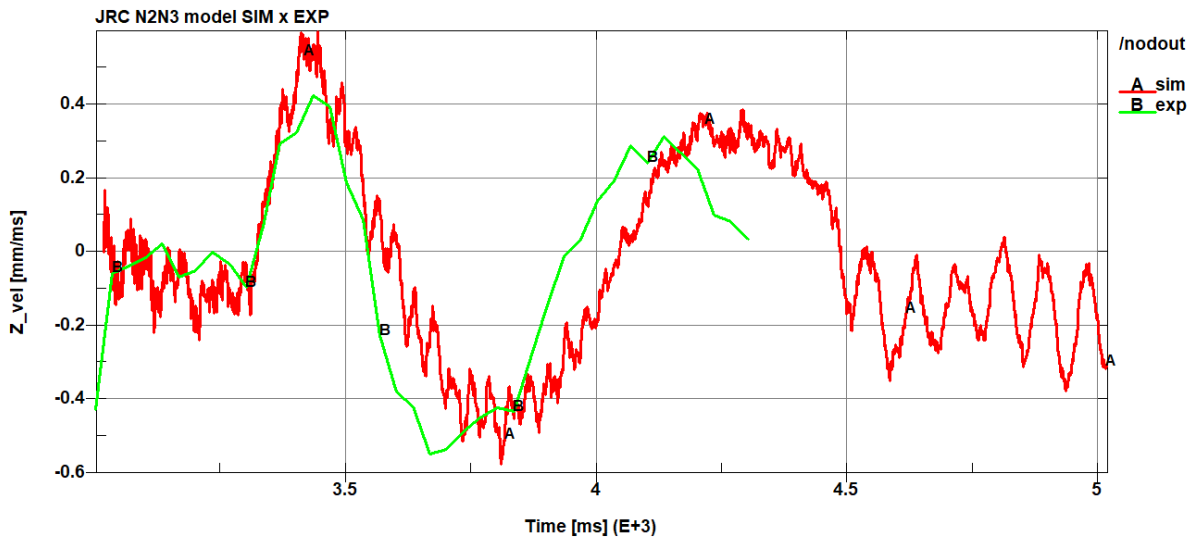


Figure 63: Front wheels at curb test – Flatbed lead edge, vertical velocity comparison

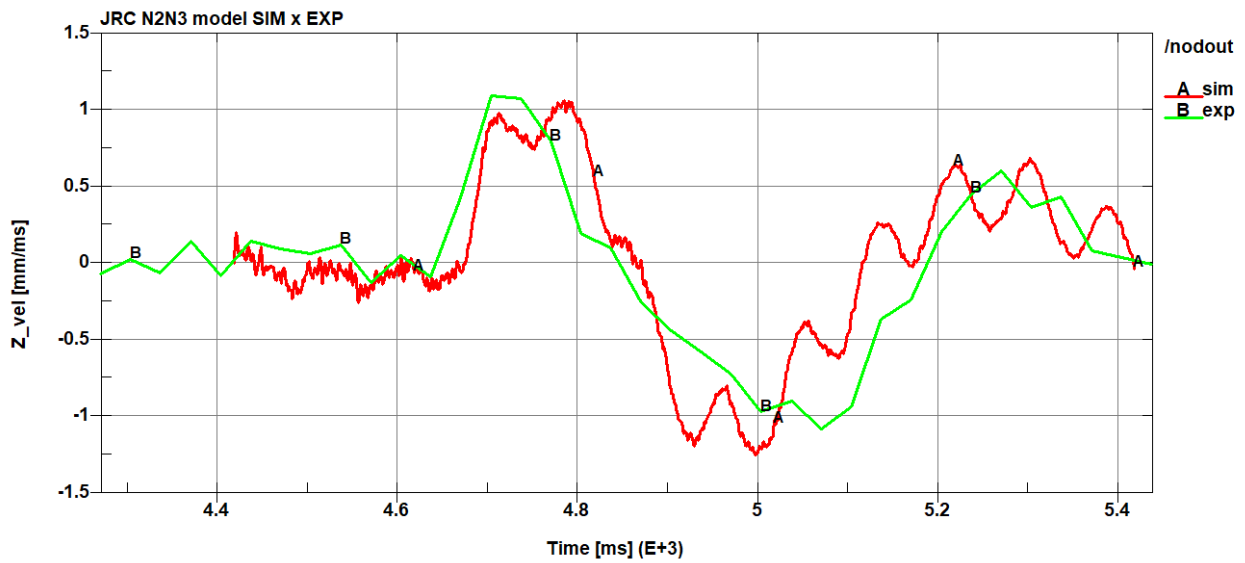


Figure 64: Rear wheels at curb test – Flatbed above rear wheels, vertical velocity comparison

4.3.3 Conclusion

The FE model proved computational stability. Comparison of trajectories and velocities of monitored points proved agreement between the behaviour of the real vehicle and vehicle model in simulation.

4.4 Crash test – rigid wall

4.4.1 Objective

Full scale crash test simulation is one of the last steps in the vehicle model validation process. In this test the vehicle model is set in front of a rigid wall, given initial velocity and global response of the model is observed as it impacts the barrier. This test was not compared with any experimental results. For this test, the parameters of the model were (in terms of dimensions and masses) adjusted to match the real vehicle from chapter “Crash test - bollard” as close as possible (see fig. 65). The impact velocity was 48 km/h.

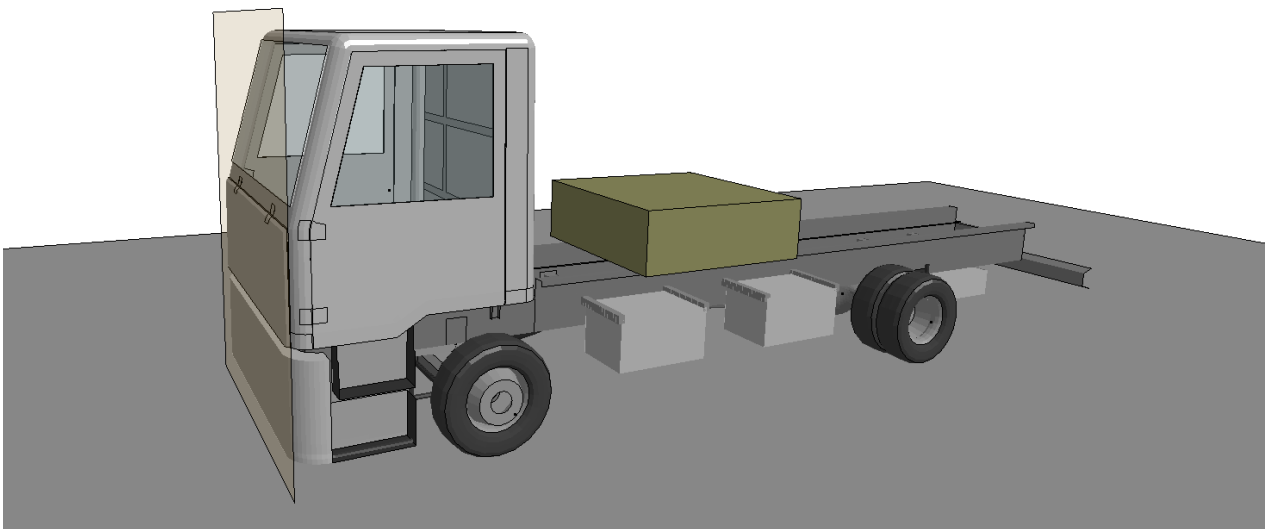
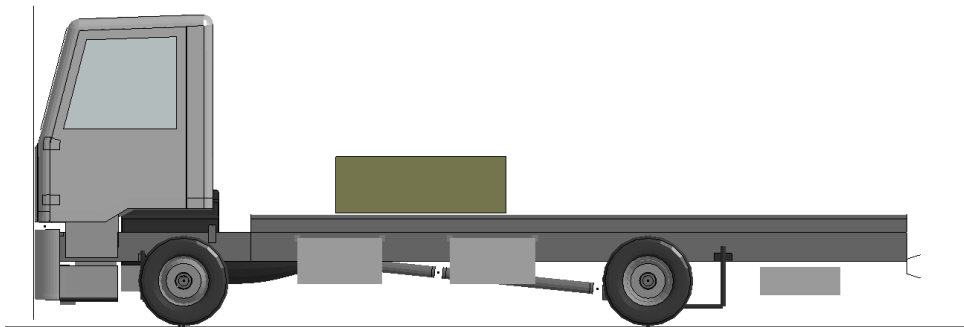


Figure 65: Crash test – impact to a rigid wall

For later comparison of simulation results with an experiment (chapter “Crash test - bollard”), measurement points were set on the vehicle cabin (measurement points M1, M2), on the front bumper (measurement point M3) and in the axis of the front and rear axles (measurement points M4, M5), see figure 66). The movement of these points during the crash simulation can be seen in the following figures. The X direction corresponds to the horizontal direction (original travel direction is -X). The Z direction corresponds to the vertical direction.



Figure 66: Positions of the measurement points

4.4.2 Results

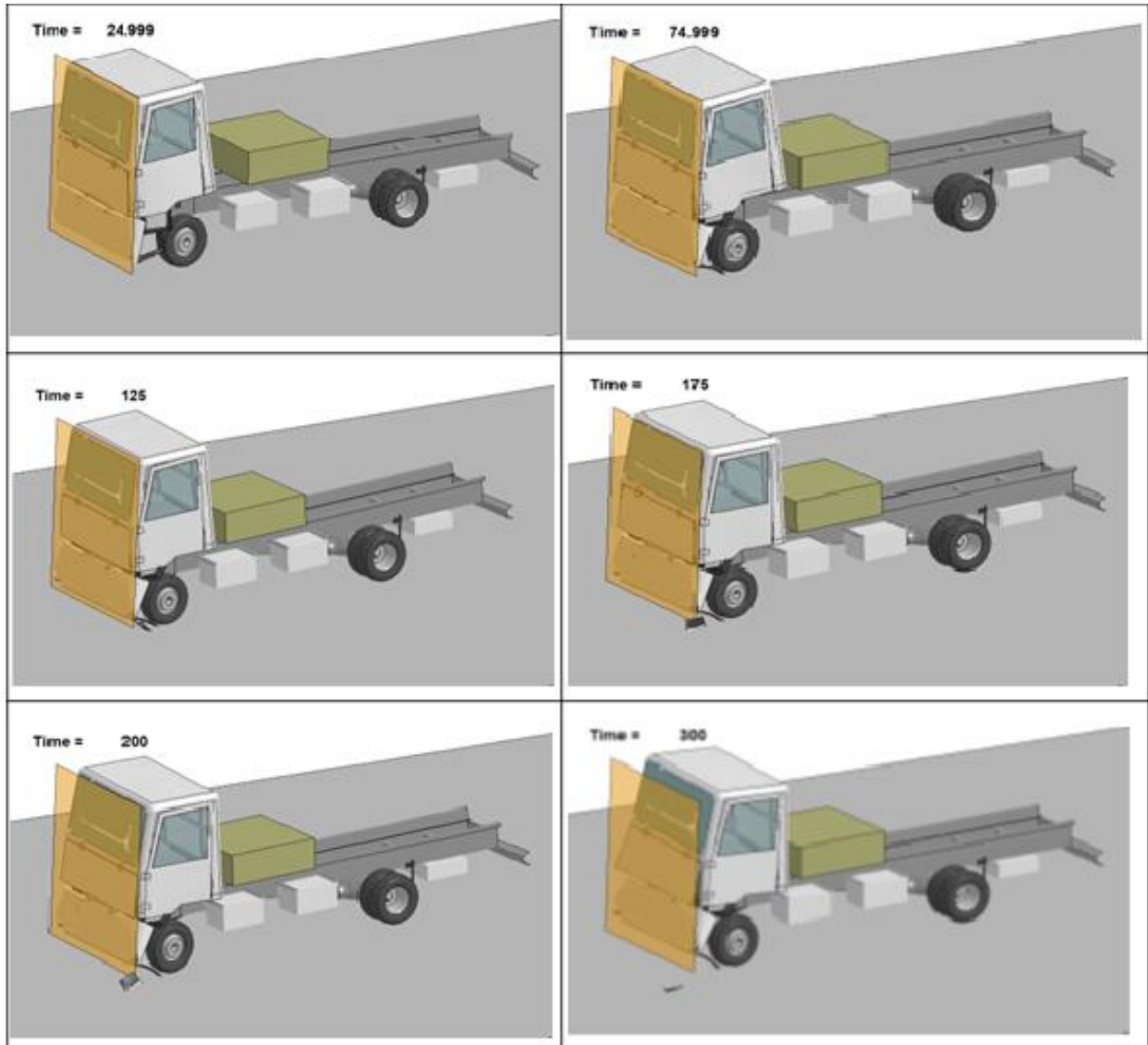


Figure 67:Crash test simulation – rigid wall, 48 km/h

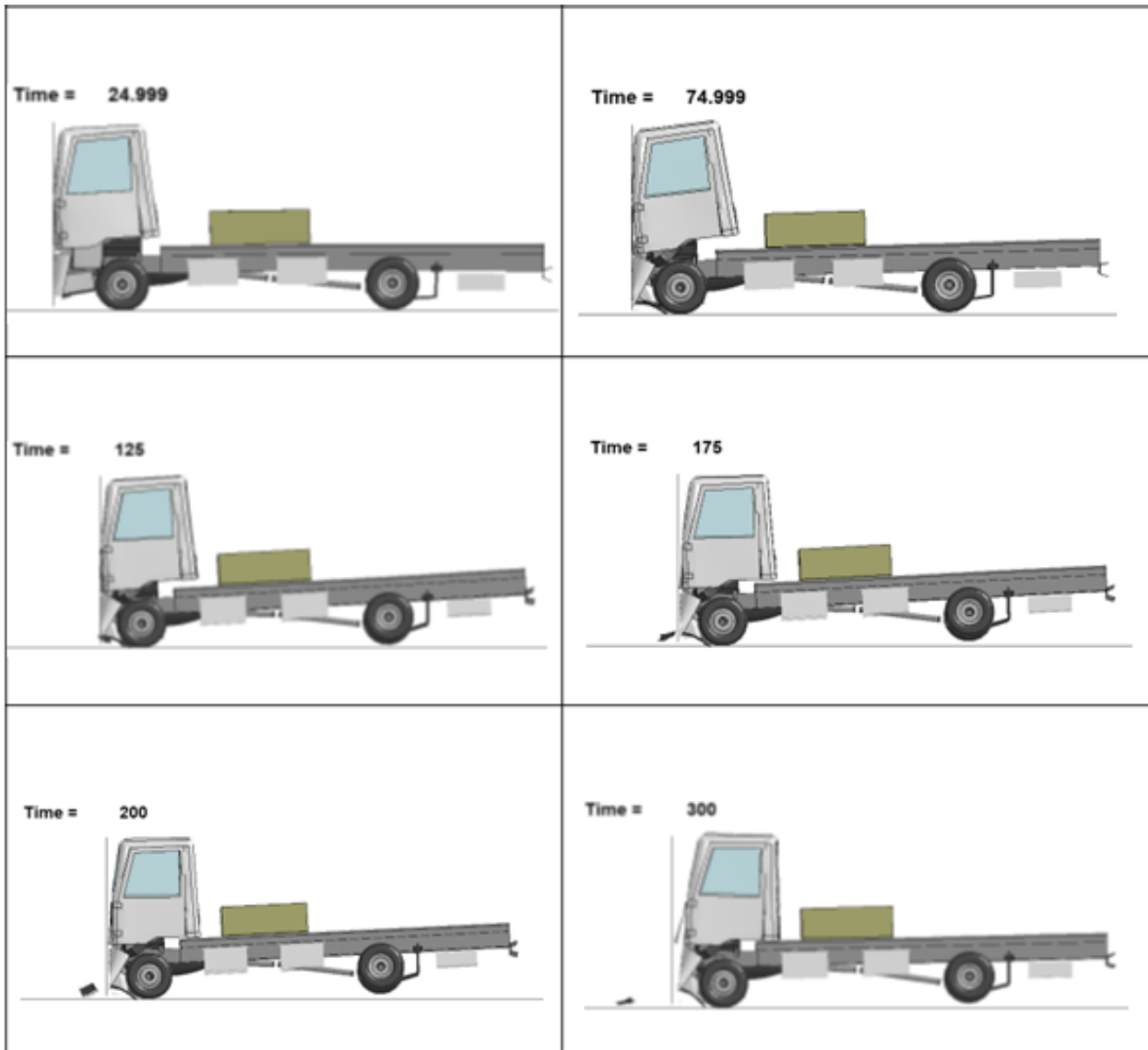


Figure 68: Crash test simulation – rigid wall, 48 km/h (side view)

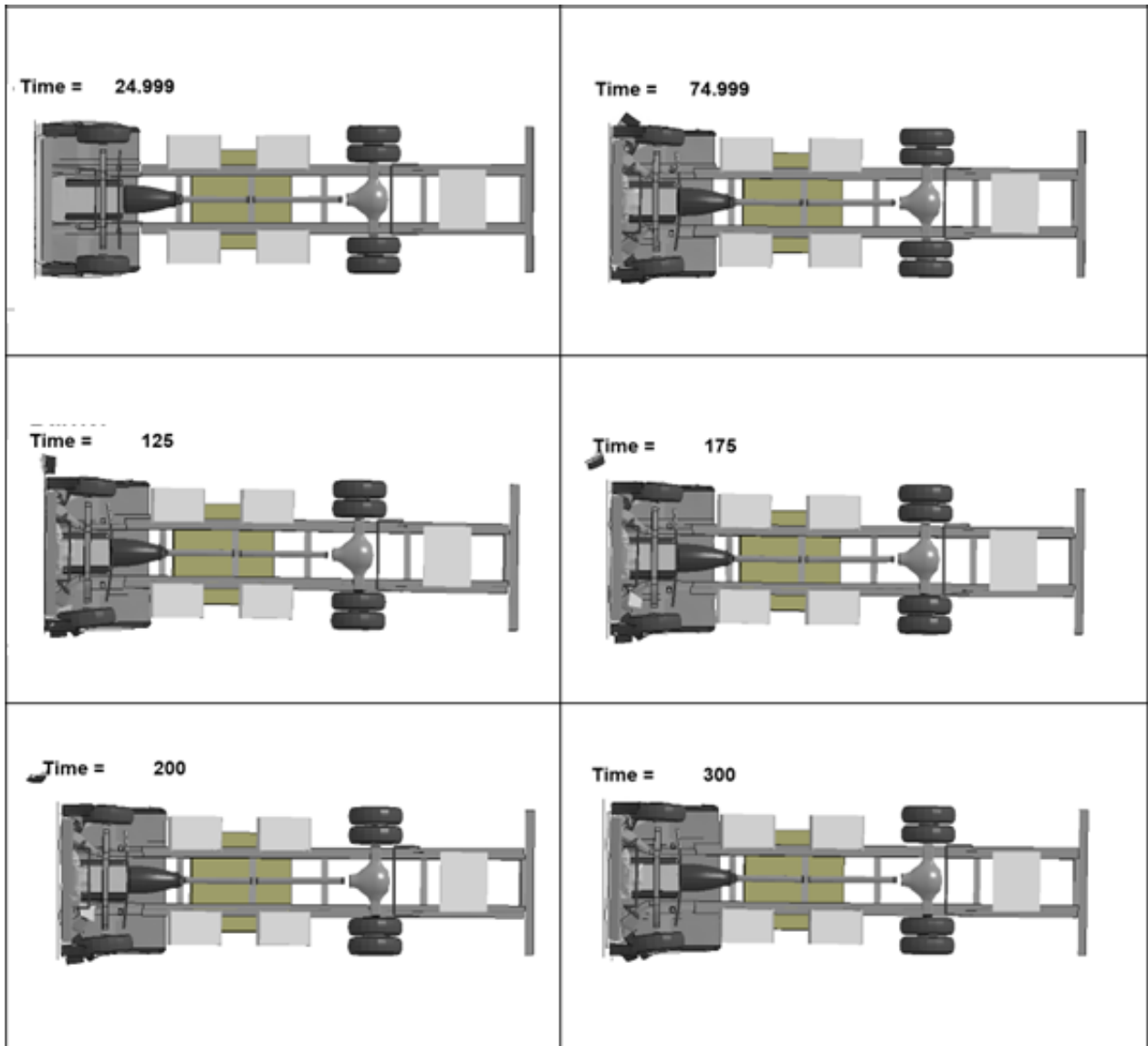


Figure 69:Crash test simulation – rigid wall, 48 km/h (bottom view)

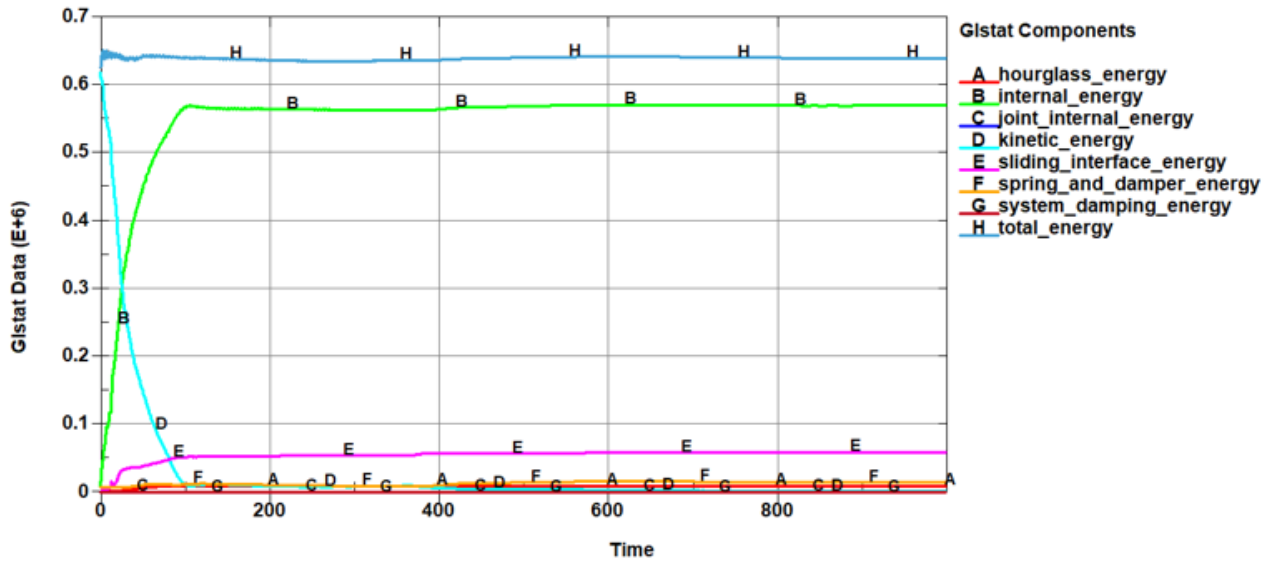


Figure 70: Crash test simulation (rigid wall) – energy balance

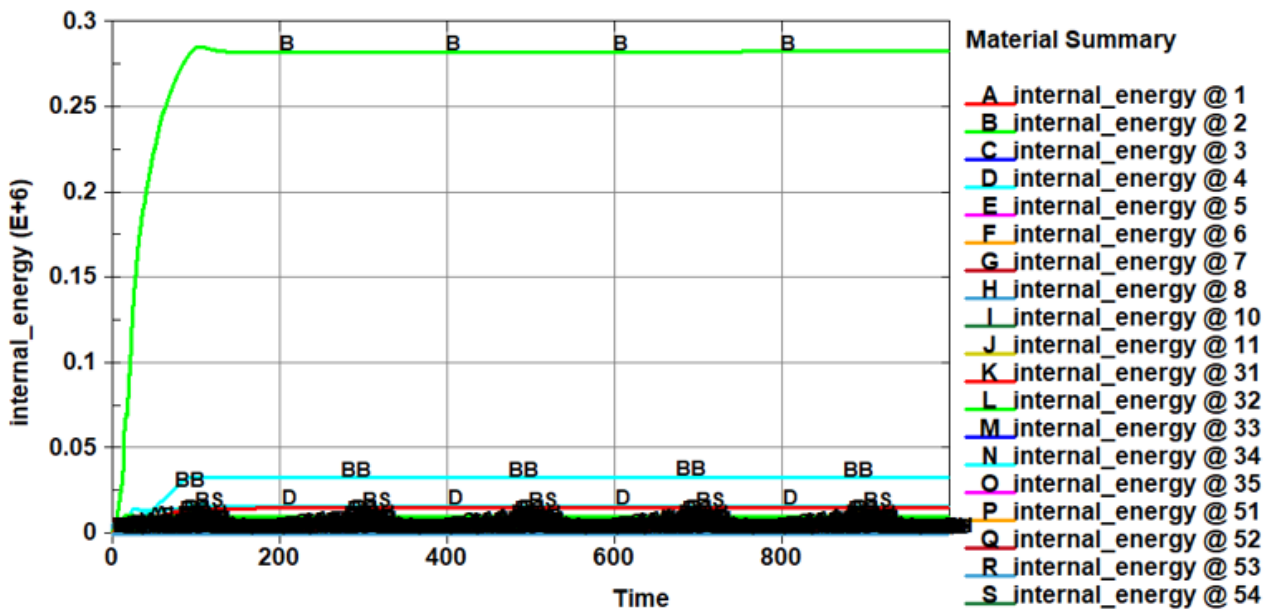


Figure 71: Crash test simulation (rigid wall) – internal energy of individual parts

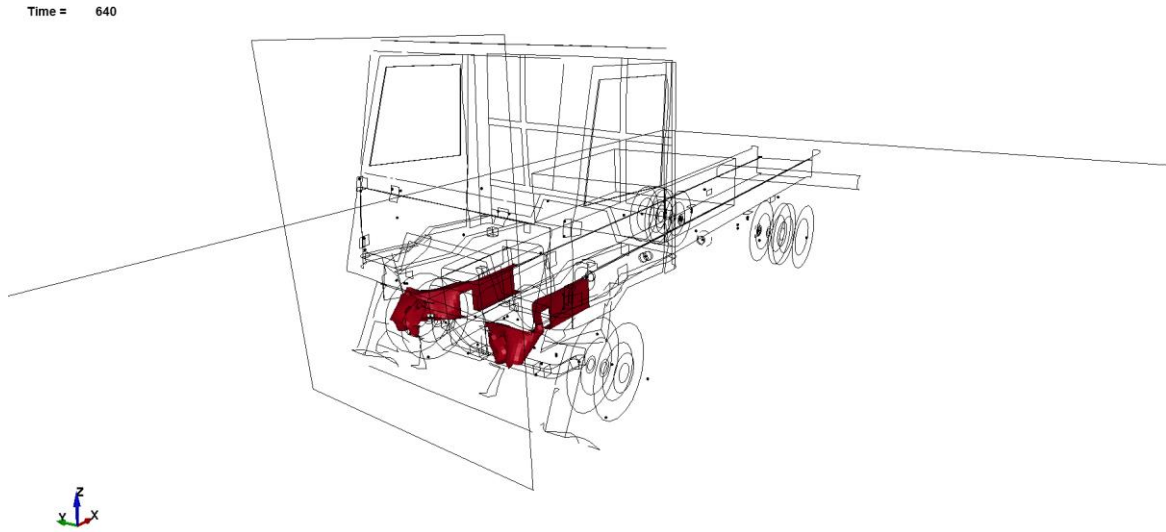


Figure 72: Crash test simulation (rigid wall) – parts with the highest internal energy

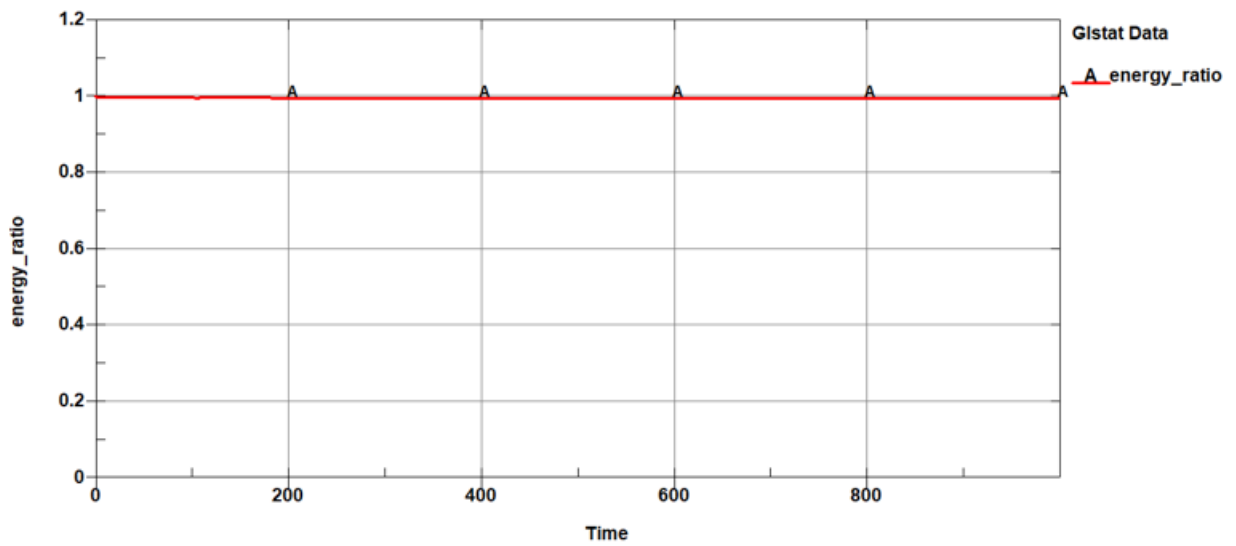


Figure 73: Crash test simulation (rigid wall) – energy ratio

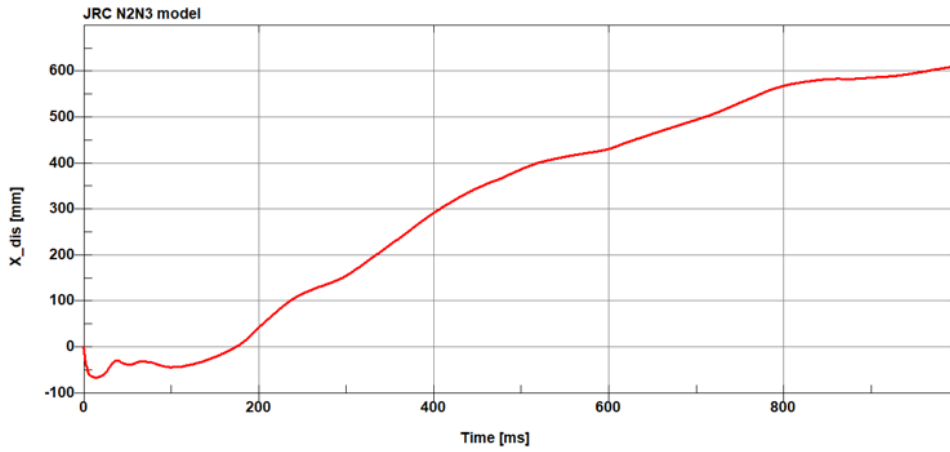


Figure 74: X Displacement of the measurement point M1 (horizontal direction)

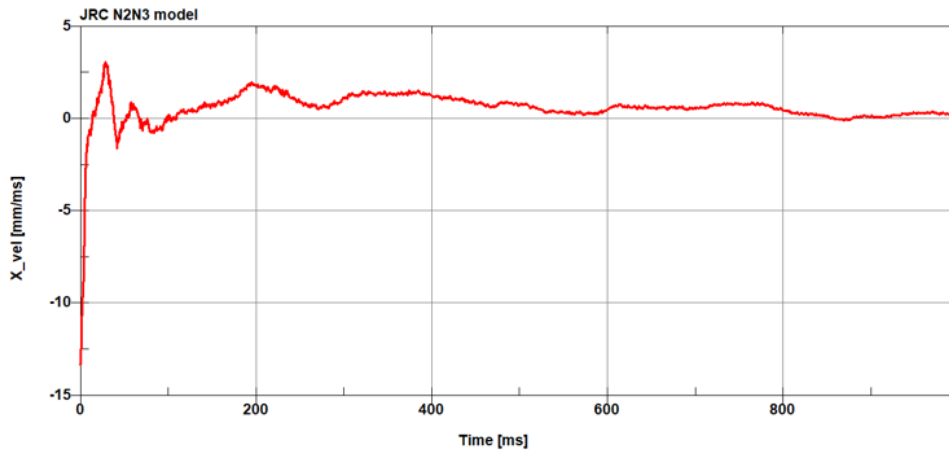


Figure 75: X Velocity of the measurement point M1 (horizontal direction)

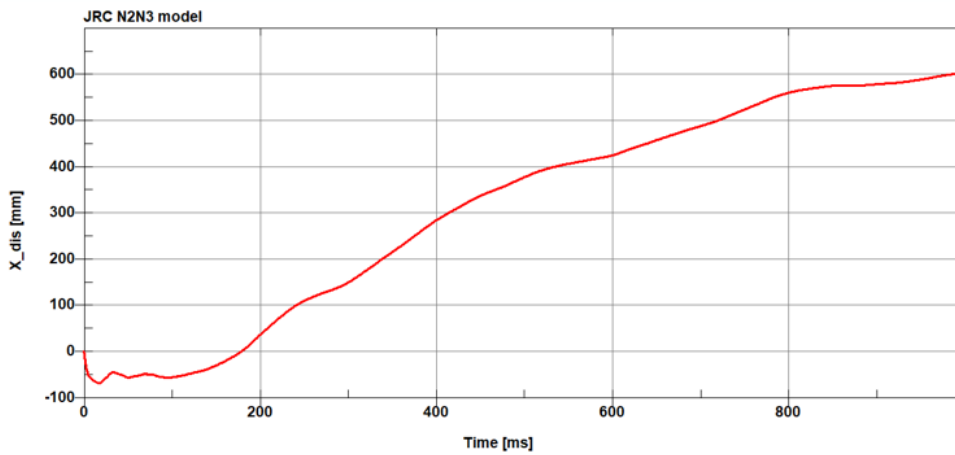


Figure 76: X Displacement of the measurement point M2 (horizontal direction)

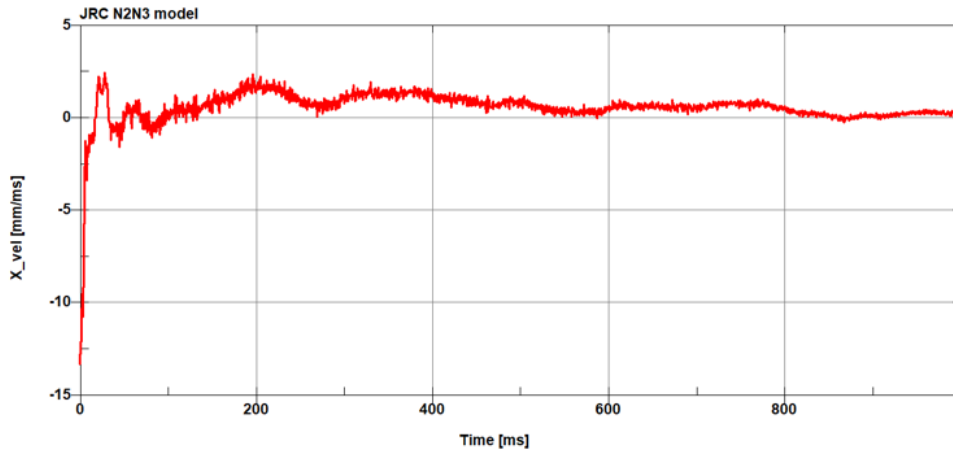


Figure 77: X Velocity of the measurement point M2 (horizontal direction)

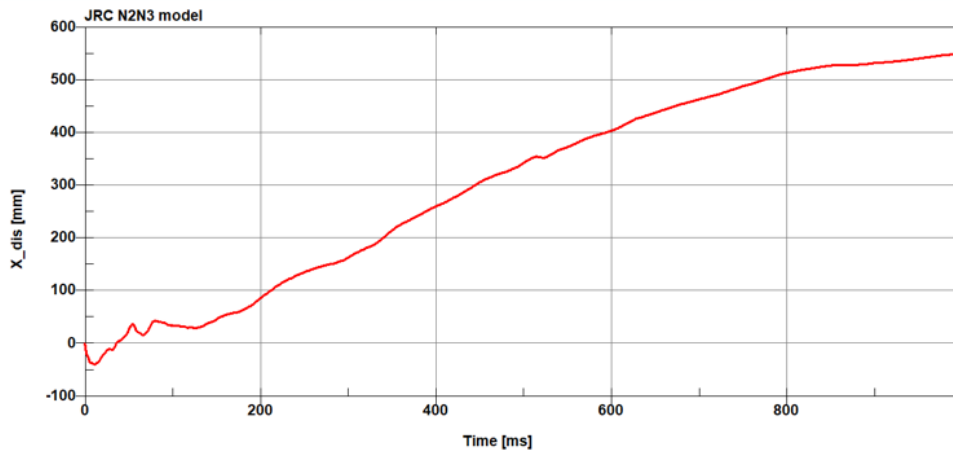


Figure 78: X Displacement of the measurement point M3 (horizontal direction)

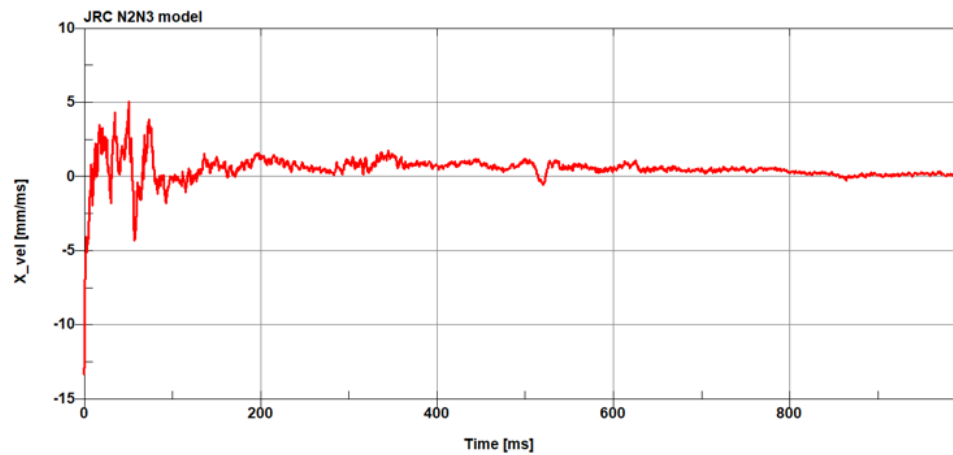


Figure 79: X Velocity of the measurement point M3 (horizontal direction)

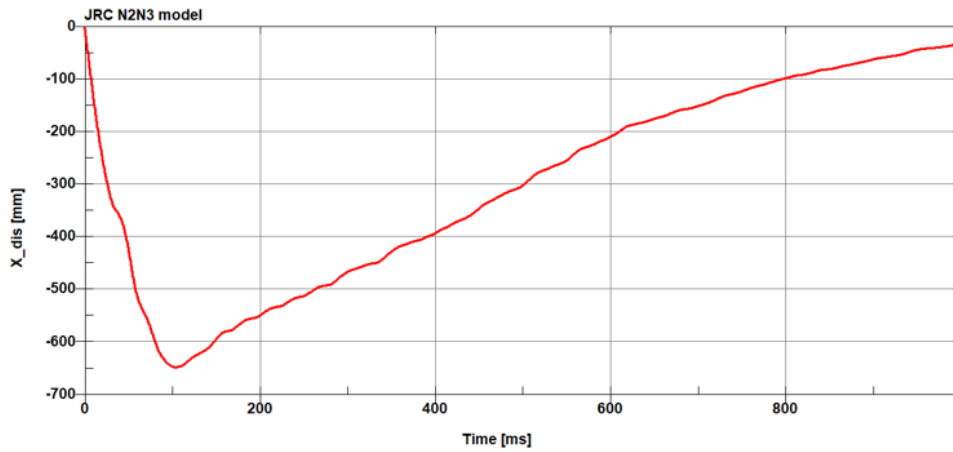


Figure 80: X Displacement of the measurement point M4 (horizontal direction)

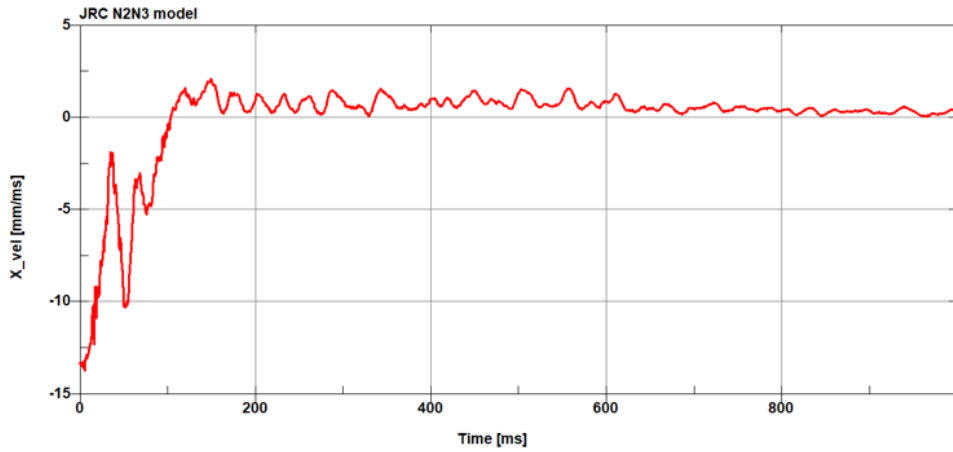


Figure 81: X Velocity of the measurement point M4 (horizontal direction)

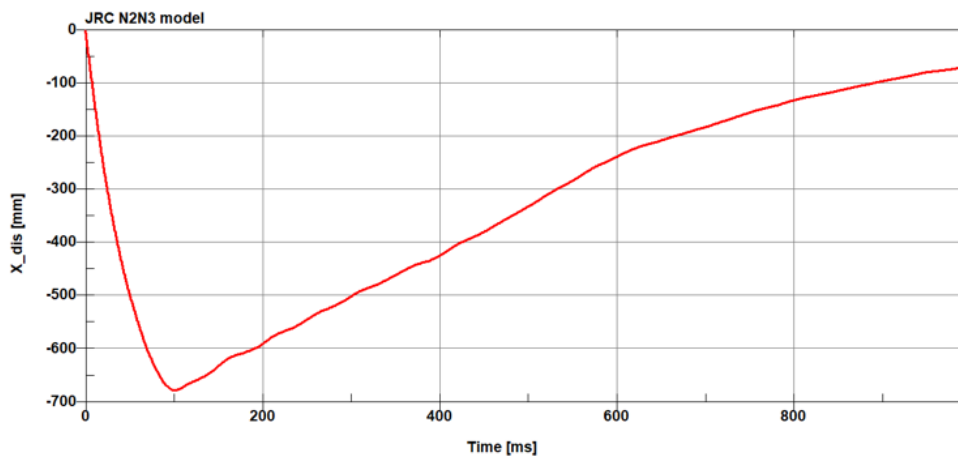


Figure 82: X Displacement of the measurement point M5 (horizontal direction)

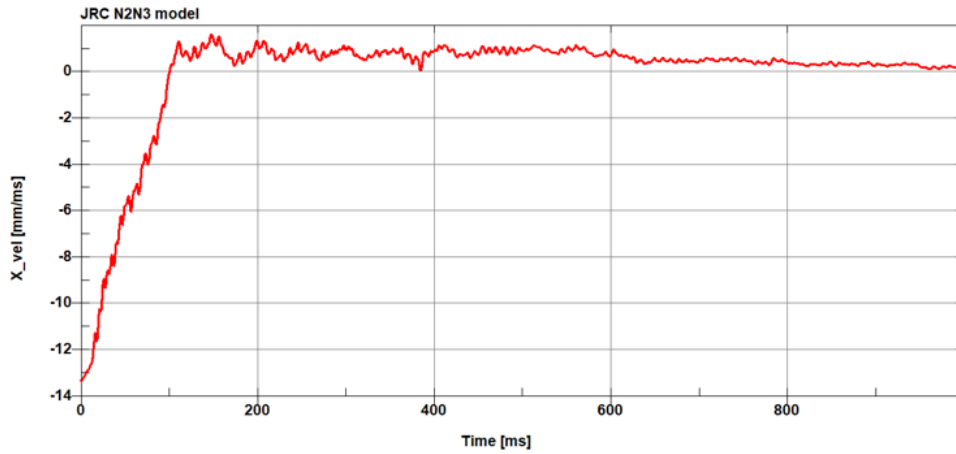


Figure 83: X Velocity of the measurement point M5 (horizontal direction)

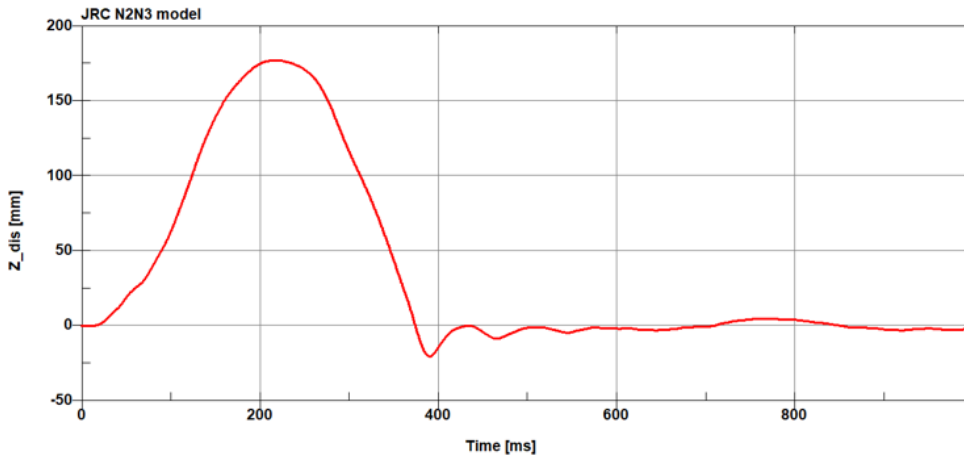


Figure 84: Z Displacement of the measurement point M5 (vertical direction)

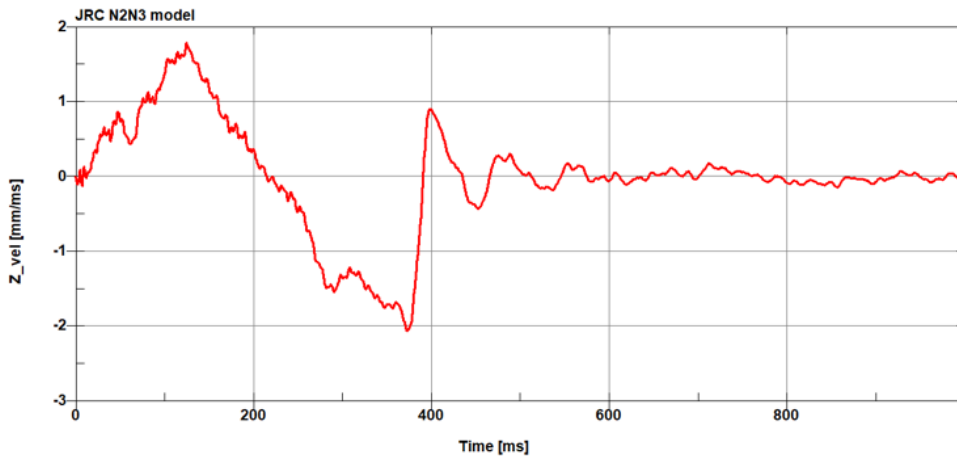


Figure 85: Z Velocity of the measurement point M5 (vertical direction)

4.4.3 Conclusion

The global response of the vehicle model, including deformations of main parts, and velocity response aligns with the expected behaviour of the real vehicle. The computational stability of the model was also confirmed during the crash test simulation. Energy balance is reasonable. Vast majority of the kinetic energy is transformed into internal energy of the vehicle parts. Majority of the internal energy after the crash is stored in the front of the vehicle frame.

4.5 Crash test – bollard

4.5.1 Objective

The simulation of the crash test to a fixed barrier, in this case, a fixed bollard, is the final step in the validation procedure of the vehicle model. In this test, the vehicle model is placed in front of a rigid cylinder, which is securely fixed to the ground. The initial velocity is given to the vehicle, and the global response of the model is observed upon the collision with the barrier (bollard). This test was compared with publicly available experimental results of the crash test with vehicle in the corresponding category [29]. The vehicle in this real test matches N2A category with total mass 7500 kg. The parameters of the model (dimensions and masses) were adjusted in order to match the real test vehicle as close as possible. The impact velocity was 48 km/h. Displacements and velocities of the measurement points (see fig. 66) in the simulation are compared with data from experiment [29].

Time = 0

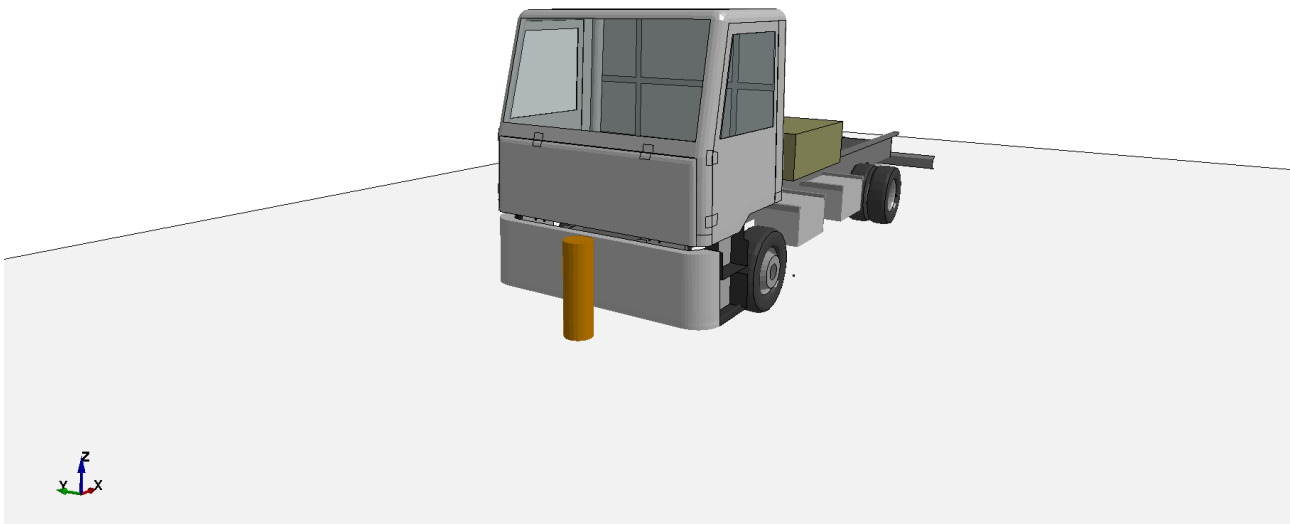


Figure 86: Crash test to bollard - simulation setup

4.5.2 Experimental data

Source of experimental data was a video from a real crash test capturing the event with high speed camera (200 Hz) from several views (front view, left view, right view, top view) [29]. The data for comparison with simulation were acquired with an open-source software Tracker [30]. This software allows capturing movement of selected points in 2D plane. The data from left view was chosen for the comparison with simulation as the left view is less affected with perspective (captured in direction perpendicular to the vehicle movement and parallel with the ground plane, the camera is also further from the event). Based on the video the time-dependent positions of key points of the vehicle were tracked. For majority of the points the automatic point tracking was not precise enough, so they were tracked manually.

Accuracy of this method of data acquisition is affected by the frequency of data acquisition, perspective, resolution of the video and quality of the point tracking (can be done automatically or manually).

4.5.3 Results









Time [ms]	Simulation	Experiment
0		
160		
500		
1000		

Figure 87: Crash test simulation and experiment – bollard, 48 km/h (side view)









Time [ms]	Simulation	Experiment
0		
160		
500		
1000		

Figure 88: Crash test simulation and experiment – bollard, 48 km/h (front view)

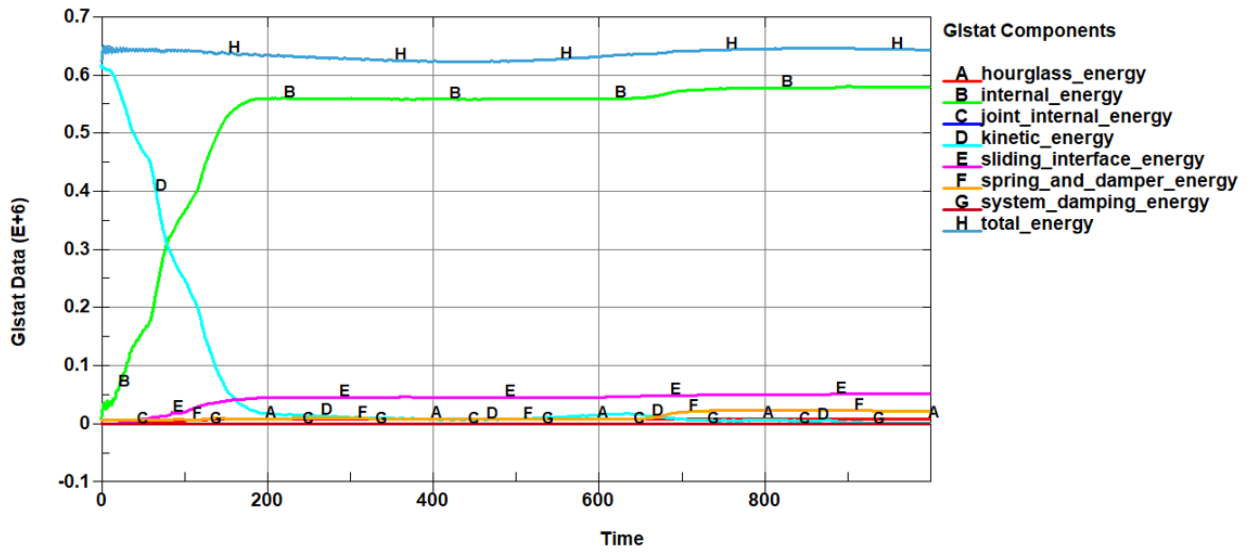


Figure 89: Crash test simulation (bollard) – energy balance

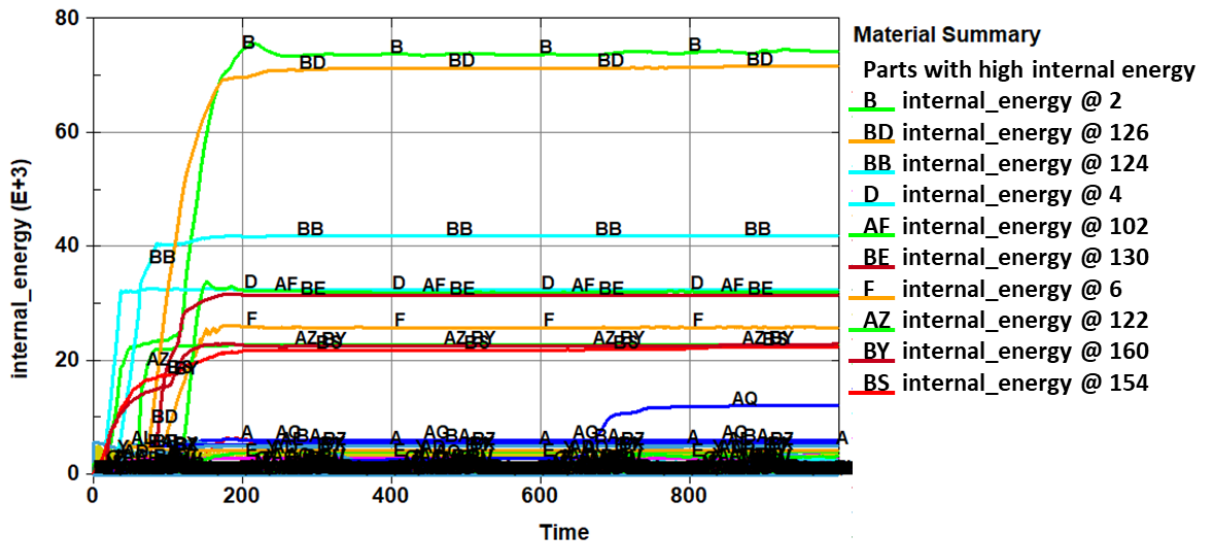


Figure 90: Crash test simulation (bollard) – internal energy of individual parts

Time = 130

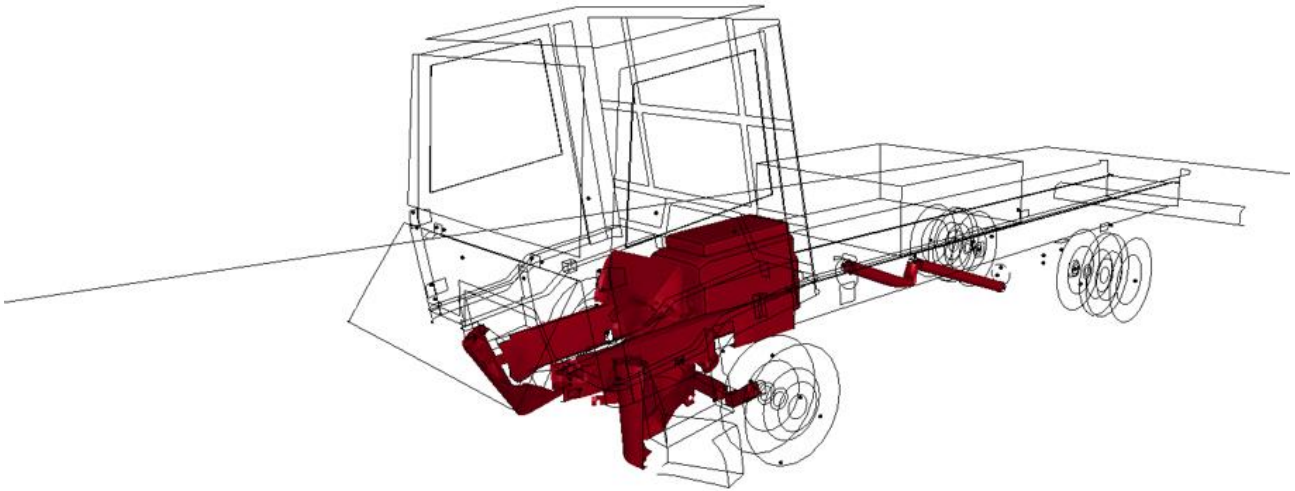


Figure 91: Crash test simulation (bollard) – parts with the highest internal energy

Time = 130

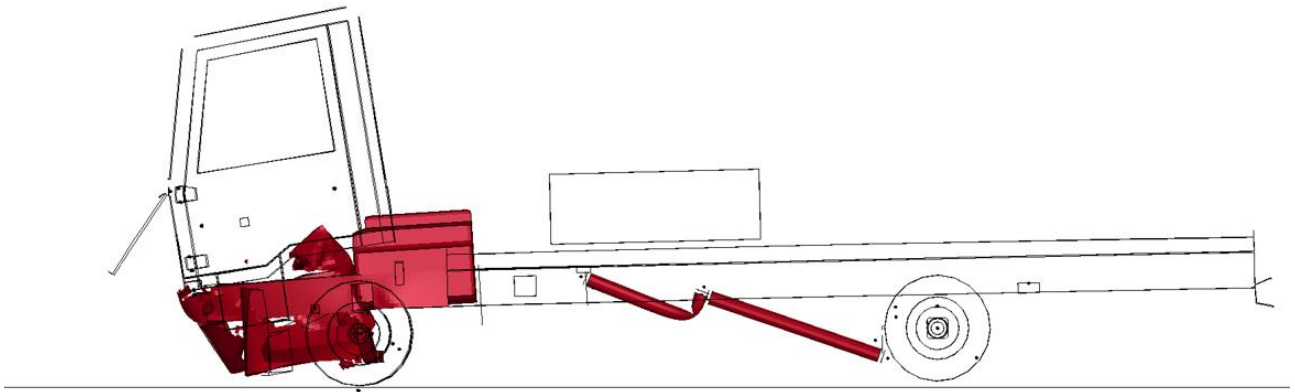


Figure 92: Crash test simulation (bollard) – parts with the highest internal energy (side view)

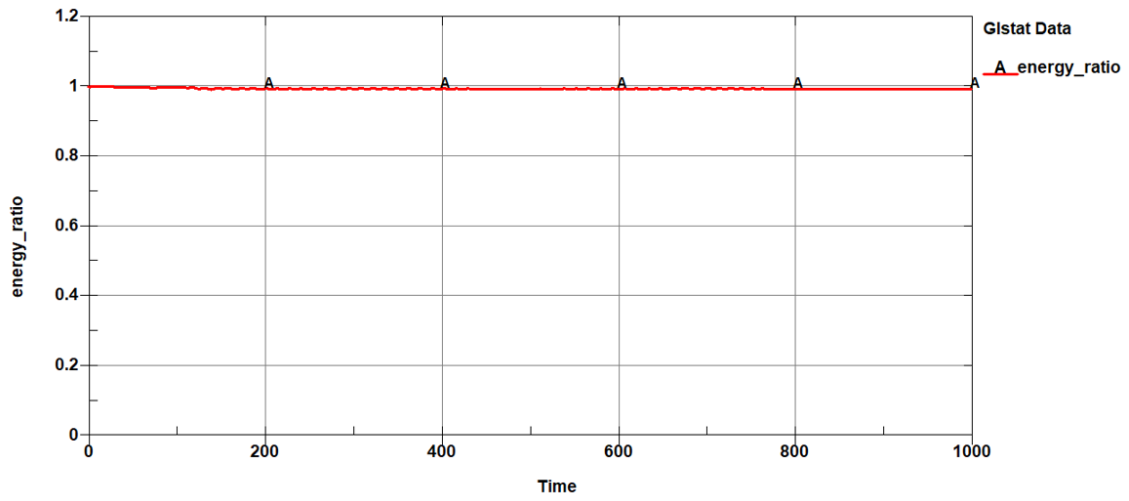


Figure 93: Crash test simulation (bollard) – energy ratio

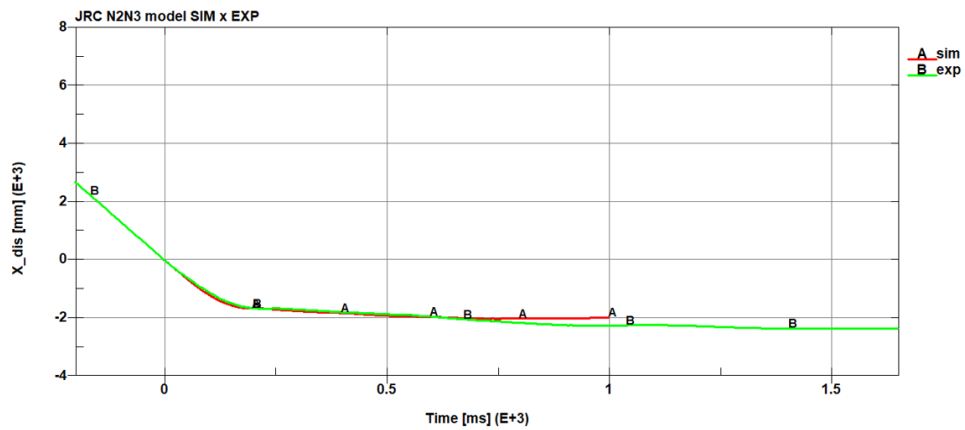


Figure 94: X Displacement of the measurement point M1 (horizontal direction): simulation, experiment

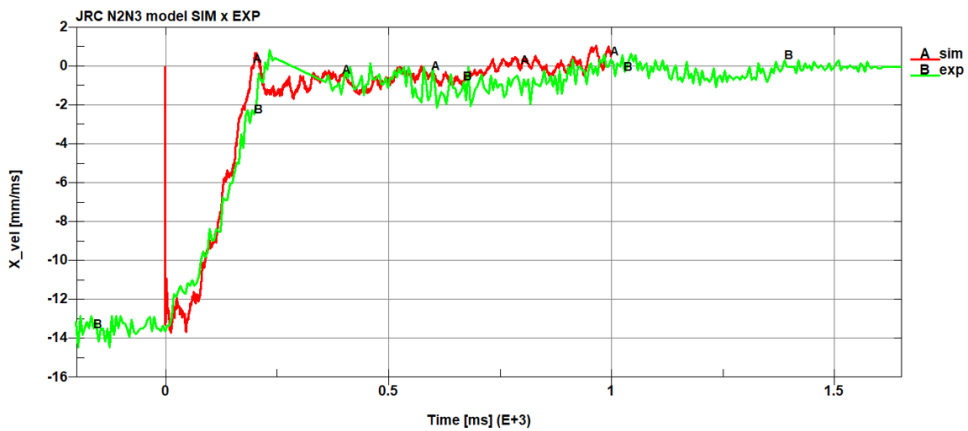


Figure 95: X Velocity of the measurement point M1 (horizontal direction): simulation, experiment

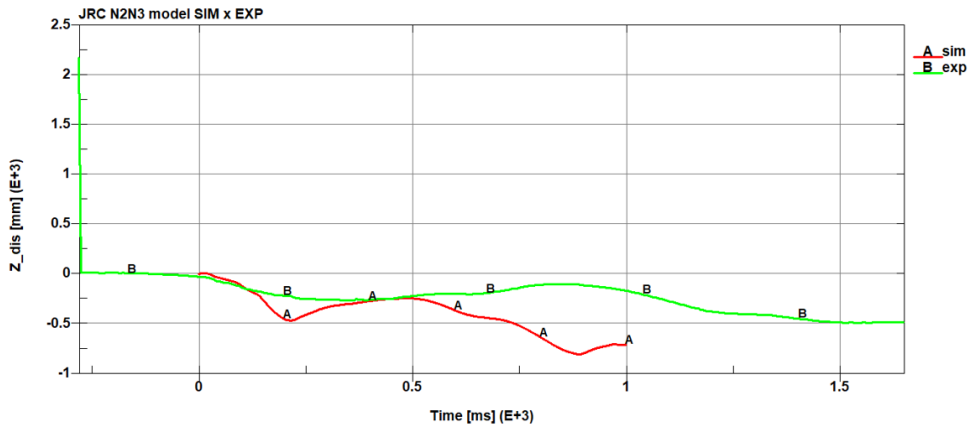


Figure 96: Z Displacement of the measurement point M1 (vertical direction): simulation, experiment

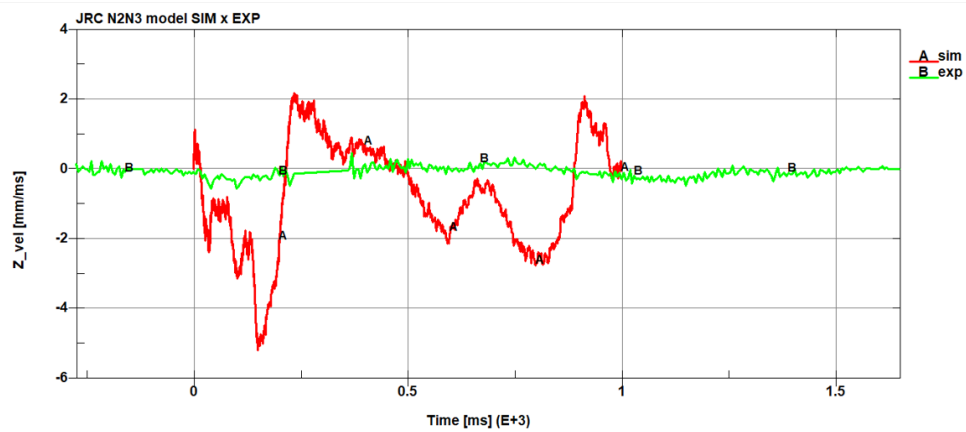


Figure 97: Z Velocity of the measurement point M1 (vertical direction): simulation, experiment

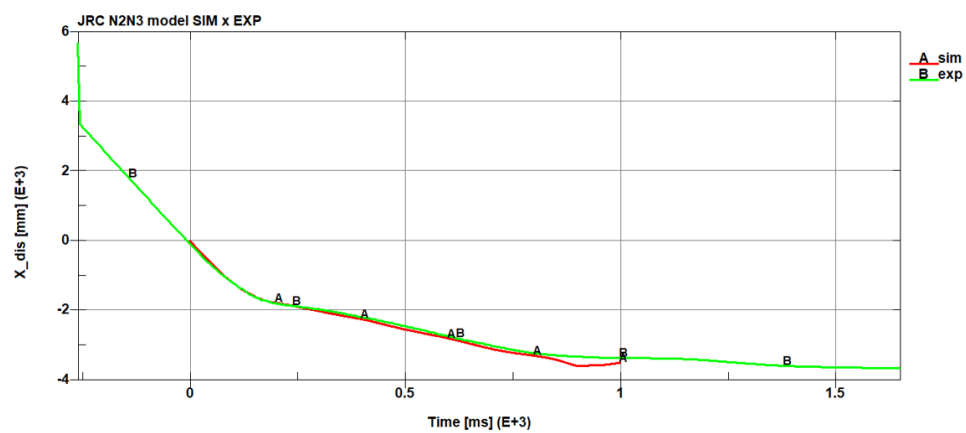


Figure 98: X Displacement of the measurement point M2 (horizontal direction): simulation, experiment

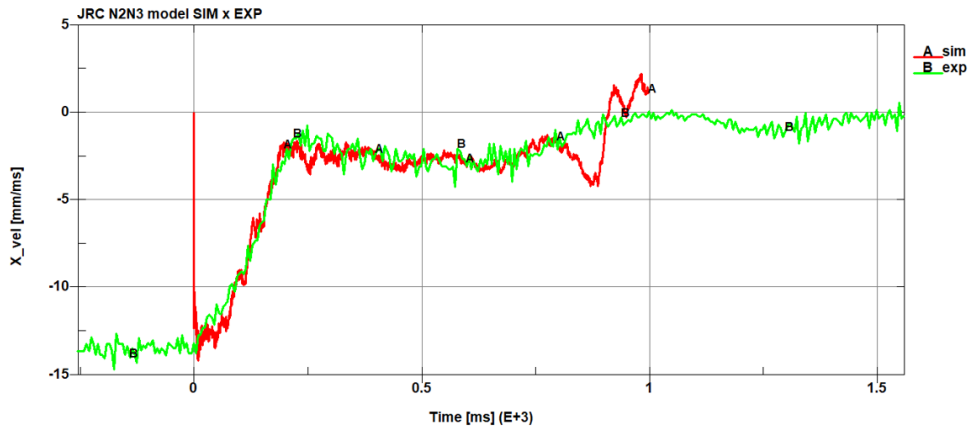


Figure 99: X Velocity of the measurement point M2 (horizontal direction): simulation, experiment

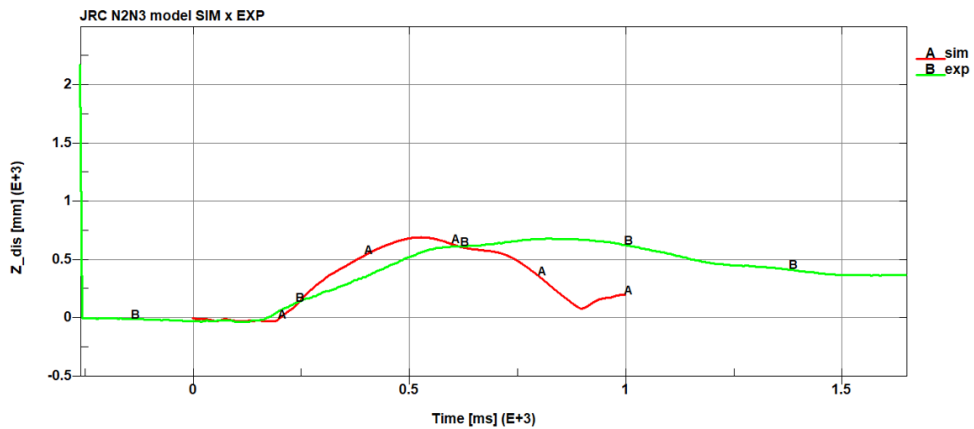


Figure 100: Z Displacement of the measurement point M2 (vertical direction): simulation, experiment

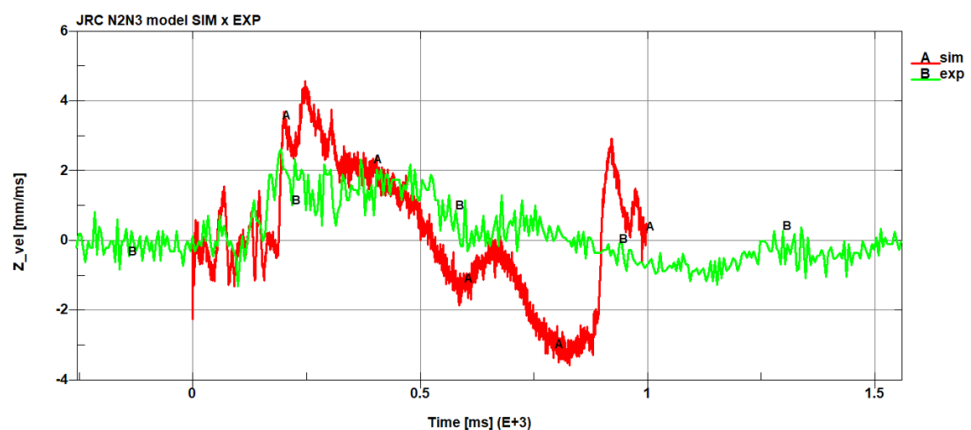


Figure 101: Z Velocity of the measurement point M2 (vertical direction): simulation, experiment

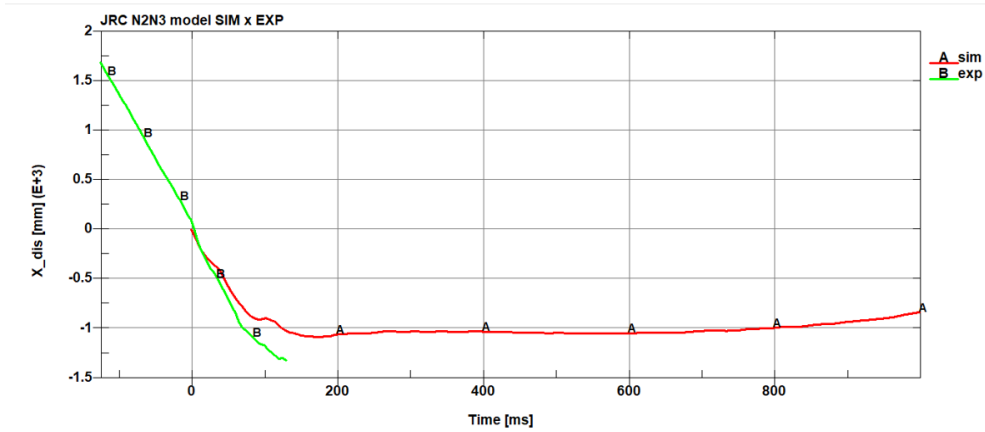


Figure 102: X Displacement of the measurement point M3 (horizontal direction): simulation, experiment

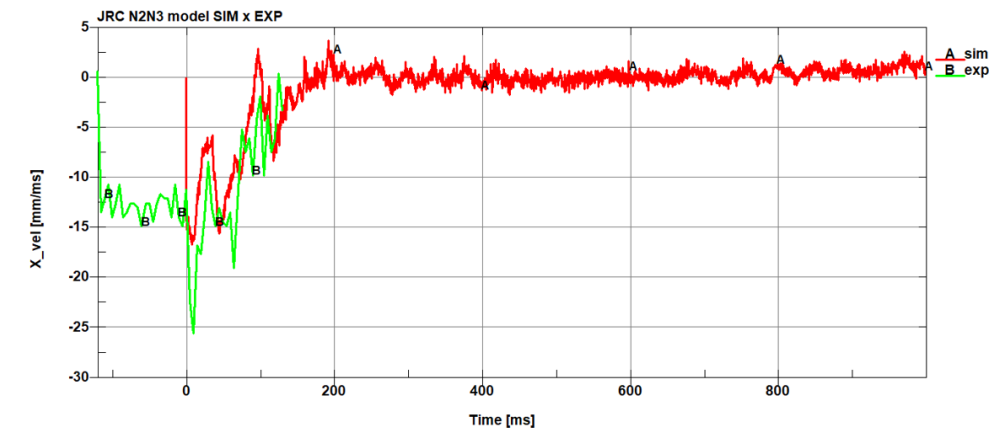


Figure 103: X Velocity of the measurement point M3 (horizontal direction): simulation, experiment

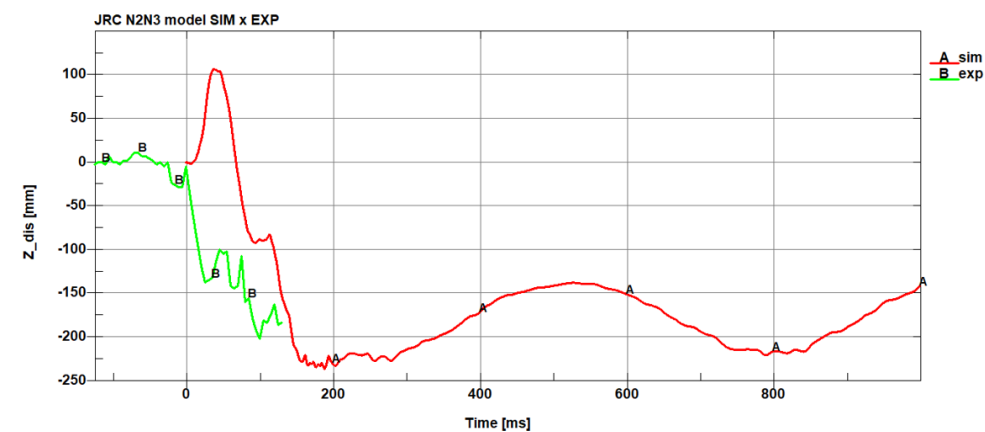


Figure 104: Z Displacement of the measurement point M3 (vertical direction): simulation, experiment

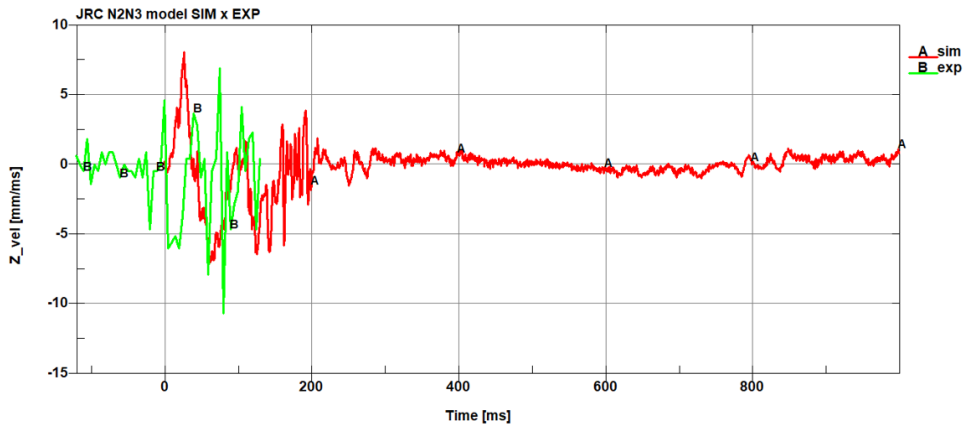


Figure 105: Z Velocity of the measurement point M3 (vertical direction): simulation, experiment

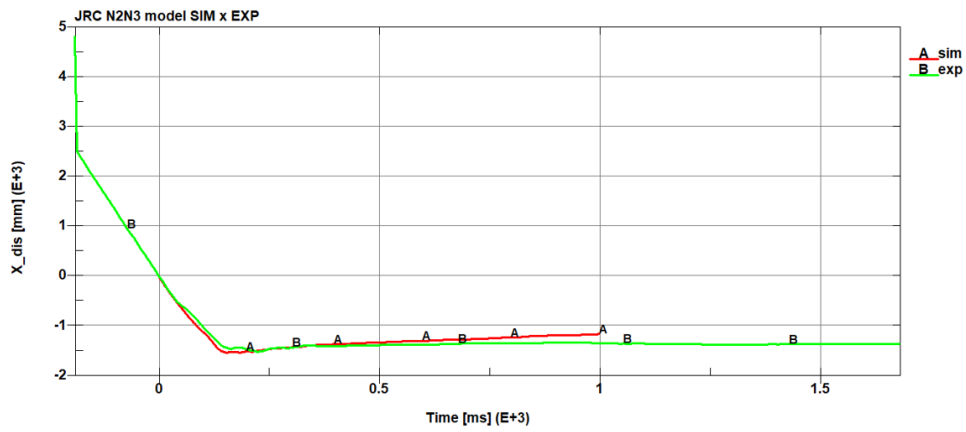


Figure 106: X Displacement of the measurement point M4 (horizontal direction): simulation, experiment

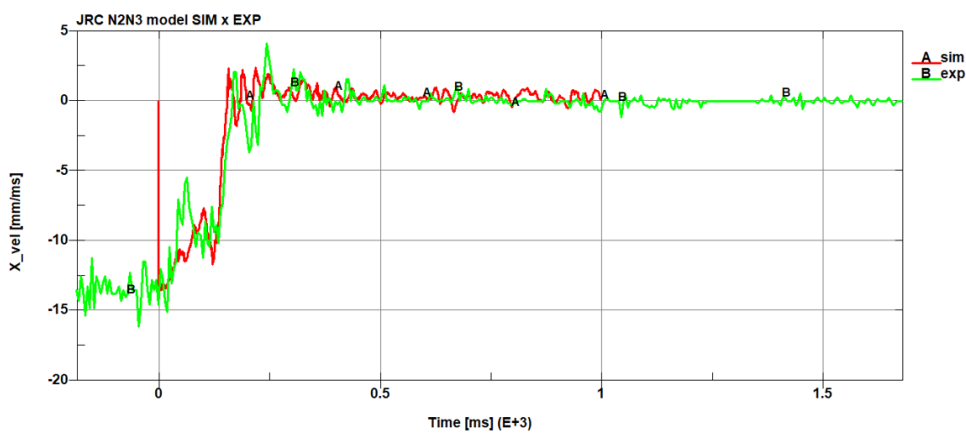


Figure 107: X Velocity of the measurement point M4 (horizontal direction): simulation, experiment

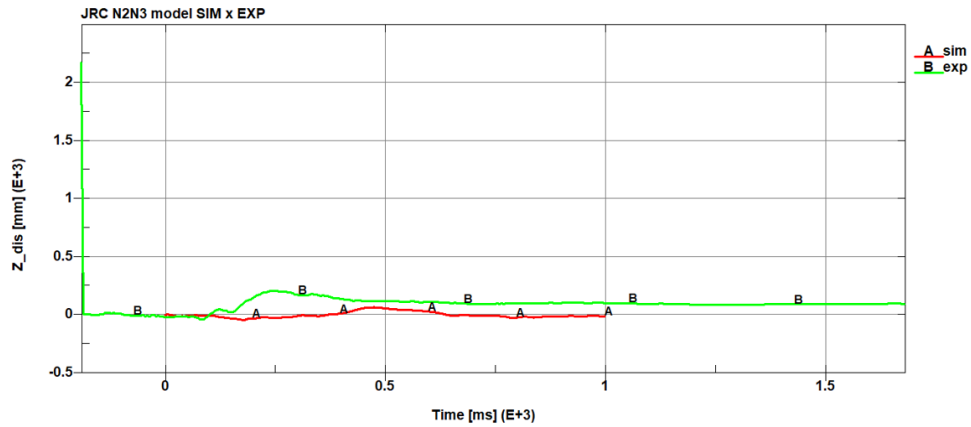


Figure 108: Z Displacement of the measurement point M4 (vertical direction): simulation, experiment

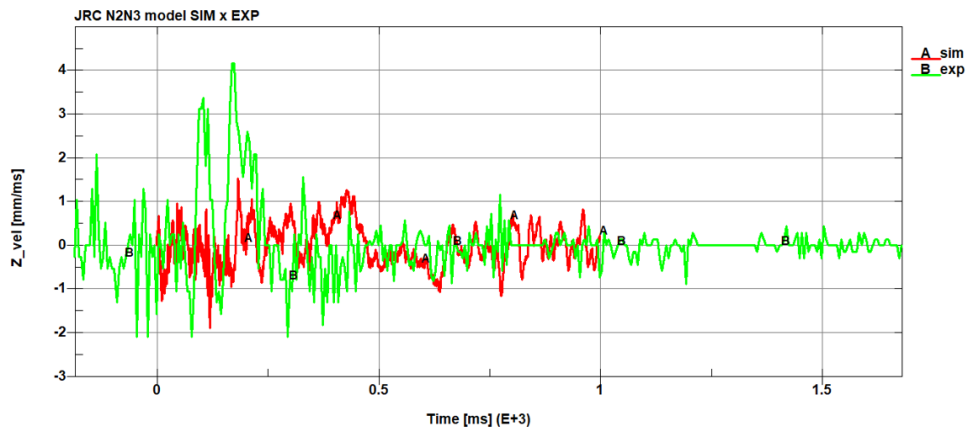


Figure 109: Z Velocity of the measurement point M4 (vertical direction): simulation, experiment

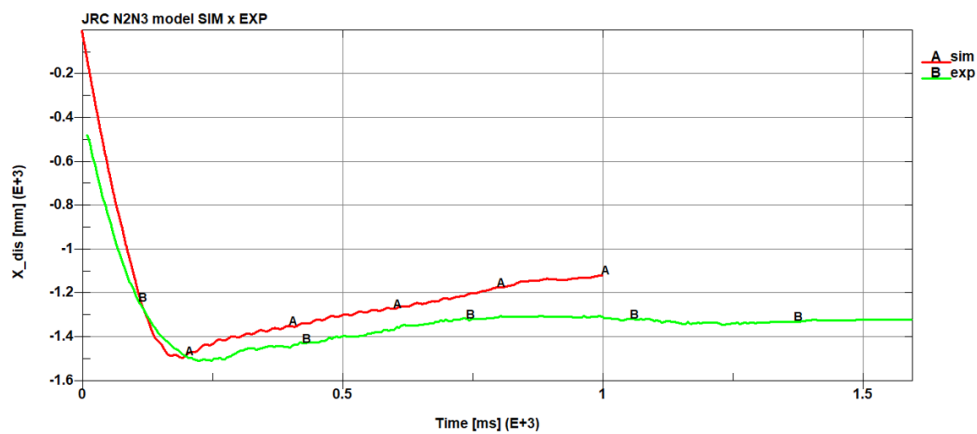


Figure 110: X Displacement of the measurement point M5 (horizontal direction): simulation, experiment

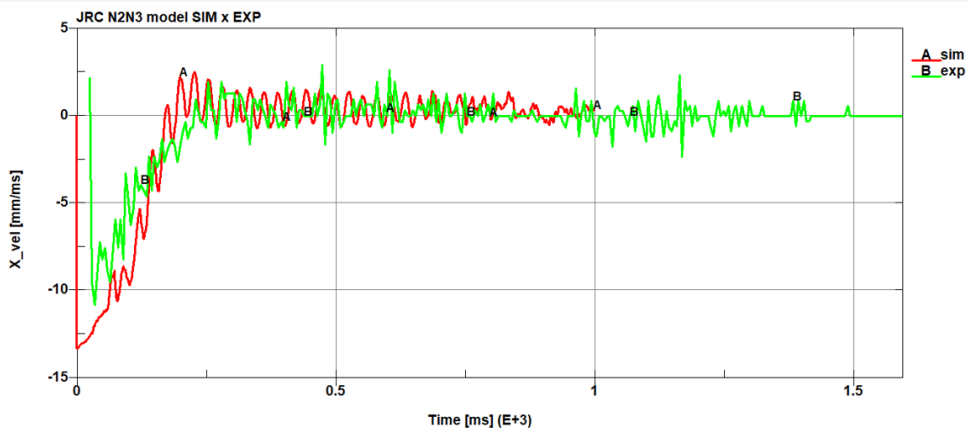


Figure 111: X Velocity of the measurement point M5 (horizontal direction): simulation, experiment

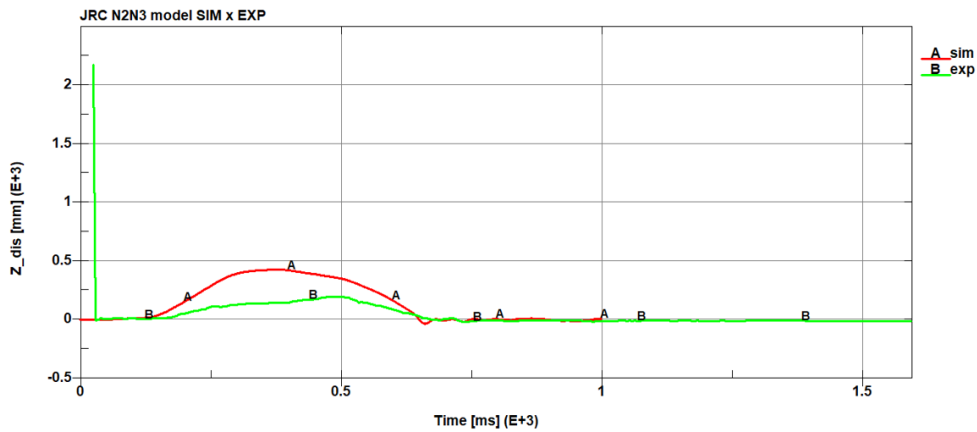


Figure 112: Z Displacement of the measurement point M5 (vertical direction): simulation, experiment

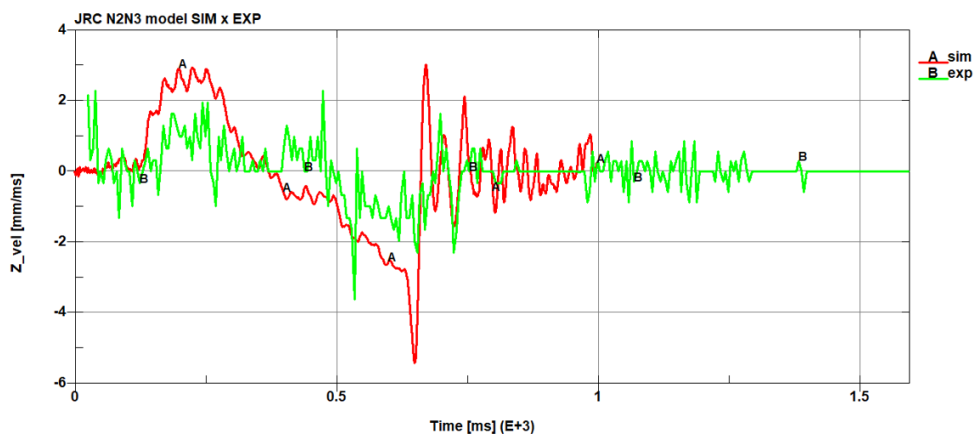


Figure 113: Z Velocity of the measurement point M5 (vertical direction): simulation, experiment

4.5.4 Conclusion

The FE model proved numerical stability throughout the computation time (1000 ms). Comparison of displacements and velocities of measurement points showed sufficient agreement between the behaviour of the real N2A vehicle and FE vehicle model. The discrepancies between the experiment and the simulation could be caused by several aspects: experiment data acquisition inaccuracy, barrier deformability, road deformability, break of symmetry at the experiment (see fig. 88) or relative movement of the cargo with respect to the vehicle frame. The most important aspects are probably break of symmetry which diminishes representativeness of the data tracked from the experiment and movement of the cargo which alters behaviour of the vehicle. In the simulation the cargo is fixed to the frame in such manner that no relative movement is allowed. On the other hand, certain relative movement of the cargo in the experiment was observed. This difference is probably the main reason why the impact in the simulation seems to be slightly harder (larger deformation of the front of the frame, rear part of the vehicle jumps higher after the impact). Despite this difference, the generic vehicle model cannot be modified in order to achieve better match with the experiment (in terms of the relative movement between the cargo and the vehicle frame). The main aim of presented work is to create a generic vehicle model representing N2A and N3D categories in accordance with IWA 14 standard. According to this standard, the cargo shall be rigidly fixed to the frame.

5 Summary

On the initiative of the JRC, SVS FEM s.r.o. prepared a generic vehicle model corresponding to the category N2A and N3D (IWA 14). This numerical model is released as Generic Vehicle N2AN3D R1.0. Key properties of the model are parametrized in order to allow convenient model modifications, which might reflect various conditions of real N2A and N3D vehicles (various dimensions, mass distribution, age, fitness, etc.). The model is therefore suitable for stochastic analyses, which allow advanced, probabilistic assessment of barrier performance. The variability of the model is its greatest strength.

The vehicle model was validated by several tests (corresponding to CEN/TR 16303). The validation procedure included tests that confirmed stability and robustness of the model and tests, which confirmed its reliability by comparing the results with experiments (curb test, full-scale bollard crash test). For further validation it would be necessary to have more experimental crash data with various N2A or N3D vehicles.

Since the variability of this vehicle model and the variability of possible impact scenarios is endless, the development and enhancement process is expected to continue among the stakeholders of the concerned working group of the JRC or other interested parties. Further development will be focused on exploration of the performance of the model in particular concerning crash scenarios, which have not been tested and compared to experiments yet. This development approach driven by researchers from various organizations and various countries will maximize the generality of the model and should lead to updated versions of the model.

6 References

- [1] WILDE K., BURZYNSKI S., BRUSKI D., CHROSCIELEWSKI J., WITKOWSKI W. TB11 test for short w-beam road barrier. 11th European LS-DYNA Conference 2017, Salzburg, DYNAmore GmbH, 2017.
- [2] SEBIK M., POPOVIC M., KLETECKOVA K. Generic vehicle model N1, JRC Technical Report 130165, 2022. Available from: https://counterterrorism.ec.europa.eu/generic_vehicle_models.php
- [3] BURZYNSKI S., CHROSCIELEWSKI J., PACHOCKI L. Finite Element Method Simulations of Various Cases of Crash Tests with N2/W4/A Steel Road Barrier. Gdansk, GAMBIT, Department of Highway and Transportation Engineering of Gdansk University of Technology, 2018.
- [4] TRAJKOVSKI J., AMBROZ M., KUNC R. The Importance of Friction Coefficient between Vehicle Tyres and Concrete Safety Barrier to Vehicle Rollover – FE Analysis Study. Strojnski vestnik - Journal of Mechanical Engineering, 64(2018)12, p. 753-762. University of Ljubljana, Faculty of Mechanical Engineering, 2018.
- [5] LS-DYNA Keyword User's Manual. R12.0, Livermore Software Technology (LST), an Ansys company, 2020.
- [6] NCAC. (2016). National crash analysis Center.
- [7] RAOUL F., INAMULLAH K., VU H. D. Impact of corrosion on mechanical properties of steel embedded in 27-year-old corroded reinforced concrete beams. Materials and Structures. 46. 10.1617/s11527-012-9941-z. 2013.
- [8] Iveco Eurocargo MLL160 [online]. [see 2023-03-20]. Available from: <https://iveco-hk.cz/wp-content/uploads/2020/12/iveco-eurocargo-ml160e32-p-my19.pdf>
- [9] Iveco technical sheet [online]. [see 2023-02-16]. Available from: https://www.iveco.com/czech/collections/technical_sheets/Documents/CargoPdfPublic/Cargo%20120EL22.pdf
- [10] Iveco cargo Stralis public [online]. [see 2023-02-16]. Available from: https://www.iveco.com/czech/collections/technical_sheets/Documents/StralisPdfPublic/ADN%20190S33.pdf
- [11] Euro4 Commercial Documentation 4x2 First Edition Commercial Documentation - EuroCargo Euro 4. [online]. [see 2023-01-19]. Available from: <https://pdf4pro.com/view/m-h-c-v-iveco-iveco-76858.html>
- [12] Iveco Eurorider Crusor 10 Euro 5 [online]. [see 2023-01-19]. Available from: https://www.iveco.com/czech/collections/technical_sheets/Documents/Irisbus/Minibus/34_Eurorider_Crusor_10_Euro5_4x2_CZ_MAY2010.pdf
- [13] Daf truck feature [online]. [see 2023-01-16]. Available from: <https://www.daftrucks.cz/api/feature/specsheet/open?container=224abfca-b4a6-46ae-b8af-0fdabacbf49&filename=TSCZCS081F3602BAAA202321>.
- [13] Daf club manual [online]. [see 2023-01-16]. Available from: https://www.daf-club.com/manual_download.php?id=189
- [14] Daf trucks club [online]. [see 2023-01-16]. Available from: <https://www.daftrucks.cz/cs-cz/trucks>
- [15] Daf truck trade, brochure [online]. [see 2023-01-16]. Available from: https://www.daftrucktrade.cz/wp-content/uploads/2017/11/DAF-XF-brochure-MY2017_CZ.pdf
- [16] Daf XF530 Specification [online]. [see 2023-01-16]. Available from: <https://www.daf.com.au/wp-content/uploads/2021/06/DAF-XF-MX13-FTT-SS-0621.pdf>
- [17] Iveco club manuals, brochure [online]. [see 2023-01-17]. Available from: https://www.iveco-club.com/manuals.php?ddlb_category=12
- [18] Hyundai Mighty EX8 chassis cab [online]. [see 2023-01-17]. Available from: <https://williamgill.co.nz/uploads/images/FINAL-EX-8.pdf>
- [19] Mitsubishi Fuso, brochure [online]. [see 2023-01-17]. Available from: <http://www.fuso.simbacolt.com/brochure/canter.pdf>
- [20] Mitsubishi Fuso full line, brochure [online]. [see 2023-01-17]. Available from: <https://www.mitfuso.com/files/FUSO-Full-Line-Brochure-EN-US.pdf>

- [21] Hyundai Mighty Truck [online]. [see 2023-01-17]. Available from: <http://trucknbus.hyundai.com/global/products/truck/mighty>
- [22] Isuzu product brochure [online]. [see 2023-01-17]. Available from: https://www.isuzucv.com/en/app/site/pdf?file=2023ProductBrochure_Final.pdf
- [23] Isuzu current special tradepack [online]. [see 2023-01-17]. Available from: https://www.isuzu.com.au/Media/Isuzu_Files/Spec_Sheets/Current_spec_sheets/NPR%2045_55-155%20TRADEPACK_ARK1367_v02.pdf
- [24] Daf truck document library [online]. [see 2023-01-17]. Available from: <https://www.daftrucks.cz/cs-cz/novinky-a-media/daf-document-library>
- [25] Hyundai Mighty EX8 Cargo long [online]. [see 2023-01-17]. Available from: <https://www.hyundai-meacv.com/en/pdf/trucks/ex-series/products-truck-qt-ex8-cargo-spec.pdf>
- [26] Man truck brochure [online]. [see 2023-01-18]. Available from: <https://www.man.eu/cz/cz/nakladni-automobil/kabiny-ridice/kabina-ridice-nn/kabina-ridice-nn.html>
- [27] Isuzu 2022 Truck, brochure [online]. [see 2023-01-18]. Available from: https://www.isuzutruckservice.com/pdf_redirect_nav.php?reference=BodyBuilder2022
- [28] Isuzu Truck Body Builder 2016 [online]. [see 2023-01-18]. Available from: https://drive.google.com/file/d/1H0rA6les1MpONl3lpyE_q0P6if7oN5v5/view
- [29] Video of Crash test DAF LF 45 vs. Bollard PAS 68 IWA 14-1 [online]. [see 2023-01-17]. Available from: https://youtu.be/7fTl4_vGyI0
- [30] Tracker, software. Available from: <https://physlets.org/tracker/>

7 Attachments

Attachment 1: Input files for Ansys LS-DYNA „ JRCVehicleN2AN3D_R1_2.zip“

Archive contains all input files for the generic vehicle model N2A/N3D release 1.2.

8 Appendix A: Geometry reverse engineering example

Collection of geometry data of mentioned vehicles was based on physical measurements, photos, and product brochures of several complete and partially disassembled vehicles. This appendix provides examples of how the direct measurements were done.



Figure 1: Representative vehicle



Figure2: Rear axle and wheel suspension



Figure 3: Representative vehicle with tilted cab



Figure 4: Measurement of frame thickness



Figure 5: Measurement of main frame dimensions



Figure 6: Measurement of main frame dimensions



Figure 7: Exposed front part of the frame and the engine



Figure 8: Measurement of a box holder

GETTING IN TOUCH WITH THE EU

In person

All over the European Union there are hundreds of Europe Direct centres. You can find the address of the centre nearest you online (european-union.europa.eu/contact-eu/meet-us_en).

On the phone or in writing

Europe Direct is a service that answers your questions about the European Union. You can contact this service:

- by freephone: 00 800 6 7 8 9 10 11 (certain operators may charge for these calls),
- at the following standard number: +32 22999696,
- via the following form: european-union.europa.eu/contact-eu/write-us_en.

FINDING INFORMATION ABOUT THE EU

Online

Information about the European Union in all the official languages of the EU is available on the Europa website (european-union.europa.eu).

EU publications

You can view or order EU publications at op.europa.eu/en/publications. Multiple copies of free publications can be obtained by contacting Europe Direct or your local documentation centre (european-union.europa.eu/contact-eu/meet-us_en).

EU law and related documents

For access to legal information from the EU, including all EU law since 1951 in all the official language versions, go to EUR-Lex (eur-lex.europa.eu).

Open data from the EU

The portal data.europa.eu provides access to open datasets from the EU institutions, bodies and agencies. These can be downloaded and reused for free, for both commercial and non-commercial purposes. The portal also provides access to a wealth of datasets from European countries.

Science for policy

The Joint Research Centre (JRC) provides independent, evidence-based knowledge and science, supporting EU policies to positively impact society



EU Science Hub

joint-research-centre.ec.europa.eu



@EU_ScienceHub



EU Science Hub - Joint Research Centre



EU Science, Research and Innovation



EU Science Hub



@eu_science